DISSERTATION

Retinol Saturase as a Novel Regulator of Thyroid Function and Energy Homeostasis

Retinol Saturase als neuer Regulator der Schilddrüsenfunktion und Energiestoffwechsel

zur Erlangung des akademischen Grades
Doctor rerum medicinalium (Dr. rer. medic.)

vorgelegt der Medizinischen Fakultät
Charité – Universitätsmedizin Berlin

von

Na Yang

Erstbetreuung: Prof. Dr. rer. nat. Michael Schupp

Datum der Promotion: 30. 06. 2024

List of Tables

List of Figures

List of Abbreviations

According to general guidelines for formatting protein and gene nomenclature, protein symbols are not italicized, and all letters are in upper case in this work, while for gene symbols, the first letter is in upper case and all letters are italicized.

ACC1/*Acc1*	acetyl-CoA carboxylase 1
AFAP1L2	actin filament-associated protein 1-like 2
AMPK	adenosine monophosphate-activated protein kinase
ANOVA	analysis of variance
APS	ammonium persulfate
atRA	all-*trans* retinoic acid
ATP	adenosine triphosphate
BAT	brown adipose tissue
BCA	bicinchoninic acid assay
BSA	bovine serum albumin
cAMP	cyclic adenosine monophosphate
cDNA	complementary DNA
ChREBP	carbohydrate responsive element binding protein
CO_2	carbon dioxide
CRTISO	carotenoid isomerase
CYP7A1	cholesterol 7-alpha-monooxygenase or cytochrome P450 7A1
ddH_2O	double distilled water
Dio1/*Dio1*	iodothyronine deiodinases 1
Dio2/*Dio2*	iodothyronine deiodinases 2
Dio3	iodothyronine deiodinases 3
DIT	diiodotyrosine
DNA	deoxyribonucleic acid
DNase	deoxyribonuclease
DTT	dithiothreitol
DUOX1/*Duox1*	dual oxidase 1
DUOX2/*Duox2*	dual oxidase 2
ECL	enhanced chemiluminescence
EDTA	ethylenediaminetetraacetic acid
EGTA	ethylene glycol-bis(β-aminoethyl ether)-N,N,N′,N′-tetraacetic acid
ELISA	enzyme-linked immunosorbent assay
ER	endoplasmic reticulum

EtOH	ethanol
FAD	flavin adenine dinucleotide
Fasn	fatty acid synthase
FDR	false discovery rate
FOXO1	forkhead box O1
fT3	free triiodothyronine
fT4	free thyroxine
GPCRs	G-protein-coupled receptors
GPX	glutathione peroxidase family
GPX2/*Gpx2*	glutathione peroxidase 2
GV-SOLAS	Society for Laboratory Animal Science
h	hour
H_2O_2	hydrogen peroxide
HEK293	human embryonic kidney 293
HFD	high-fat diet
HIF-1α	hypoxia-inducible factor 1-alpha
HMG-CoA	β-hydroxy-β-methylglutaryl-CoA
HMGCR	3-hydroxy-3-methylglutaryl-CoA reductase
HNF4α	hepatocyte nuclear factor 4 alpha
HPT	hypothalamic-pituitary-thyroid
HRP	horseradish peroxidase
HSA	human serum albumin
ipGTT	intraperitoneal glucose tolerance test
ipITT	intraperitoneal insulin tolerance test
KOH	potassium hydroxide
LAT2	L-type amino acid transporters 2
LDL	low-density lipoprotein
loxP	locus of X-over P1
MDA	malondialdehyde
min	minute
MIT	monoiodotyrosine
mRNA	messenger ribonucleic acid
NAD	nicotinamide adenine dinucleotide
NADP/NADPH	nicotinamide adenine dinucleotide phosphate
NAFLD	nonalcoholic fatty liver disease
NaI	sodium iodide
NEFA	non-esterified fatty acid

NHRs	nuclear hormone receptors
NIH	National Institutes of Health
NIS/*Nis*	sodium-iodide symporter
NMR	nuclear magnetic resonance
NQO1/*Nqo1*	NAD(P)H quinone dehydrogenase 1
NRF2/*Nrf2*	NFE2-related transcription factor 2
O_2	oxygen
PBS	phosphate-buffered saline
PCR	polymerase chain reaction
PDAC	pancreatic ductal adenocarcinoma
PPARα/*PPARα*	peroxisome proliferator-activated receptor α
PPARγ	peroxisome proliferator-activated receptor γ
Ppia	peptidylprolyl isomerase A
Ppsig	starvation-induced gene
PVDF	polyvinylidene fluoride
qPCR	quantitative real-time polymerase chain reaction
RAR	retinoic acid receptor
RBP4	retinol binding protein 4
RetSat/*RetSat*	retinol saturase
RER	respiratory exchange ratio
Rmt7	rat mammary tumor 7
RNA	ribonucleic acid
RNase	ribonuclease
RNAseq	RNA sequencing
ROS	reactive oxygen species
rT3	reverse triiodothyronine
RXR	retinoid x receptor
SDS	sodium dodecyl sulfate
SDS-PAGE	sodium dodecyl sulphate-polyacrylamide gel electrophoresis
sec	second
SEM	standard error of the mean
Spot14	thyroid hormone-responsive spot 14
SREBP1C	sterol regulatory element-binding protein 1C
SREBP2	sterol regulatory element-binding protein 2
T2	diiodothyronine
T3	triiodothyronine
T4	thyroxine

TAE	tris acetate-EDTA
TBARS	thiobarbituric acid reactive substances
TBG/*Tbg*	thyroxine-binding globulin
TBHP	*tert*-butylhydroperoxide
TEMED	tetramethylethylenediamine
TG/*Tg*	thyroglobulin
TH	thyroid hormone
TRs	thyroid hormone receptors
TPO/*Tpo*	thyroid peroxidase
TRH	thyrotropin-releasing hormone
TSH	thyroid-stimulating hormone
TSHR	thyroid-stimulating hormone receptor
TTR/*Ttr*	transthyretin
UCP1	uncoupling protein 1
UPR	unfolded protein response
UV	ultraviolet
WAT	white adipose tissue
wt	wild-type
XBP1/*Xbp1*	X-box binding protein 1
Zfx	zinc finger protein X-linked

Abstract

Background: Retinol Saturase (RetSat), an oxidoreductase, is expressed in metabolically active tissues and plays a role in adipocyte differentiation, hepatic glucose and lipid metabolism, macrophage function, vision, and ROS production. However, its function in the thyroid remains unexplored.

Methods: RetSat expression in the mouse thyroid was examined under various physiological conditions, including normal diet, high-fat diet, hyperthyroidism, hypothyroidism, and iodide overload. To elucidate the functional significance of RetSat in the thyroid, a thyrocyte-specific *RetSat* knockout mouse model was generated and evaluated, and its effects were systematically studied under various experimental conditions. Serum samples were collected to quantify thyroid hormone levels by radioimmunoassay, TSH levels by Luminex immunoassay, and triglyceride and non-esterified fatty acids (NEFA) levels by colorimetric enzymatic assay. Thyroid and liver tissues were obtained for comprehensive evaluation of thyroid morphology using H&E staining, analysis of gene expression patterns using real-time polymerase chain reaction, examination of protein expression profiles using immunoblotting and immunohistochemistry techniques, determination of Dio1 activity using the non-radioactive Sandell-Kolthoff method, and quantification of triglyceride levels.

Results: RetSat exhibited strong expression in the thyroid, with induction under hypothyroidism and reduction upon iodide overload. Thyrocyte-specific *RetSat* deletion resulted in elevated circulating TSH levels, alterations in thyroid morphology, and disruption of metabolic homeostasis, influenced by diet and gender. However, it did not significantly affect circulating thyroid hormone levels.

Conclusion: This study unveils the previously unexplored function of RetSat in the thyroid and establishes its role as a novel regulator of thyroid function and metabolic homeostasis.

Zusammenfassung

Hintergrund: Retinol Saturase (RetSat), ein Oxidoreduktase, wird in metabolisch aktiven Geweben exprimiert und spielt eine Rolle bei der Adipozytendifferenzierung, dem hepatischen Glukose- und Lipidstoffwechsel, der Makrophagenfunktion, Sehvorgang und der ROS-Produktion. Seine Funktion in der Schilddrüse ist jedoch noch unerforscht.

Methoden: Die Expression von RetSat in der Mausschilddrüse wurde unter verschiedenen physiologischen Bedingungen untersucht, einschließlich normaler Ernährung, fettreicher Ernährung, Hyperthyreose, Hypothyreose und Iodüberladung. Um die funktionelle Bedeutung von RetSat in der Schilddrüse aufzuklären, wurde das Mausmodell mit schilddrüsenspezifischer *RetSat*-Deletion erzeugt und bewertet, und seine Auswirkungen wurden systematisch unter verschiedenen experimentellen Bedingungen untersucht. Serumproben wurden gesammelt, um die Schilddrüsenhormonspiegel mittels Radioimmunoassay, die TSH-Spiegel mittels Luminex Immunassay und die Triglycerid- und NEFA-Spiegel mittels farbmetrischem enzymatischem Reaktionen zu quantifizieren. Schilddrüsen- und Lebergewebe wurden zur umfassenden Bewertung der Schilddrüsenmorphologie mittels H&E-Färbung, zur Analyse der Genexpression mittels Echtzeit-Polymerase-Kettenreaktion, zur Untersuchung der Proteinexpression mittels Immunoblotting- und Immunohistochemiemethoden, zur Bestimmung der Dio1-Aktivität mittels der nicht-radioaktiven Sandell-Kolthoff-Methode und zur Quantifizierung der Triglyceridspiegel gewonnen.

Ergebnisse: RetSat zeigte eine starke Expression in der Schilddrüse, mit Induktion bei Hypothyreose und Reduktion bei Iodüberladung. Die schilddrüsenspezifische *RetSat*-Deletion führte zu erhöhten zirkulierenden TSH-Spiegeln, Veränderungen der Schilddrüsenmorphologie und Störungen der metabolischen Homöostase, beeinflusst durch Ernährung und Geschlecht. Allerdings hatte sie keine signifikanten Auswirkungen auf die zirkulierenden Schilddrüsenhormonspiegel.

Schlussfolgerung: Diese Studie enthüllt die bisher unerforschte Funktion von RetSat in der Schilddrüse und etabliert seine Rolle als neuartigen Regulator der Schilddrüsenfunktion und metabolischen Homöostase.

1 Introduction

1.1 Thyroid Gland

The thyroid is an endocrine gland in the front of the neck, as shown in Figure 1, shaped like a butterfly and made up of two lobes of equal size. It is located just below the larynx, next to the Adam's apple. The thyroid gland is made up of thyrocytes (also called thyroid epithelial cells or thyroid follicular cells) that synthesise and release thyroid hormones (TH), which are essential for normal growth, development and metabolism in the body.

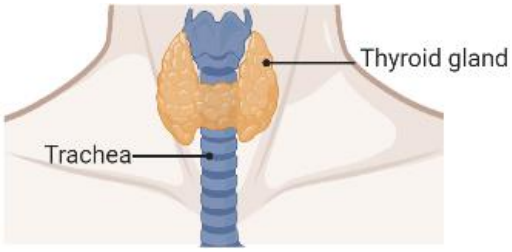

Figure 1: The position of the thyroid gland in the neck. The thyroid gland is a small gland located beside the trachea, below the larynx in the front part of the neck, and forms part of the endocrine system. Created with BioRender.com.

The main function of the thyroid gland is to synthesise, store, and release TH, the two most important of which are triiodothyronine (3,5,3'-triiodo-l-thyronine, T3) and thyroxine (3,3',5,5'-tetraiodo-l-thyronine, T4). The chemical structures of T3 and T4 are shown in Figure 2. These hormones regulate various aspects of the body, such as the basal metabolic rate, heart function, and digestive and nervous systems (1-7). TH also affect body temperature regulation, bone health, reproductive health, and emotional state, among others (8-13).

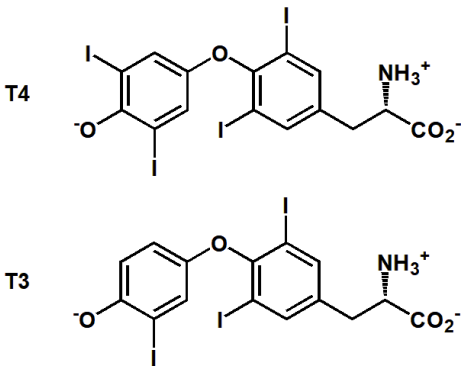

Figure 2: Chemical structures of T4 and T3. T4 is composed of four iodine atoms attached to a tyrosine residue, and T3 has three iodine atoms attached to a tyrosine residue. Created with ChemDraw software.

The thyroid gland plays an important role in overall health. Abnormal thyroid function can lead to hyperthyroidism or hypothyroidism. Hyperthyroidism can cause a rapid metabolic rate, with symptoms including anxiety, weight loss, rapid heartbeat and neck swelling (14). Hypothyroidism causes a decrease in metabolism, with symptoms including fatigue, weight gain, dry skin and depressed mood (15).

1.1.1 Histological Structure of the Thyroid Gland

The thyroid follicle is considered to be the functional unit required for TH biosynthesis, consisting of a single layer of polarized follicular epithelial cells, known as thyrocytes, as shown in Figure 3, organized into a three-dimensional ovoid structure surrounding the follicular lumen. The follicle is filled with colloid, which contains thyroglobulin (TG), a very large glycoprotein (660 kDa) that is the precursor and storage form of TH (16). The follicles vary greatly in size, and the calcitonin-producing C-cells are located between the thyroid follicles (16). The exterior of the follicle is bounded by the basolateral plasma membrane of the thyrocytes and is in contact with a vast network of capillaries, as shown in Figure 3, where an intense exchange with blood takes place (17).

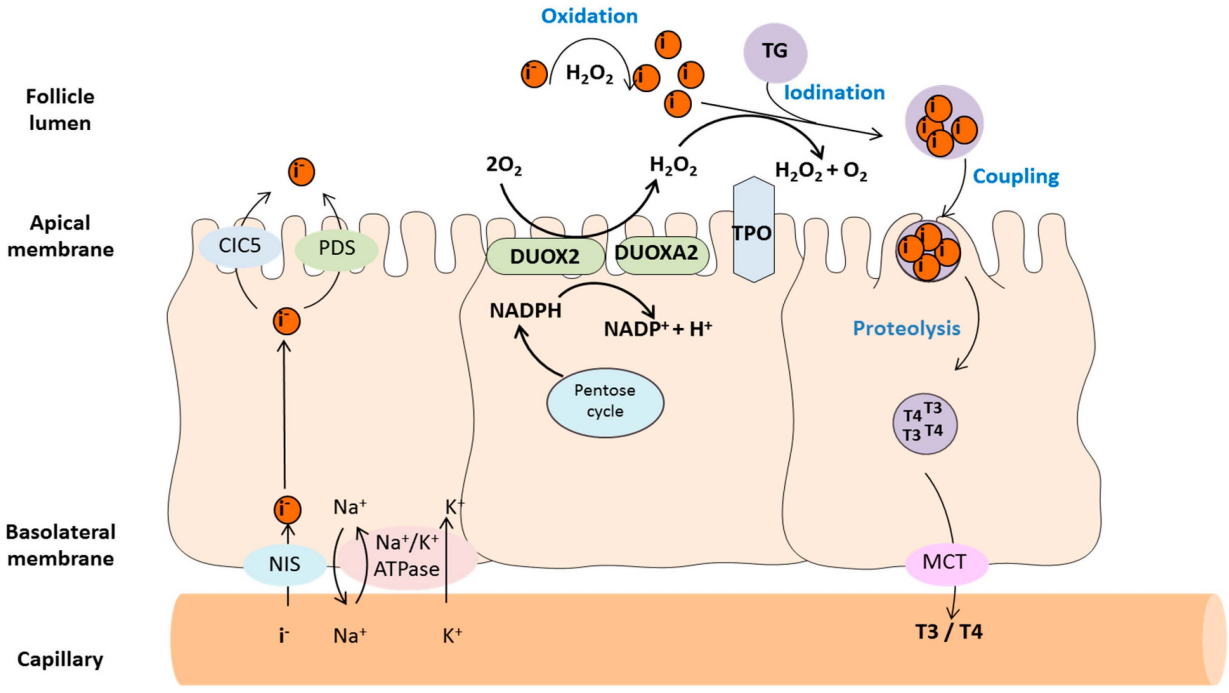

Figure 3: Synthesis of thyroid hormones. Iodine is transported into thyroid cells through the sodium-iodine symporter (NIS) and subsequently enters the follicular lumen by the transporter pendrin (PDS) and the voltage-gated chlorine channel 5 (CIC-5). In the colloid, the iodide is rapidly oxidized by thyroid peroxidase (TPO) with hydrogen peroxide (H_2O_2) provided by dual oxidase 2

(DUOX2). Iodine is very reactive and iodinates the thyroglobulin (TG) at tyrosyl residues, which is then endocytosed into the follicular cells. The TG undergoes hydrolysis, resulting in the release of triiodothyronine (T3) and thyroxine (T4). These hormones are finally transported into the circulation through the monocarboxylate transporter 8 (MCT8). Figure taken from Szanto *et al*. (18).

1.1.2 Synthesis of Thyroid Hormones (TH)

The synthesis of TH occurs within the thyroid follicles and involves a series of specific biochemical reactions that are closely related to the histology of the thyroid tissue.

TH synthesis involves the uptake of iodide, its incorporation into TG, and the coupling of iodinated tyrosine residues to form mainly T4 and along with some T3. The biosynthesis and metabolism of TH requires the involvement of several minerals and trace elements such as iodide, selenium and iron (19). TH contain iodine atom as an essential component, and the transmembrane Na+ gradients mediated by the sodium-iodide symporter (NIS) facilitate iodide transport to thyrocytes (20, 21). Iodide transport is also stimulated by thyroid stimulating hormone (TSH) (22, 23). TSH stimulates cyclic adenosine monophosphate (cAMP) synthesis by binding to the TSH receptor (TSHR), a member of the class A G-protein-coupled receptors (GPCRs) located on the basolateral plasma membrane of thyrocytes (24-29). TSH stimulates NIS activity and regulates *Nis* mRNA levels through the cAMP pathway (21).

TG plays a crucial role in iodine metabolism, serving as a scaffold for TH biosynthesis and for iodide storage in the thyroid, which is essential for maintaining thyroid homeostasis (30, 31). TG is a high molecular weight glycoprotein homodimer with two subunits of 330 kDa, primarily located in the follicular lumen. The expression of *Tg* mRNA is regulated by TSH through the stimulation of thyroid adenylate cyclase (32), which plays an important role in GPCR signaling through the generation of the soluble second messenger cAMP (29). Upon TSH-induced stimulation of exocytosis, newly synthesized non-iodinated TG is secreted into the follicular lumen (33). Thyroid peroxidase (TPO), a transmembrane protein present in the apical plasma membrane, catalyzes the iodination of some amino acid residues of TG (31).

TPO is a critical enzyme in TH synthesis, as it catalyzes the oxidative coupling of iodotyrosine residues to produce T4 and T3 iodothyronine. *TPO* gene expression is primarily restricted to the thyroid gland and is regulated by at least three transcription

factors, including paired box gene 8 (*PAX8*), NK2 homeobox 1 (*NKX2-1*), and forkhead box E1 (*FOXE1*), along with the p300 coactivator (34, 35). TSH stimulates *TPO* gene expression via the cAMP pathway, and it also increases *TPO* levels in the apical plasma membrane by stimulating cytokinesis (36). However, TSH does not appear to play a direct role in regulating protein peroxidase activity. Interestingly, the oxidized form of iodide, generated by TPO catalysis, negatively regulates *TPO* mRNA levels (37, 38). Similar to other heme peroxidases, TPO requires oxidation by H_2O_2 to catalyze substrate oxidation. The enzyme responsible for H_2O_2 production in TH synthesis is the calcium-dependent nicotinamide adenine dinucleotide phosphate (NADPH) oxidase, also known as dual oxidase 2 (DUOX2) (18). H_2O_2 initiates the oxidation of TPO, which subsequently oxidizes iodide ions to enable their binding to tyrosyl residues of TG. This leads to the formation of iodothyronine T4 and T3 in the TG molecule via the oxidation and coupling of hormonal iodotyrosines (39).

Transporter proteins located in the basolateral plasma membrane of thyrocytes play a critical role in regulating the cellular uptake and efflux of TH (17). Several transporter proteins from different protein families are involved in facilitating these processes (40). Among these, SLC16A2 monocarboxylate transporter 8 (MCT8) has been characterized as the most important and specific transporter responsible for TH transport (40, 41). Studies in mice have shown that MCT8 deficiency results in increased thyroid hormone levels in the thyroid gland and decreased serum levels of T4 (42, 43). Mutations in MCT8 cause severe psychomotor retardation associated with a severe syndrome called Allen-Herndon-Dudley syndrome, as reported in several studies (44-47). Research has demonstrated that short-term iodide overload can lead to a significant reduction in thyroid MCT8 expression in rats, which explains the acute decrease in serum T4 caused by iodide overload (48).

Overall, the synthesis and transport of TH depend on the complex regulation of multiple enzymatic steps and regulators to maintain thyroid function and physiological regulation.

1.1.3 TH Serum Transport Proteins

More than 99% of circulating TH is bound to three types of serum proteins (thyroxine-binding globulin (TBG), transthyretin (TTR), and human serum albumin) and transported to target tissues (49, 50). Of these proteins, TBG is responsible for binding approximately

75% of serum T4, while TTR and human serum albumin (HSA) bind approximately 20% and 5% of T4, respectively (49). They act as a buffering system to maintain a stable concentration of extrathyroidal TH and to facilitate the even distribution of TH throughout various tissues (51).

TBG is synthesized in the liver. The TBG molecule has a single iodothyronine binding site with a slightly higher affinity for T4 than for T3 (49). Although TBG carries most of the TH, its concentration in serum is much lower than that of TTR and HSA (52).

TTR is synthesized mainly by the liver and the choroid plexus, which are the major sources of TTR in serum and cerebrospinal fluid, respectively (53). In humans, 90% of serum TTR is secreted by the liver (54). Alternatively, retinol binds to retinol binding protein 4 (RBP4), which forms a complex with TTR, and can be secreted in hepatocytes (54). TTR is involved in the systemic circulation of TH and retinol (53).

HSA is the most abundant circulating protein synthesized by the liver, but compared to TBG, HSA has a much lower affinity for T4 and T3 (49, 51). Drastic changes in HSA concentration do not have a noticeable effect on TH levels (51).

1.1.4 TH Function

1.1.4.1 Role of the Thyroid Gland in Normal Growth

The thyroid gland plays a pivotal role in facilitating normal growth and development, particularly during infancy and childhood, through the secretion of TH, which regulate metabolism and control cellular growth and differentiation (55, 56). These hormones are essential for the optimal functioning of all body cells, and play a critical role in regulating protein synthesis, which is vital for cellular growth and division (57-59). TH is especially crucial for the normal development of the central nervous system as well as the growth and maturation of bones and muscles during childhood (60, 61). Hypothyroidism resulting from an insufficiency of TH during this time may lead to growth retardation and developmental delays (62). Furthermore, the thyroid gland is also involved in maintaining healthy body weight and regulating body temperature, as well as affecting the functioning of the cardiovascular, gastrointestinal, and other body systems (2, 63, 64).

1.1.4.2 Effects of TH on Thermogenesis

TH have a major influence on the modulation of thermogenesis in the human body. Through their actions on various tissues and cell types, such as skeletal muscle, heart, liver, and adipose tissue, they promote energy metabolism and heat production (65). One of the important mechanisms of thermogenesis is via the action of TH on brown adipose tissue (BAT), where they stimulate the expression of proteins, such as uncoupling protein 1 (UCP1), that dissipate energy of the mitochondrial respiratory chain in the form of heat instead of synthesizing adenosine triphosphate (ATP) (66, 67).

1.1.4.3 Role of TH in Lipid Metabolism

TH exert a complex control over lipid metabolism by regulating lipogenesis, lipolysis, and lipid transport processes in the body (68, 69). Individuals diagnosed with hypothyroidism display altered lipid profiles, characterized by elevated levels of low-density lipoprotein (LDL), triglycerides, and apolipoprotein B (70). In addition to dyslipidemia, low levels of free thyroxine (fT4) also increase the risk of nonalcoholic fatty liver disease (NAFLD) (71).

TH can increase lipolysis in adipose tissue, leading to increased circulating free fatty acids, which are then taken up by the liver and oxidized to produce energy as well as synthesize and secrete ketone bodies (69, 72). In addition, TH can also stimulate the expression of genes involved in *de novo* lipogenesis, resulting in increased production of triglycerides and other lipids in the liver (68, 69).

TH is also essential in regulating the expression of key enzymes involved in cholesterol metabolism, such as β-hydroxy-β-methylglutaryl-CoA (HMG-CoA) reductase, which is responsible for the rate-limiting step in cholesterol synthesis (73). TH can increase the expression of HMG-CoA reductase and other enzymes involved in cholesterol biosynthesis, leading to increased hepatic cholesterol production (73).

Moreover, TH can also influence the expression and activity of several other important enzymes involved in hepatic lipid metabolism, including lipoprotein lipase, acyl-CoA synthase, and carnitine palmitoyltransferase 1 (74, 75). These enzymes are critical for facilitating lipid uptake, transport, and metabolism/oxidation in the liver.

1.1.4.4 Effect of TH on Cardiac Function

TH has an important role in the modulation of cardiac function, and the heart is the primary

target organ for its physiological effects (3). Thyroid dysfunction can significantly impact cardiovascular health. Hypothyroidism can lead to decreased heart rate and cardiac output, while hyperthyroidism can cause an increased heart rate, arrhythmias, hypertrophied hearts and increased cardiac output, which can put significant stress on the heart (63, 76). TH is pivotal in regulating the growth and development of cardiac muscle, promoting the growth of cardiomyocytes, increasing the number of blood vessels in the heart, and improving the function of heart valves (77).

1.1.5 Hypothalamic-Pituitary-Thyroid Axis

TH production is regulated by the hypothalamic-pituitary-thyroid (HPT) axis, which has several key components. The hypothalamus secretes thyrotropin-releasing hormone (TRH), which stimulates the pituitary gland to synthesize and secrete TSH (78) (Figure 4). TSH then acts on the thyroid gland to stimulate the biosynthesis and secretion of TH, primarily T4, and a lesser amount of biologically active T3 (78) (Figure 4). T4 and T3 are released into the bloodstream and exert specific actions on target organs, as illustrated in Figure 4. To maintain physiological levels of the main hormones of the HPT axis, T4 and T3 control the secretion of TRH and TSH through a negative feedback mechanism (79). Primary thyroid failure can result in decreased levels of circulating TH, leading to increased secretion of TRH and TSH, while excess circulating TH has the opposite effect (80). The HPT axis is also modulated by other neural, humoral and local factors that determine changes in its physiological function (81). The collective actions of the hypothalamus, pituitary, and thyroid constitute the HPT axis, which adjusts TH levels in accordance with the body’s physiological needs.

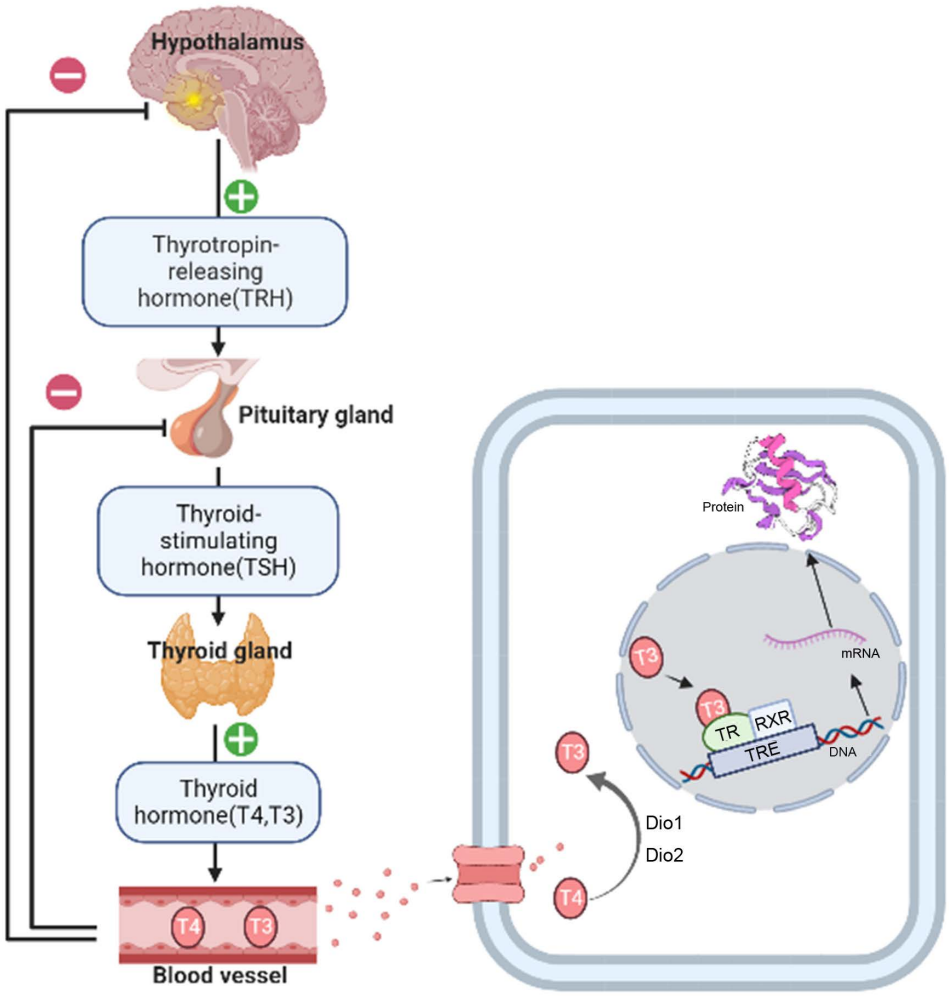

Figure 4: Hypothalamic-Pituitary-Thyroid Axis. Thyrotropin-releasing hormone (TRH) is produced and secreted by the hypothalamus, which prompts the release of thyroid-stimulating hormone (TSH) by the pituitary gland. TSH binds to membrane receptors on thyroid follicular cells, causing the synthesis and secretion of thyroid hormones such as thyroxine (T4) and triiodothyronine (T3). A negative feedback loop is established when the concentrations of T4 and T3 in the blood increase, resulting in the inhibition of the pituitary response to TRH and a decrease in TSH secretion. Thyroid hormones enter target cells through specific transmembrane transporters. T4 is converted to T3 by iodothyronine deiodinase 1 and 2 (Dio1, Dio2). Once inside the nucleus, T3 binds to thyroid hormone receptors and forms homodimers or heterodimers with Retinoid-X receptor (RXR) or others on the thyroid hormone response elements (TREs) to activate the transcription of target genes. Created with BioRender.com.

TH is central to several physiological processes, including nervous system development, energy metabolism, linear growth, thermogenesis, fluid balance and cardiovascular function. TH modifies gene expression through the action of nuclear TH receptors (*TRs*). T3 is the preferred ligand for *TR*, while T4 has a much higher serum concentration than T3 and is locally converted to T3 by TH-activating enzymes - mainly iodothyronine

deiodinase 1 (Dio1) and iodothyronine deiodinase 2 (Dio2) (80, 82). In addition, T4 can be converted to reverse triiodothyronine (rT3) by iodothyronine deiodinase 3 (Dio3) and Dio1, which reduces its affinity for *TR* (80, 83).

1.2 Retinol Saturase (RetSat)

1.2.1 Discovery of RetSat

Moise *et al.* identified a family of vertebrate enzymes with significant similarity and a putative phytoene desaturase domain to plant carotenoid isomerase (CRTISO) (84) and some cyanobacteria (85), but not in mice (86). The CRTISO-related mouse enzyme is a retinol saturase that saturates the 13-14 double bond of all-*trans*-retinol to produce all-*trans*-13,14-dihydroretinol (Figure 5), hence the name retinol saturase, abbreviated RetSat (86).

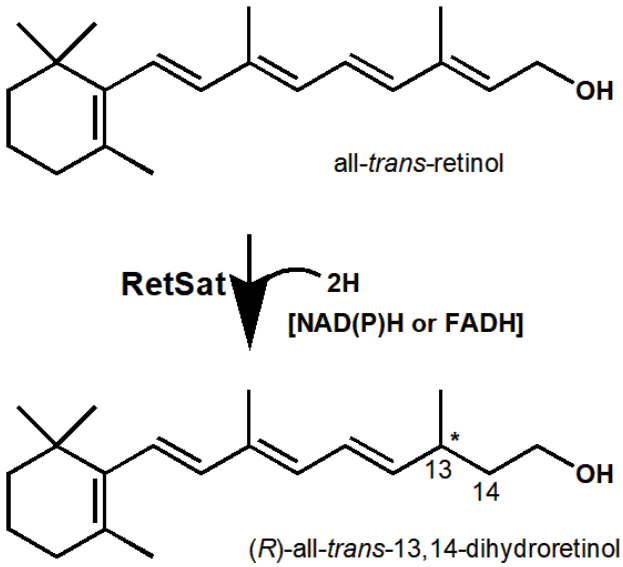

Figure 5: RetSat-catalyzed reaction that converts all-*trans*-retinol to all-*trans*-13,14-dihydroretinol. The NAD(P)H- or FADH-dependent oxidoreductase RetSat catalyzes the 13-14 double bond of all-*trans*-retinol to form all-*trans*-13,14-dihydroretinol. Created with ChemDraw software.

1.2.2 Protein Structure of RetSat

The homologs of humans and rodents have a high degree of similarity, sharing 90% of their protein sequence and having the same genic organization with 11 exons and identical exon-intron boundaries (86, 87). The mouse protein, which consists of 609

amino acids, is predicted to be about 67 kDa in size and includes a signal peptide at its N-terminus (amino acids 1-18) that directs the protein to the endoplasmic reticulum (ER). It also contains a dinucleotide-binding domain (amino acids 73-118), which is a common feature among oxidoreductases (87, 88). This domain acts as a binding site for either flavin adenine dinucleotide (FAD) or nicotinamide adenine dinucleotide (NAD)/NADP cofactors. RetSat, the enzyme in question, uses all-*trans*-retinol as its substrate and is likely to saturate the retinol double bond by transferring a hydride ion from the reduced cofactor NAD(P)H or $FADH_2$ along with a proton, as suggested by the presence of the dinucleotide-binding motif (87).

1.2.3 RetSat Catalyzed Enzymatic Reactions

Murine RetSat catalyzes the conversion of all-*trans*-retinol to all-*trans*-13,14-dihydroretinol (86, 89, 90). In contrast, the zebrafish RetSat saturates either the 7-8 or the 13-14 double bonds of the retinol side chain (91). Toomey *et al.* reported that the RetSat of zebra finch exhibited the ability to catalyze the conversion of 10'-apo-β-carotene-3,10'-diol (galloxanthin) to 11',12'-dihydro-10'-apo-β-carotene-3,10'-diol (dihydrogalloxanthin), thereby indicating a functional role of RetSat in avian vision (86, 92). This finding extends previous knowledge that RetSat is capable of saturating not only the double bond of the polyene chain of all-*trans*-retinol, but also the polyene chain of galloxanthin.

1.2.4 Expression of RetSat

Although *RetSat* mRNA was cloned from the retina and retinal pigment endothelium, it has been detected in numerous tissues, primary cells, and cultured cell lines. In mice, the expression of both mRNA and protein were most prominent in the liver and kidney, followed by BAT and white adipose tissue (WAT) (86, 87, 89, 93-95). According to the mRNA expression profiles provided by BioGPS (96, 97) and the Human Protein Atlas (98) (www.proteinatlas.org), RetSat is also highly expressed in the thyroid gland, which is shown in Figure 6A. RETSAT protein localizes predominantly to hormone-synthesizing follicular thyrocytes surrounding the TG colloid in immunohistochemical staining of healthy human thyroids (Figure 6B).

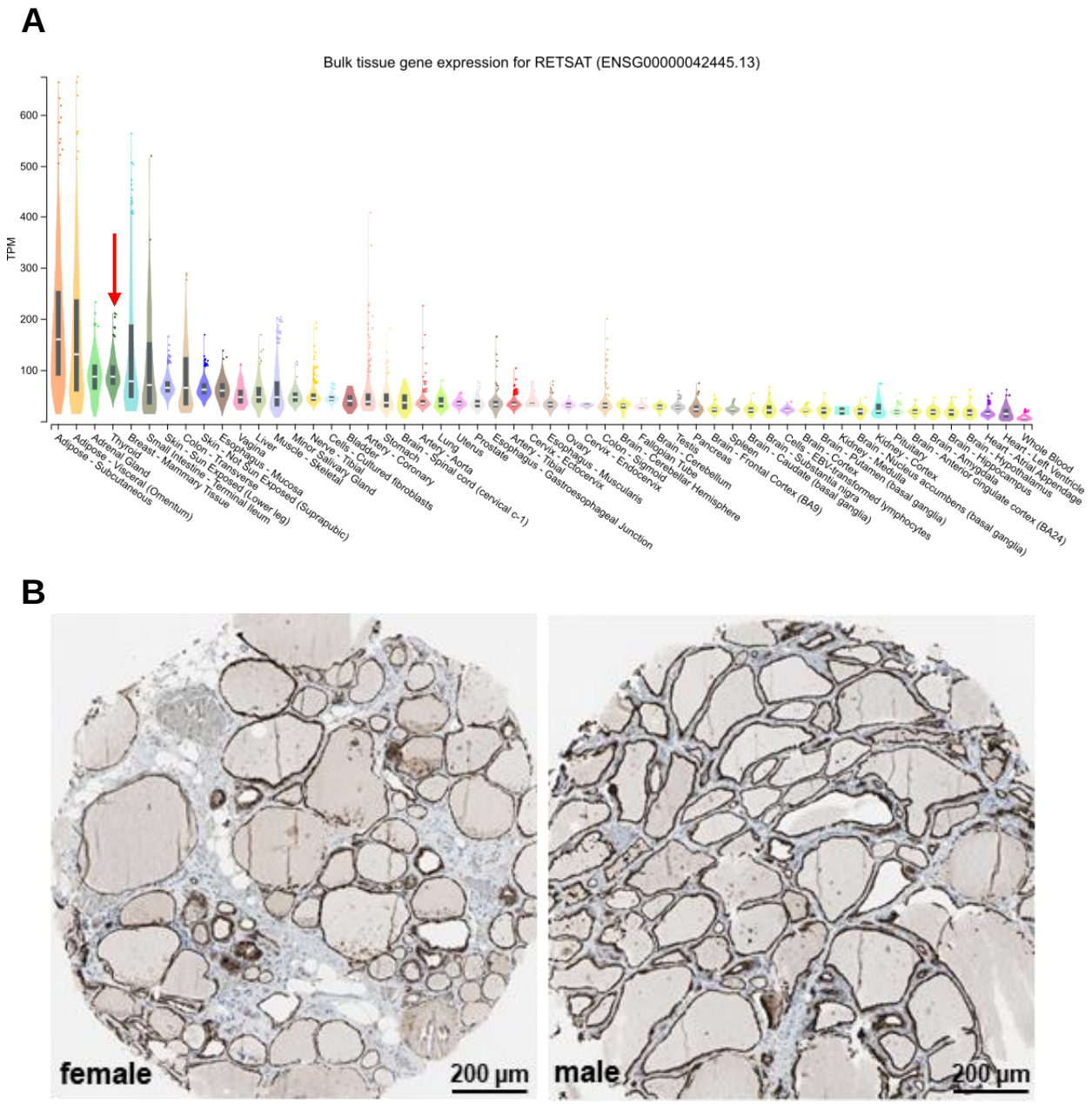

Figure 6: Expression of RetSat in human tissues and thyroid sections. A) Tissue distribution of *RetSat* mRNA expression from https://gtexportal.org/home/gene/RETSAT. The red arrow highlights *RetSat* expression in the thyroid, one of the highest among the organs with strong expression. B) RETSAT immunohistochemistry in sections of thyroid glands from human individuals, downloaded from the Human Protein Atlas, available from http://www.proteinatlas.org (98).

1.2.5 Transcriptional Regulation of RetSat

RetSat is regulated by nuclear peroxisome proliferator-activated receptor α (PPARα) in liver and PPARγ in adipose tissue via a PPAR response element in intron 1 of both murine and human genes (87, 89, 95, 99). RetSat is also induced by fasting in a PPARα-

dependent manner and was alternatively named PPARα-regulated and starvation-induced gene (*Ppsig*) (95). Additionally, *RetSat* is transactivated by forkhead box O1 (FOXO1) in mouse liver, a transcription factor that regulates gluconeogenesis (100).

1.2.6 Role of RetSat in Adipocyte Differentiation and its Impact on Adipose Tissue Physiology

RetSat expression has been detected in preadipocytes, and both RetSat mRNA and protein levels are upregulated during adipocyte differentiation (89). Treatment with the thiazolidinedione pioglitazone resulted in increased *RetSat* mRNA expression, while knockdown of PPARγ caused a noticeable decrease in *RetSat* mRNA levels in adipocytes (87, 89). Depletion of RetSat in 3T3-L1 preadipocytes impaired adipocyte differentiation, and even the addition of all-*trans*-13,14-dihydroretinol did not rescue the effects of RetSat deficiency (89, 101). Interestingly, overexpression of RetSat did not result in detectable amounts of all-*trans*-13,14-dihydroretinol even after incubation with retinol, suggesting that RetSat promotes adipocyte differentiation independently of dihydroretinol formation (89). Moreover, RetSat overexpression was found to increase the activity of PPARγ, and supplementation with the PPARγ agonist pioglitazone overcame the differentiation defects caused by RetSat knockdown. These findings suggest that RetSat is required for adipogenic differentiation and may promote it by activating PPARγ.

RetSat is highly expressed in white adipose tissue and has been found to be decreased in expression in diabetic *ob/ob* mice and in human obesity (89). In obese individuals, the macrophage content in adipose tissue is significantly increased, whereas in lean subjects it is only around 5-10% (102). The downregulation of RetSat expression has been observed when adipocytes and macrophages are cultured together, which suggests a relationship between RetSat expression and the impact of inflammatory cells on adipocytes *in vivo* (89). However, the impact of RetSat expression on adiposity is not clear, as whole-body knockout of *RetSat* in mice has been found to increase adipose tissue (103). It is unclear why this *in vivo* finding differs from *in vitro* observations. The accumulation of triglycerides and development of adiposity occurs only when an individual’s energy equation is out of balance, not as a consequence of adipocyte differentiation (104). RetSat deficiency in other cell types may affect the energy equation, taking into account that the mouse model used in the Moise *et al.* study was a whole body *RetSat* knockout model (87).

Further characterizing confirmed that mice lacking RetSat exhibited an increase in body weight gain on normal chow or when fed a high-fat diet (HFD), but food intake and energy expenditure remained unchanged (87). In addition, locomotor activity was increased, which indicates that energy efficiency may have been altered (87, 103). *RetSat* expression is also high in BAT, but its function in BAT is still unclear. One study showed that RetSat protein expression in BAT can be induced when mice are exposed to cold temperatures (105), but whether *RetSat* is related to thermogenesis requires further investigation.

1.2.7 Role of RetSat in Liver Metabolism

RetSat global deficiency did not induce variation in hepatic triglycerides, cholesterol, phospholipids or NEFA levels and did not affect hepatic and serum retinol or hepatic retinyl ester in the mixed genetic background (129sv/C57BL6) mouse (87, 103). However, it induced an increase in hepatic triglycerides under normal chow or HFD conditions after the mouse was backcrossed to C57BL/6N, but the whole-body and liver-specific insulin sensitivity were not impaired (94).

Nevertheless, in the mouse model with acute liver-specific knockdown of RetSat, no significant changes were observed when fed a normal chow diet. However, when subjected to HFD challenge, the mice exhibited lower levels of liver and serum triglycerides, serum NEFA, and glucose levels (87, 94). Furthermore, blood glucose and insulin levels also decreased, while glucose tolerance increased and insulin sensitivity did not change (94). From a mechanistic perspective, this was linked to reduced mRNA, protein, and target gene expression of carbohydrate response element binding protein (ChREBP) (87). The essential role of RetSat in glucose-induced ChREBP activity and its nuclear accumulation in primary mouse hepatocytes indicates that RetSat acts as an upstream regulator of the glucose-sensing transcription factor ChREBP (87). Notably, RetSat's regulation of ChREBP is independent of dihydroretinol formation (94). In humans, *RetSat* expression correlates with obesity, hepatic steatosis and ChREBP target gene expression in liver (87, 94). Overall, the involvement of *RetSat* extends to hepatic glucose and lipid metabolism.

1.2.8 Role of RetSat in Macrophage Function and Autoimmunity

The expression and regulation of *RetSat* mRNA in mouse thymus were reported. The results showed that under the induction of dexamethasone, the apoptosis-phagocytosis process of thymocytes led to an increase in the expression of RetSat (106). Then the researchers observed impaired long-term phagocytosis of apoptotic cells by peritoneal and bone marrow-derived macrophages in mice with *RetSat* deletion (87). This effect was rescued by administration of the recombinant bridging molecule milk fat globule-EGF factor 8, which was expressed at lower levels in RetSat-deficient macrophages (107). Furthermore, female *RetSat* knockout mice were more susceptible to developing mild systemic lupus erythematosus-like autoimmunity as they aged (87). These mice displayed increased spleen weight, delayed clearance of apoptotic cells, and deposition of immune complexes in organs such as the kidney (87, 107). The authors concluded that the function of RetSat in macrophages was likely unrelated to dihydroretinol production based on their analysis of the effects of all-*trans*-13,14-dihydroretinol on macrophage gene expression and phagocytosis (87).

1.2.9 Role of RetSat in Oxidative Stress Sensitivity

Nagaoka-Yasuda *et al.* found that RetSat can modulate the NIH/3T3 cells' response to oxidative stress, and the expression of si-RetSat significantly enhanced the viability of primary fibroblasts exposed to *tert*-butylhydroperoxide (TBHP) (108). Another study later found that as the dose of the oxidative stress inducer TBHP increased, cell survival in the RetSat knockdown group was significantly higher than in the control group, and the addition of all-*trans*-13,14-dihydroretinol did not alter the results, indicating that RetSat modulates the cellular response to oxidative stress independently of retinol saturation (109). Overexpression or knockdown of RetSat in NIH/3T3 cells leads to an increase or decrease, respectively, in TBHP-induced reactive oxygen species (ROS) production (109). Liver thiobarbituric acid reactive substances (TBARS), a byproduct of lipid peroxidation, are decreased in *RetSat* knockout normal chow and HFD mice (109). In summary, RetSat has been shown to modulate peroxide sensitivity and ROS production in cells and mouse liver, and its mechanism remains to be further studied (87).

Through evolutionary genomic comparisons, the researchers identified *RetSat* as a convergent gene that contributes to mammalian adaptation to hypoxia on the Tibetan

Plateau (110). The amino acid substitution at position 247 of RetSat (Q247R), from glutamine (Q) to arginine (R), was found to result in higher enzymatic activity in HEK293T cells (110). Mice carrying the Q247R mutation show a significant increase in heart mass, pulmonary artery diameter and pulmonary stroke volume compared to wt mice (110). In addition, mice with the Q247R mutation show significantly longer survival times under acute hypoxia conditions, indicating their increased resistance to hypoxia-induced stress compared to the wt littermates (110).

However, suppression of RetSat expression had no effect on UV- or paraquat-induced cell death (108). This implies that RetSat deficiency only provides protection against specific types of oxidative stress, suggesting that RetSat may have an undiscovered function in maintaining oxidative balance.

1.2.10 Role of RetSat in Ferroptosis

Ferroptosis, a recently discovered form of cell death, is characterized by a reduction in antioxidant capacity and the accumulation of lipid ROS in cells, resulting in oxidative cell death (111). Dubreuil *et al.* identified *RetSat* as one of the cytoprotective genes under H_2O_2 treatment by genome-wide CRISPR/Cas9 and shRNA screening in K562 chronic myelogenous leukemia cells (112). Subsequently, *RetSat* was found to be specifically required for H_2O_2-driven, iron-dependent cell death in HAP1 cells, a human leukemic cell line (113). A recent study indicated that both knockdown and knockout *RetSat* in cells showed significant resistance to ferroptosis induced by ferroptosis inducers (114). The study provided evidence that the pro-ferroptosis activity of RetSat functioned independently of the conventional ferroptosis mechanism, as *RetSat* knockout had no significant effect on the expression of established key ferroptosis-related factors such as acyl-CoA synthetase long chain family member 4 (ACSL4), glutathione peroxidase 4 (GPX4), and solute carrier family 7 member 11 (SLC7A11) in cells (114). They postulated that the regulation of ferroptosis by RetSat may be due to its capacity to attenuate the free radical scavenging properties of retinoids and inhibit the retinoic acid receptor (RAR) signaling pathway (114).

1.2.11 Role of RetSat in Cancer

The reduction of RetSat expression by zinc finger protein X-linked (*Zfx*) deletion in stem

cells and its role in retinoid homeostasis may imply a correlation with cell proliferation and tumor development (87, 115). Indeed, compared to normal control tissues in rats, *RetSat*, also known as Rat Mammary Tumor 7 (*Rmt7*), exhibits decreased transcription levels in breast cancer and proliferative bladder tissue (87). Furthermore, *RetSat* mutations have been identified in rare undifferentiated pleomorphic sarcoma (116) and malignant melanoma (117), and its expression is positively associated with tumor immune infiltration (87, 118). Recent studies have shown a correlation between high RetSat expression in pancreatic ductal adenocarcinoma patients and poor survival outcomes (119). RetSat is believed to be a novel replication fork protein that is upregulated by hypoxia-inducible factor 1-alpha (HIF-1α) under hypoxic conditions, which avoids replication fork restarting and fork damage to prevent cell apoptosis, thus conferring chemoresistance to the pancreatic ductal adenocarcinoma (PDAC) cells against the chemotherapeutic drug gemcitabine (119). These findings link expression or mutation of RetSat with tumorigenesis. However, it remains unclear whether loss of RetSat function can induce carcinogenesis, and further investigation is needed to address this question.

1.3 Aims of This Study

TH is important regulators of food intake, energy expenditure, glucose and lipid metabolism, and cardiovascular function (1, 120). Thyrocytes produce large amounts of extracellular H_2O_2 in a NADPH-dependent manner and oxidize iodide and iodinate TG during the synthesis of TH in the follicular cavity formed by thyrocytes (17). The major TH is T4, while the more active T3 is produced mainly by local T4 deiodination in the target tissues (83). Recent studies have shown an association between adiposity and serum TSH and T3 in individuals with normal thyroid function, suggesting that obesity may potentially affect HPT axis function (121, 122). Even within the physiological range, alterations in thyroid function may lead to exacerbation of metabolic complications and the development of thyroid disease. *In vitro* and *in vivo* studies present evidence supporting the potential therapeutic benefits of activating T3-dependent pathways in metabolic syndrome, NAFLD, and the treatment of hepatocellular carcinoma (HCC) (123).

Whole-body knockout of *RetSat* in mice results in increased adiposity, increased body weight under HFD conditions, increased hepatic triglyceride levels, and decreased hepatic ROS levels (103, 109). However, there is still a lack of tissue-specific knockout

models that could help us to understand the functions of RetSat. Although strong expression of RetSat has been observed in the thyroid (https://gtexportal.org/home/, phs000424.vN.pN), its functional relevance in this organ has not yet been demonstrated. However, RetSat may play an important role in the thyroid based on the following three factors: First, RetSat is highly expressed in the thyroid; moreover, peroxide sensitivity and H_2O_2 production have been shown to be associated with RetSat (108, 109); additionally, mice with global *RetSat* deletion exhibit enhanced locomotor activity (109), possibly due to alteration of the TH axis. Therefore, it is hypothesized that RetSat plays an important role in the thyroid gland. To substantiate the aforementioned hypothesis, the following research objectives were formulated:

Objective 1: To investigate the regulation of RetSat in the mouse thyroid

Objective 2: To establish a mouse model of thyrocyte-specific deficiency of RetSat

Objective 3: To investigate whether *RetSat*-specific deletion in the thyroid gland of mice affects basal energy homeostasis in a metabolically challenged state

Objective 4: To investigate whether *RetSat*-specific deletion in the thyroid gland of mice affects oxidative stress in mice with iodide overload.

The above objectives will enable us to further investigate the role of RetSat in the thyroid gland and provide new therapeutic strategies for the treatment of hormonal dysfunction and metabolic diseases.

2 Materials

2.1 Chemicals and Reagents

The chemicals and reagents used are listed in Table 1.

Table 1: Chemicals and reagents

Substance	Supplier
$(NH_4)_4Ce(SO_4)_4$	Sigma Aldrich (USA)
0.9% saline solution	B. Braun Melsungen AG (DE)
2-mercaptoethanol	Sigma Aldrich (USA)
5x PCR master mix “ready-to-load”	Bio & Sell (DE)
Acetic acid (CH_3COOH)	Carl Roth GmbH & Co. KG (DE)
Acetone ($(CH_3)_2CO$)	Sigma Aldrich (USA)
Acrylamide solution 30%	AppliChem GmbH (DE)
Ammonium persulfate (APS)	Sigma Aldrich (USA)
Bovine serum albumin fatty acid free (BSA)	Sigma Aldrich (USA)
Bromophenol blue	Sigma Aldrich (USA)
Chloroform ($CHCl_3$)	Merck KGaA (DE)
Sodium citrate	Carl Roth GmbH & Co. KG (DE)
D-(+)-glucose	Sigma Aldrich (USA)
Dibromotyrosine	Tokyo Chemical Industry (JP)
dNTP Mix	Thermo Fisher Scientific Inc. (USA)
DPX mountant for histology	Sigma Aldrich (USA)
Dithiothreitol (DTT)	Sigma Aldrich (USA)
Entellan	Sigma Aldrich (USA)
Eosin Y	Merck KGaA (DE)

Ethanol (EtOH, C_2H_5OH)	Merck KGaA (DE)
Ethylenediaminetetraacetic acid (EDTA)	Sigma Aldrich (USA)
Formaldehyde solution 4%, buffered	Merck KGaA (DE)
Glycine	Carl Roth GmbH & Co. KG (DE)
Hematoxylin	Carl Roth GmbH & Co. KG (DE)
HEPES	Thermo Fisher Scientific Inc. (USA)
Hydrogen peroxide (H_2O_2) 30%	Merck KGaA (DE)
Insulin solution human	Sigma Aldrich (USA)
Isoflurane (Forene)	AbbVie Inc. (USA)
Isopropanol	Merck KGaA (DE)
Ketamine 100 mg/ml	CP-Pharma Handelsgesellschaft mbH (DE)
Potassium hydroxide (KOH)	Sigma Aldrich (USA)
Proteinase K	Sigma Aldrich (USA)
Magnesium chloride ($MgCl_2$)	Sigma Aldrich (USA)
Methanol (CH_3OH)	Sigma Aldrich (USA)
Methimazole (MMI)	Sigma Aldrich (USA)
Milk powder	Carl Roth GmbH & Co. KG (DE)
M-MLV reaction buffer (5x)	Promega Corporation (USA)
M-MLV reverse transcriptase	Promega Corporation (USA)
Molecular weight marker ProSieve color protein marker	Lonza (CH)
NADPH tetrasodium salt	Carl Roth GmbH & Co. KG (DE)
Neo-Clear	Merck KGaA (DE)
Neomount	Merck KGaA (DE)
No ROX SYBR MasterMix blue dTTP	Eurogentec (BE)

Non-reducing lane marker sample buffer (5x)	Thermo Fisher Scientific Inc. (USA)
Paraffin type 6 & 9	Thermo Fisher Scientific Inc. (USA)
Phosphate-buffered saline (PBS) (pH 7.2; without $CaCl_2$ and $MgCl_2$)	Thermo Fisher Scientific Inc. (USA)
PhosSTOP phosphatase inhibitor cocktail tablets	F. Hoffmann-La Roche AG (CH)
Pierce ECL western blotting substrate	Thermo Fisher Scientific Inc. (USA)
Ponceau S	Cayman Chemical Company (USA)
Propylthiouracil	Sigma Aldrich (USA)
Protease Inhibitor Cocktail Tablets (complete, EDTA-free)	F. Hoffmann-La Roche AG (CH)
Protein A sepharose CL-4B	GE Healthcare Bio-Sciences AB (SE)
Qiazol lysis reagent	Quiagen GmbH (DE)
Random hexamer primer	Thermo Fisher Scientific Inc. (USA)
RNase A	Thermo Fisher Scientific Inc. (USA)
RNase-free water	Thermo Fisher Scientific Inc. (USA)
Roti-ImmunoBlock	Carl Roth GmbH & Co. KG (DE)
Reverse-T3 (rT3)	Cayman Chemical (USA)
Saccharine	Sigma Aldrich (USA)
Sodium arsenite ($NaAsO_2$)	Sigma Aldrich (USA)
Sodium chloride (NaCl)	Merck KGaA (DE)
Sodium dodecyl sulfate (SDS)	Carl Roth GmbH & Co. KG (DE)
Sodium hydroxide solution (NaOH)	Sigma Aldrich (USA)
sodium iodide (NaI)	VWR International (USA)
Sodium Perchlorate Monohydrate ($NaClO_4.H_2O$)	Sigma Aldrich (USA)

Sodium pyruvate	Sigma Aldrich (USA)
Sulfuric acid (H_2SO_4)	Sigma Aldrich (USA)
Sybrgreen PCR Mastermix	Eurogentec (BE)
Tetramethylethylenediamine (TEMED)	Sigma Aldrich (USA)
Tris hydrochloride (Tris-HCl)	Carl Roth GmbH & Co. KG (DE)
Tris(hydroxymethyl)-aminomethane (Tris base)	Merck KGaA (DE)
Triton X-100	Carl Roth GmbH & Co. KG (DE)
Trizol reagent	Thermo Fisher Scientific Inc. (USA)
Tween 20	Merck KGaA (DE)
Ultrapure distilled water DNase/RNase Free	Thermo Fisher Scientific Inc. (USA)
Xylene	Sigma Aldrich (USA)

2.2 Kits

The kits used are listed in Table 2.

Table 2: Kits

Kit	Supplier
NEFA-HR (2) Kit	FUJIFILM Wako Chemicals Europe GmbH (DE)
peqGOLD Total RNA Kit	VWR International (USA)
DAB substrate kit K3466	Dako Denmark A/S (DK)
MPTMAG-49K TSH kit	Merck, Millipore (DE)
NEBNext Ultra II RNA Library Prep Kit	New England Biolabs (USA)
Pierce BCA Protein Assay Kit	Thermo Fisher Scientific Inc. (USA)
RNA Clean & Concentrator Kit	Zymo Research (USA)
Rneasy Mini Kit	Qiagen GmbH (DE)
SuperSignal Chemiluminescent Substrate	Thermo Fisher Scientific Inc. (USA)

Total T3 RIA Kit RIA-4534	DRG Diagnostics GmbH (DE)
Total T4 RIA Kit RIA-4533	DRG Diagnostics GmbH (DE)
Triglycerides FS	DiaSys Diagnostic Systems GmbH (DE)
Vectastain ABC Kit, Rabbit IgG, PK-4001	Vector Laboratories, Inc. (USA)

2.3 Buffers and Solutions

All buffers and solutions were prepared in double distilled water (ddH_2O) unless declared otherwise and are listed in Table 3.

Table 3: Buffers and solutions

Buffer/Solution	Purpose	Composition
APS solution	Preparation of gels for SDS-PAGE	10% (m/v) APS in ddH_2O
Blocking solution	Blocking of membrane after Western blot	4% (m/v) Milk powder in 1:1 TBS/TBST buffer
Citrate buffer (pH 6/9)	Buffer for immunohistochemical staining	0.1 M Sodium citrate in ddH_2O
Electrophoresis buffer (pH 8.3-8.8)	Buffer for SDS-PAGE	16.7 mM Tris base 8.3 mM Tris-HCl 192 mM Glycine 0.1% (m/v) SDS
Loading buffer	Buffer for sample to load on gel for SDS-PAGE	87.5% (m/v) 5x Pierce lane marker non-reducing sample buffer 12.5% (m/v) 2-Mercaptoethanol
Loading buffer non-denaturing (pH 6.8)	Buffer for sample to load on gel for non-denaturing gel	1.25 mM Tris base 27.4 mM Glycerol 15 µM Bromophenol blue
Protein homogenization buffer (pH 7.4)	Buffer for protein extraction	250 mM Sucrose, 20 mM HEPES 1 mM EDTA in ddH_2O

Protein lysis buffer	Lysis buffer for protein extraction	2 mM EDTA (pH 8.0) 150 mM NaCl 50 mM NaF 50 mM Tris-HCl (pH 7.2) 0.5% (m/v) Sodium deoxycholate 1% (v/v) IGEPAL CA-630 0.1% (v/v) SDS 1 Protease inhibitor cocktail tablet (complete, EDTA-free) per 50 ml buffer
SDS solution	Compound of gel for SDS-PAGE	10% SDS
Stripping buffer	To remove already bound antibodies on membranes in Western blot analysis	6 M Guanidine hydrochloride 0.3% (v/v) TritonX-100 20 mM Tris-HCl (pH 7.5) 0.1 M 2-Mercaptoethanol
Tailcut buffer (pH 8.5)	Isolation of DNA from mouse tail biopsies	0.1 M Tris base 0.2 M NaCl 5 mM EDTA 0.2% (w/v) SDS
TE buffer (pH 7.5)	Isolation of DNA from mouse tail biopsies	10 mM Tris base 1 mM EDTA
Tris-buffered saline (TBS) buffer	Washing buffer for PVDF membranes; antibody dilution	40.1 mM Tris base 159.9 mM Tris-HCl 137 mM NaCl
Tris-buffered saline buffer with tween (TBST)	Washing buffer for PVDF membranes; antibody dilution	40.1 mM Tris base 159.9 mM Tris-HCl 137 mM NaCl 0.1% (v/v) Tween 20
Transfer buffer (pH 8.1-8.5)	Buffer for Western blot transfer	25 mM Tris base 192 mM Glycine 20% (v/v) Methanol

		0.05% (v/v) SDS
Tris-HCl buffer 0.5 M (pH 6.8)	Buffer for stacking gel for SDS-PAGE	15.3 mM Tris base 485 mM Tris-HCl
Tris-HCl buffer 1.5 M (pH 8.8)	Buffer for separation gel for SDS-PAGE	0.3 M Tris base 1.2 M Tris-HCl

2.4 Antibodies

Western blot analysis used the antibodies listed in Table 4.

Table 4: Antibodies for Western blot analysis

Antibody	Species	Product ID	Supplier	Dilution
Alpha-Tubulin	Rabbit	2144s	Cell Signaling Technology, Inc. (USA)	1:1000
Gapdh	Rabbit	14C10	Cell Signaling Technology, Inc. (USA)	1:1000-1:5000
I-thyroglobulin	Rabbit	Self-generated (124)	provided by Dr. Carrie Ris-Stalpers (University of Amsterdam) and Dr. Xavier De Deken (Université libre de Bruxelles)	1:1000
RetSat	Rabbit	HPA046513	Sigma Aldrich (USA)	1:1000
Thyroglobulin	Rabbit	A0251	Dako Denmark A/S (DK)	1:10000
Mouse	Goat	31430	Thermo Fisher Scientific Inc. (USA)	1:1000
Rabbit	Goat	31460	Thermo Fisher Scientific Inc. (USA)	1:1000

Immunohistochemical staining was performed using the antibodies listed in Table 5.

Table 5: Antibodies for immunohistochemical staining analysis

Antibody	Species	Product ID	Supplier	Dilution
RetSat	Rabbit	Self-generated (89)	Dr. Michael Schupp	1:100
Rabbit	Goat	P0448	Dako Denmark A/S (DK)	1:500

2.5 Oligonucleotides

The primers used for quantitative real-time polymerase chain reaction (qPCR) were

designed using Primer Premier software (125) and the online tool Primer-BLAST (126). The primers were produced by Thermo Fisher Scientific Inc. (Waltham, USA). The sequences of primers (from 5' to 3') used in this study are listed in Table 6 and Table 7.

Table 6: Primers for qPCR

Gene	Primer direction	Sequences
36B4	forward	TCATCCAGCAGGTGTTTGACA
	reverse	GGCACCGAGGCAACAGTT
Acc1	forward	GGTGAAGCTGGACCTAGAAGAGAA
	reverse	AAAGGCCAAACCATCCTGTAAGC
Cre	forward	GCTTGCATGATCTCCGGTAT
	reverse	ATACCTGGCCTGGTCTGGA
Dio1	forward	AAGTGCAACATCTGGGATTTC
	reverse	AGAAATGAAGGTCAGGTGCAA
Duox1	forward	GTCTGGCTTCCAGGACAAGG
	reverse	CATGTTGTTTCGGGCACAGT
Fasn	forward	CACCAATACAGATGGCAGCA
	reverse	CCAGCTGGCTGATACAGAGA
Gpx2	forward	CTCAATGAGCTGCAATGTCG
	reverse	GCTGTTCAGGATCTCCTCGT
Nis	forward	AAGTGACCGGGTTGGACATC
	reverse	ATCAGGTTGATCCGGGAATG
Nqo1	forward	TTCAACCCCATCATTTCCAG
	reverse	GCTCAGGCGTCCTTCCTTAT
Ppia	forward	TCAACCCCACCGTGTTCTTC
	reverse	CCAGTGCTCAGAGCTCGAAA
RatSat exon 1-2	forward	CGACAAGGAGGCTAGGAAGA
	reverse	ATCACCACTGCATCCAGCTT

RatSat exon 2-3	forward	GCGGCTGTTGTCATACCTTT
	reverse	CCAAGATAAAACGGCCAATG
RatSat exon 8-9	forward	CCCATCAAGCAAGGATCCAA
	reverse	ATGGGTACCAGCGCAGTCA
Spot14	forward	GAGGTGACGCGGAAATACCA
	reverse	TGTCCAGGTCTCGGGTTGAT
Tbg	forward	AAGAGGGACACATGGAATGG
	reverse	ATTCAACCCATCCTTTCTGC
Tg	forward	TGTGGCCAGCATACACCTTC
	reverse	TGGCGGAGACATGATACCAC
Tpo	forward	CAGCGGTACACACCTTGTGG
	reverse	AGGGTTCACAGTGGGGTTGT
Ttr	forward	CGTACTGGAAGACACTTGGCATT
	reverse	GAGTCGTTGGCTGTGAAAACC
Xbp 1 total	forward	TGAAAAACAGAGTAGCAGCGCAGA
	reverse	CCCAAGCGTGTTCTTAACTC
Xbp1 spliced	forward	GCTGAGTCCGCAGCAGGT
	reverse	CAGGGTCCAACTTGTCCAGAAT
Xbp1 unspliced	forward	CAGACTATGTGCACCTCTGC
	reverse	CAGGGTCCAACTTGTCCAGAAT

Table 7: Primers for genotyping

Cre	forward	AGGTGTAGAGAAGGCACTTAGC
	reverse	CTAATCGCCATCTTCCAGCAGG
olMR7338/7339	forward	CTAGGCCACAGAATTGAAAGATCT
	reverse	GTAGGTGGAAATTCTAGCATCATCC
RetSat	forward	CTCCTTTTCTGAGGCTGGTG
	reverse	AAGGCAGACCTTTCTTTTAAGG

2.6 Equipment

Table 8 lists all of the equipment used in this study.

Table 8: Equipment

Equipment	Supplier
Analytical balance	Sartorius AG (DE)
AU480 chemistry analyzer	Beckman Coulter (DE)
Biofuge 13-R centrifuge	Heraeus (DE)
Biofuge universal 32-R centrifuge	Heraeus (DE)
Bruker minispec liver mice analyzer (LF50)	Bruker Optics, Inc. (USA)
CFX connect real-time PCR detection system	Bio-Rad Laboratories (USA)
Chemidoc imaging system	Bio-Rad Laboratories (USA)
ContourXT glucose meter	Bayer Vital GmbH (DE)
Equipment for polyacrylamide gels	Bio-Rad Laboratories (USA)
Equipment for Western blot	Bio-Rad Laboratories (USA)
FreeStyle precision neo	Abbott Laboratories (USA)
GammaMaster 1277	LKB Wallac (FIN)
Heating plate MR 2002	Heidolph Instruments GmbH & Co. KG (DE)
Luminex 200 system	Luminex Corporation (USA)
TSE LabMaster Indirect Calorimetry System	TSE Systems (DE)
Microm EC-350 tissue embedding Center	Thermo Fisher Scientific Inc. (USA)
Microscope Keyence BZ-9000	Keyence (DE)
Mikrotom Leica 1130	Leica Biosystems Nussloch GmbH (DE)
MiniSpin plus benchtop centrifuge	Eppendorf AG (DE)
NanoDrop ND-1000 spectrophotometer	PEQLAB Biotechnologie GmbH (DE)
RNA ScreenTape System	Agilent Technologies Inc. (USA)
NovaSeq 6000 system	Illumina Inc. (USA)
PTC-200 peltier thermal cycler	Bio-Rad Laboratories (USA)

Restrainer rotating tail injector RTI	Braintree Scientific, Inc. (USA)
Rotamax 120 shaker	Heidolph Instruments GmbH & Co. KG (DE)
Thermomixer comfort	Eppendorf AG (DE)
Thermo Microm HM 325 Rotary Microtome	Thermo Fisher Scientific Inc. (CN)
Vortex genie 2	Scientific Industries, Inc. (USA)
xMark microplate spectrophotometer	Bio-Rad Laboratories (USA)
Zeiss Axioscope 2mot plus	Carl Zeiss (DE)

2.7 Software

All the software used to obtain, analyze, process, and present data is listed in Table 9.

Table 9: Software

Software	Purpose	Supplier
CFX Manager, software Version 3.1	qPCR signal detection	Bio-Rad Laboratories (USA)
EndNote X9, software version 9.3.3	References management	Clarivate Analytics (USA)
GraphPad PRISM 9, software version 9.3.0	Scientific graphing and statistical analysis	GraphPad Software Inc. (USA)
ImageJ, software version 1.53k	Protein signal quantification for Western blot analysis	National Institutes of Health (USA)
Image Lab, software version 6.1.0	Protein signal detection for Western blot	Bio-Rad Laboratories (USA)
Keyence BZ-X analyzer software	Modification of microscope images	Keyence (DE)
Microplate Manager 6, software version 6.2	Measurement of colorimetric signals	Bio-Rad Laboratories (USA)
MS Office 2019	Data processing and presentation	Microsoft Corporation (USA)

ND-1000, software version 3.8.1	RNA quantification	Thermo Fisher Scientific Inc. (USA)
Primer-BLAST	Design tool for primers	https://www.ncbi.nlm.nih.gov/tools/primer-blast/
R-Studio	Analyzing RNA-Seq data	https://www.r-studio.com
R-Project	Analyzing RNA-Seq data	www.r-project.org

3 Methods

3.1 Animal Experiments

3.1.1 Breeding and Housing

Male and female *RetSat* flox mice and *TPO*-Cre mice were housed in the Research Institute for Experimental Medicine (FEM, Charité, Berlin). *RetSat* flox mice were generated in our laboratory by Steffi Heidenreich (127). *TPO*-Cre mice were used in cooperation with Dr. Eva Katrin Wirth (Department of Endocrinology and Metabolic Diseases, Charité, Berlin) and provided by Dr. Shioko Kimura (128). All mice were maintained at 23°C with a 12 h light/dark cycle (light: 6 am to 6 pm). Food and water were provided ad libitum.

Mice were transferred to the animal facility of the Max Rubner Center (MRC) for Cardiovascular Metabolic Renal Research (Charité, Berlin) before the start of the experiments. All experiments were performed under the license numbers G0130/17, T0283/19 and T-CH_0014_21 in accordance with the German Regulations for the Protection of Laboratory Animals (GV-SOLAS).

3.1.2 Generation of Mice with Thyrocyte-specific Knockout of *RetSat*

To generate inducible thyrocyte-specific *RetSat* knockout mice, *RetSat*$^{flox/flox}$ mice were crossed with *TPO*-Cre mice for three generations. The offspring carry either wild-type (wt) or floxed *RetSat* alleles, and *RetSat*$^{flox/flox}$ homozygous mice with or without Cre recombinase are used for experiments.

3.1.3 Genotyping

3.1.3.1 Isolation of Genomic DNA

Genomic DNA was extracted from mouse ear/tail biopsies using Proteinase K solution (0.6 mg/ml) in 100 µl Tailcut Buffer and digested overnight at 55°C. To inactivate Proteinase K, samples were incubated at 95°C for 10 min followed by -20°C for 10 min. After a 1:5 dilution of the samples with TE buffer (containing 1.3 µg/ml RNase A), the sample was used directly for the genotyping PCR.

3.1.3.2 Polymerase Chain Reaction (PCR)

The standard PCR approach (Table 10) was used for all genotyping with the specific primers. The primers used are listed in Table 7. To activate the hot start polymerase, PCR samples were incubated in a thermal cycler at 95°C for 2 min. Then, this was followed by 35 cycles, each consisting of 15 sec at 95°C, 30 sec at an annealing temperature of 60°C and 1 min at 72°C. The PCR samples were then incubated at 72°C for 5 min and cooled to 4°C as shown in Table 11.

Table 10: PCR reaction system for genotyping

Components	Volume
5x PCR master mix	4 µl
10 µM forward primer	0.8 µl
10 µM reverse primer	0.8 µl
DNA template	1 µl
ddH_2O	13.4 µl
total volume	20 µl

Table 11: Standard PCR process for genotyping

Step No.	Temperature	Time
1	95°C	2 min
2	95°C	15 sec
3	60°C	30 sec
4	72°C	1 min
step 2 - 4, x35 cycles		
5	72°C	5 min
6	4°C	∞

For genotyping heterozygous *RetSat* mice with conditional alleles, primers were used whose PCR fragments extended the wt *RetSat* locus by 123 base pair (bp). The extension is due to the presence of loxP (34 bp), the flippase recognition target (Frt) site (34 bp) and the insertion of an additional 55 bp (127). Agarose gel electrophoresis can separate

DNA fragments by length and is therefore used to identify mouse genotypes. 10 µl PCR products were loaded onto a 1% agarose gel, run at 130 volts for 30 min in 1% TAE buffer and photographed using Bio-Rad's ChemiDoc imaging system. This led to the emergence of three potential band distribution patterns: a 416 bp PCR fragment indicating the presence of the wt *RetSat* locus; a 539 bp PCR fragment indicating the presence of a homozygous loxP fragment; and in the case of heterozygosity, two PCR fragments were detected (Figure 7A). Mice carrying the Cre recombinase fragment exhibited discernible bands, while mice lacking the fragment exhibited no observable bands (Figure 7B).

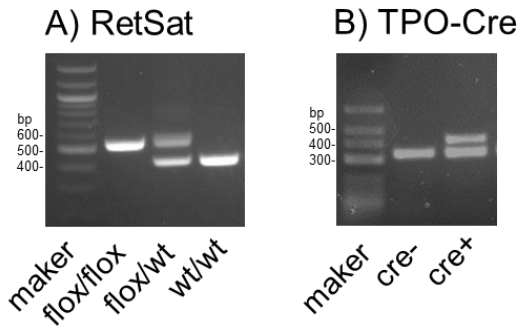

Figure 7: PCR-genotyping of the *RetSat* allele and the *Cre* transgene. (A) flox/flox = homozygous (539 bp), flox/wt = heterozygous, wt/wt= wild-type (416 bp), (B) Cre(+) (412 bp), internal positive control *oIMR7338/7339* (324bp). The sequences of primer pairs used in this study are listed in Table 7.

3.1.4 Intraperitoneal Glucose Tolerance Test (ipGTT)

Mice were fasted for 16 h and each mouse was injected intraperitoneally with a glucose solution at 0.5 g/kg. After glucose injection, blood was collected from the tail vein for glucose measurement at 0 min, 15 min, 30 min, 60 min, 120 min and 180 min using the ContourXT glucose meter.

3.1.5 Intraperitoneal Insulin Tolerance Test (ipITT)

Mice were fasted for 6 h in the morning and each mouse was injected with an insulin solution at 0.75 U/kg. After insulin injection, blood was collected from the tail vein for glucose measurement at 0 min, 15 min, 30 min, 60 min, and 120 min with the ContourXT glucose meter.

3.1.6 Nuclear Magnetic Resonance (NMR) Analysis

The Bruker Minispec Live Mice Analyzer LF50 analyzer was used, which is based on

NMR technology, and the data of fat, free body fluid and lean tissue values of each mouse were obtained after scanning.

3.1.7 Indirect Calorimetry

TSE LabMaster Indirect Calorimetry System was used to measure the metabolism parameters, with each mouse being placed in a single cage with sufficient water and food. The metabolic data were collected for 48 h, such as food and water intake, activity, volume of O_2 and CO_2, energy expenditure and respiratory exchange ratio (RER).

3.1.8 Mouse Sacrifice

Mice were placed in a vial of isoflurane for 1 min, then the blood and organs were collected after confirming that the mice were deeply anesthetized. The whole blood was collected from the heart using a 1 ml needle-tipped syringe. The blood was then incubated at room temperature for 1 h, followed by centrifugation at 3000 rpm, 4°C for 15 min. The resulting serum was transferred to tubes intended for the mouse phenotyping platform, and all samples were immediately stored at -80°C.

3.1.9 Animal Experiment Cohorts

3.1.9.1 Normal Chow Mouse Cohort

Mice were bred with *RetSat*$^{flox/flox}$ and *RetSat*$^{flox/wt}$/*TPO*-Cre(+), genotyped, and *RetSat*$^{flox/flox}$/*TPO*-Cre(-) and *RetSat*$^{flox/flox}$/*TPO*-Cre(+) littermate female and male mice were fed normal chow (ssniff R/M-H, V1534-300, Soest, Germany). All mice were anesthetized with isoflurane and sacrificed at 3, 6 and 15 months. 3-, 6- and 15-month mouse cohorts were performed under the license numbers T0283/19 (approval date 31.10.2019), G0130/17 (approval date 24.10.2018) and T-CH_0014_21 (approval date 25.02.2021), respectively, in accordance with GV-SOLAS guidelines. No further experiments were performed in the 3-month- and 15-month-old mouse groups, and the experimental procedure for the 6-month-old mouse group is shown in Figure 8.

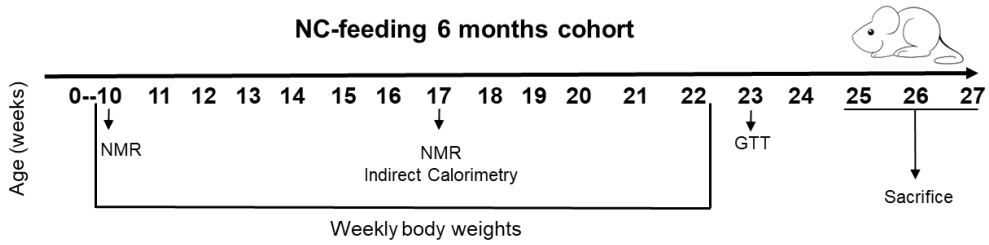

Figure 8: Procedure for normal chow 6-month-old mouse cohort. Female (n=14,19) and male (n=11,9) mice were weighed weekly starting at 10 weeks of age. Their body composition was measured by NMR at 10 and 17 weeks of age and metabolic parameters were measured by the TSE LabMaster Indirect Calorimetry System at 17 weeks of age. Blood and tissue samples were collected when the animals were sacrificed at the end of the experiment.

3.1.9.2 HFD Mouse Cohort

The procedure for the HFD mouse cohort is shown in Figure 9. *RetSat*$^{flox/flox}$/*TPO*-Cre(-) and *RetSat*$^{flox/flox}$/*TPO*-Cre+ littermate male mice were fed a 60% kcal high-fat/high-sucrose diet (HFD, D12492, Research Diets) for 12 weeks and the blood glucose was measured monthly. Body composition was assessed before and after the HFD diet. After 12 weeks of HFD, ipGTT and ipITT were performed, and then the mice were placed in cages of the TSE labmaster indirect calorimetry system to collect data on energy expenditure, calorimetry, food/water intake, and so on (Figure 9). All experiments were performed under the license number G0130/17, which was approved on 24.10.2018.

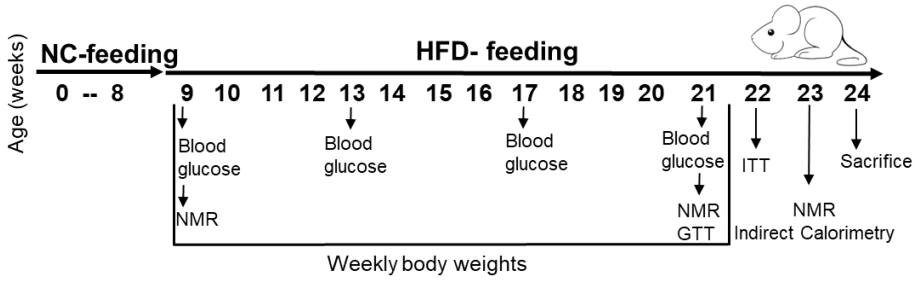

Figure 9: Procedure for the high-fat diet (HFD) mouse cohort. Male mice (n=9,11) were used and administered the experimental manipulations and testing procedures as indicated below the timeline.

3.1.9.3 Hyperthyroidism Mouse Cohort

RetSat$^{flox/flox}$/*TPO*-Cre(-) and *RetSat*$^{flox/flox}$/*TPO*-Cre(+) littermate male mice aged 10-12 weeks were injected intraperitoneally (0.5 µg/g body weight) twice weekly for a total of 6 injections (Figure 10). All experiments were performed under license number G0130/17, approved on 24.11.2020.

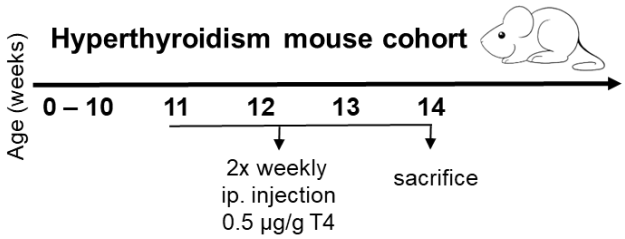

Figure 10: Procedure for the hyperthyroidism mouse cohort. Male mice (n=10,10) were used and administered the experimental manipulations and testing procedures as indicated below the timeline.

3.1.9.4 Hypothyroidism Mouse Cohort

RetSat$^{flox/flox}$/*TPO*-Cre(-) and *RetSat*$^{flox/flox}$/*TPO*-Cre+ littermate male mice of 10-12 weeks old were fed water containing 0.1% methimazole (MMI), 1% perchlorate and 0.3% saccharin for 3 weeks (Figure 11). All experiments were performed under license number G0130/17, approved on 24.11.2020.

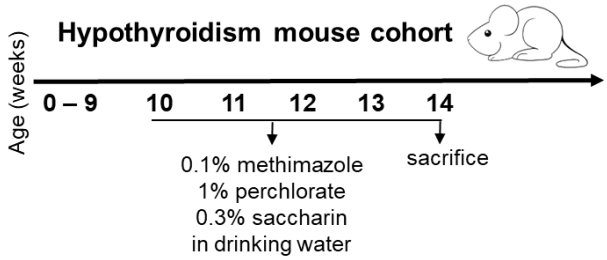

Figure 11: Procedure for the hypothyroidism mouse cohort. Male mice (n=11,9) were used and administered the experimental manipulations and testing procedures as indicated below the timeline.

3.1.9.5 High Iodide Cohort

RetSat$^{flox/flox}$/TPO-Cre(-) and *RetSat*$^{flox/flox}$/TPO-Cre(+) littermate male mice aged 14-16 weeks were given water containing 0.05% sodium iodide (NaI) for 1 week, then the mice were sacrificed under anesthesia (Figure 12). All experiments were performed under license number G0130/17, approved on 28.2.2022.

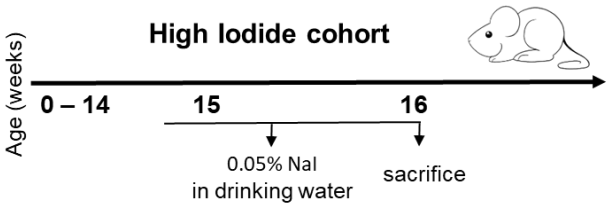

Figure 12: Procedure for the high Iodide mouse cohort. Mice (n=9,10) were used and administered the experimental manipulations and testing procedures as indicated below the timeline.

3.2 Gene Expression Analysis

3.2.1 RNA Isolation from Thyroid Gland

The thyroid gland was completely homogenized by a homogenizer in 350 µl lysis buffer. RNA was then isolated according to the manufacturer's instructions for the VWR peqGold Total RNA Kit. The homogenized liquid was transferred to the filter of the supplied RNA homogenization column and centrifuged at 13000 rpm for 2 min. A volume of 70% ethanol equivalent to the volume of the filtrate was added, thoroughly mixed, and then transferred to the RNA mini-column filter. After centrifugation at 10000 rpm for 1 min, the filter was washed by adding 500 µl of RNA Wash Buffer I and this was followed by centrifugation at 10000 rpm for 30 sec. Subsequently, 500 µl of 80% EtOH was added and centrifuged at 10000 rpm for 1 min, then this step was repeated once. The filter was then dried by centrifugation at 13000 rpm for 2 min, and 30 µl of RNase-free water was added to elute the RNA into a new tube by centrifugation at 13000 rpm for 2 min. The concentration of the RNA samples was measured using a NanoDrop ND-1000 spectrometer and the samples were stored at -80°C.

3.2.2 RNA Sequencing

RNA sequencing library preparation, sequencing and data processing were performed at the BIH Core Facility Genomics, Charité, Berlin. A total of 5 thyroid samples from each genotype (Cre(-) and Cre(+)) were used for RNA sequencing. To remove residual DNA, samples were treated with the RNA Clean & Concentrator Kit. RNA integrity was assessed using the RNA ScreenTape System, and the NEBNext Ultra II RNA Library Prep Kit and Module was used for poly(A) mRNA magnetic isolation. Sequencing was performed on a NovaSeq 6000 system using a paired-end approach, and analysis was performed using R-Studio in conjunction with R-Project. The publicly available DESeq2 package was used with the default parameters to process the mapped counts from FeatureCounts.

3.2.3 Complementary DNA (cDNA) Synthesis

For cDNA synthesis, 500 ng of RNA was diluted to a final volume of 13 µl with RNase-/DNase-free water and mixed with 2 µl of random hexamer primer. After incubation at 70°C for 5 min and cooling to 4°C, 10 µl of the mixture (Table 12) was added to each

sample for cDNA synthesis using reverse transcriptase at 37°C for 60 min, and the cDNA samples were stored at -20°C.

Table 12: Standard PCR procedure for cDNA synthesis

Components	Volume
5x M-MLV Reaction Buffer	5 µl
10 mM dNTPs	1.25 µl
200 U/µl M-MLV Reverse Transcriptase	1 µl
RNase-/DNase-free water	2.75 µl
total volume	10 µl

3.2.4 qPCR

Quantification of transcripts by qPCR. 5 µl of each sample was transferred to a new tube and mixed with water to a total volume of 220 µl, then diluted 1:10 three times, and the samples obtained were used for the standard curve (100%, 10%, 1% and 0.1%).

Primers were designed using the Primer BLAST tool. The reaction system is shown in Table 13. qPCRs were conducted using Sybrgreen PCR MasterMix (Eurogentec, Belgium) on a Bio-Rad CFX96 and a Bio-Rad CFX384 instrument (Table 14). Evaluation of the qPCR results was performed using the standard curve method. In this study, mRNA expression levels were normalized to either the housekeeping gene *Ppia* or *36B4*.

Table 13: Components for qPCR reactions

Components	Volume
2x Fast Start Universal SYBR Green	2.5 µl
5 µM forward primer	0.1 µl
5 µM reverse primer	0.1 µl
cDNA template	2 µl
ddH_2O	0.3 µl

Table 14: Standard qPCR procedure

Steps	Temperature	Time	Cycles
Initial Denaturation	95°C	3 min	1
Denaturation	95°C	15 sec	40
Annealing, Extension	60°C	30 sec	40
Melt curve	70°C	5 sec	1
	95°C	5 sec	

3.3 Protein Analysis

3.3.1 Isolation of Thyroid Protein Samples

Thyroid gland or liver was homogenized in 100 µl of homogenization buffer or lysis buffer using a VWR Cordless Pestle Motor, followed by sonication for 10 sec using a sonicator. The samples were then stored at -20°C for further analysis.

3.3.2 Determination of Protein Concentration

Protein concentration was determined according to protocol of the Pierce BCA Protein Assay Kit (Thermo Scientific, Rockford, USA).

3.3.3 Western Blot Analysis

Based on the measured protein concentration, 15 µg of protein was extracted and mixed with 20 µl of homogenization buffer or lysis buffer. Then, 5 µl of 5x loading buffer containing 12.5% β-mercaptoethanol (β-ME) and 87.5% loading buffer was added to the protein sample. The samples were heated at 95°C for 5 min as protein samples for Western blotting. SDS-PAGE gels formulated for protein separation by molecular weight, and the separating gel and stacking gel preparation methods are shown in Table 15.

Protein samples and markers (ProSieve® Color Protein Marker) were added to the wells of the SDS-PAGE gel and proteins were separated in a Bio-Rad gel electrophoresis chamber using electrophoresis buffer (Table 3). Voltage was set at 80 volts for the stacking gel and 120 volts for the separating gel, and the electrophoresis program was started on the Bio-Rad electrophoresis instrument.

Table 15: Components for SDS-PAGE gels

Reagent	10% Separating gel	Stacking gel
ddH_2O	4.1 ml	3.05 ml
1.5 M Tris-HCl (pH 8.8)	2.5 ml	-
0.5 M Tris-HCl (pH 6.8)	-	1.25 ml
10% SDS	100 µl	50 µl
30% acrylamide	3.3 ml	0.65 ml
10% APS	75 µl	50 µl
TEMED	7.5 µl	6 µl

In Western blotting, the electrophoretically separated proteins were transferred to a membrane by SDS-PAGE and detected by chemiluminescence. Proteins were transferred to a polyvinylidene fluoride (PVDF) membrane using a Bio-Rad wet blotting chamber in a specially prepared cooled transfer buffer (Table 3). The PVDF membrane was first activated in methanol for 1 min and the stacking gel was removed from the SDS gel. All components of the transfer were then assembled according to the sandwich principle: anode-sponge-filter, paper-membrane-gel-filter, paper-sponge-cathode. The proteins were transferred to the PVDF membrane at 80 volts for 2 h or 29 volts overnight.

After transfer blotting, the membrane was incubated in blocking solution for 90 min at room temperature with gentle shaking. The primary antibody was diluted with blocking solution according to its dilution (Table 4) and incubated with the membrane for 90 min at room temperature or overnight at 4°C. Unbound antibodies were removed by washing three times for 10 min at room temperature with TBST buffer. Peroxidase-conjugated secondary antibody (Table 4) was then incubated in blocking buffer for 1 h at room temperature. After washing three times with TBST for 10 min each at room temperature, protein bands were detected using a Thermo Scientific ECL Western blotting substrate solution according to the manufacturer’s instructions. Imaging was performed using x-ray film after an adequate exposure time of 30 sec to 2 h or using the ChemiDoc imaging system from Bio-Rad. Densitometry was performed using ImageJ (129).

3.4 Histology Analysis

3.4.1 Thyroid Paraffin Embedding and Sectioning

(1). Materials: Fresh thyroids were fixed in 4% formaldehyde for more than 24 h and then placed in an embedding cassette.

(2). Dehydration: The dehydration box was placed in the following solutions for dehydration (Table 16).

Table 16: Tissue dehydration

Components	Temperature	Time
70% EtOH	60°C	15 min
96% EtOH	60°C	15 min
100% EtOH	60°C	15 min
Acetone	60°C	15 min
Paraffin 6	65°C	15 min
Paraffin 9	65°C	30 min
Paraffin 9	65°C	20 min

(3). Embedding: The wax-soaked tissue was embedded in an embedding machine. Before the wax solidified, the tissue was removed from the dehydration box and placed in the embedding frame according to the requirements of the embedding surface. Freeze at -20°C. When the wax has set, remove the wax block from the mounting frame and trim the wax block.

(4). Cut: Place the trimmed paraffin block on a paraffin microtome and cut 5 μm thick sections. The sections were floated on the 40°C warm water of the slicer to flatten the tissue, and the tissue was collected with a glass slide and placed in a 60°C oven to bake the sections. After the water has dried and the wax has been baked, it was removed and stored at room temperature.

3.4.2 Hematoxylin-Eosin (H&E) Staining

H&E staining is a staining technique that combines hematoxylin and eosin dyes, where

hematoxylin is a basic dye and eosin is an acidic dye. The hematoxylin staining solution can stain basophilic structures such as the nucleus in a blue-violet color, and eosin can stain basophilic structures such as the cytoplasm, making the morphology of the entire cellular organization clearly visible.

The samples were deparaffinized, hydrated, stained with hematoxylin and eosin and dehydrated according to the steps in Table 17, then mounted on slides and carefully covered with coverslips.

Table 17: H&E staining procedure

Components	Time
Neo-Clear	10 min
Neo-Clear	10 min
Neo-Clear	10 min
100% EtOH	10 min
96% EtOH	2 min
80% EtOH	2 min
70% EtOH	2 min
tap H_2O	2 min
Hematoxylin	5 min
flowing tap H_2O	1 sec
tap H_2O	5 min
Eosin	5 min
under tap H_2O	5 min
EtOH	2 sec
80% EtOH	2 sec
96% EtOH	2 sec
100% EtOH	30 sec
Neo-Clear	5 min

3.4.3 Peroxidase Staining of Paraffin Sections

Immunohistochemical staining of paraffin sections using the biotin-streptavidin-peroxidase method was performed with the Dako Cytomation system according to the manufacturer's instructions.

Briefly, the paraffin was removed with xylene and the sections were rinsed in a descending alcohol series: 2x 5 min xylene, 2x 2 min 100% EtOH, 2x 2 min 96% EtOH, 1x 2 min 70% EtOH, 1x 2 min 40% EtOH, and 2x 5 min ddH_2O. This was followed by heat-induced antigen retrieval to remove aldehyde cross-links that would interfere with epitope antibody recognition by boiling the sections in pre-warmed citrate buffer for 2x 5 min.

To block endogenous peroxidase, the paraffin sections were incubated in 3% H_2O_2 for 10 min followed by washing in 1x PBS for 2x 5 min. Non-specific binding sites were blocked with blocking serum for 30 min at room temperature. During this time, the sections were stored in a humid chamber and covered with foil to prevent individual sections from drying out. Primary antibodies (Table 5) were diluted in the blocking serum. Incubation was performed overnight at 4°C in a humidity chamber. The sections were then washed three times with PBST for 5 min and incubated with the biotinylated secondary antibody for 30 min at room temperature. A further washing step (as above) followed before the paraffin sections were incubated with the streptavidin-HRP complex for 30-60 min at room temperature. After further washing (as above), the signal was visualized using DAB chromogen. The DAB chromogen was diluted 1:50 in DAB buffer just before use and the sections were developed with the diluted DAB chromogen.

The DAB chromogen was incubated for 3 min at room temperature. Staining was observed under the microscope and stopped by transferring the sections to 1x PBS. Tissue sections were then washed in 1x PBS for 2x 5 min. The stained sections were dehydrated through a graded series of alcohols (in reverse order as described above) and mounted in entellane.

3.5 Thyroid Function Analysis

3.5.1 Thyroid Follicle Analysis

To determine the epithelial extension, which is the height of the thyroid epithelium, as well

as the whole follicle, thyrocyte area and colloid-containing area, micrographs of Cre(+) and Cre(-) paraffin sections of the thyroid were analyzed using ImageJ software. The inner and outer circles of the follicles were marked as shown in Figure 13A, the structure of the thyroid follicle is shown in Figure 13B, the epithelial extension and thyrocyte area were calculated according to published procedures (130) as shown in Figure 13C.

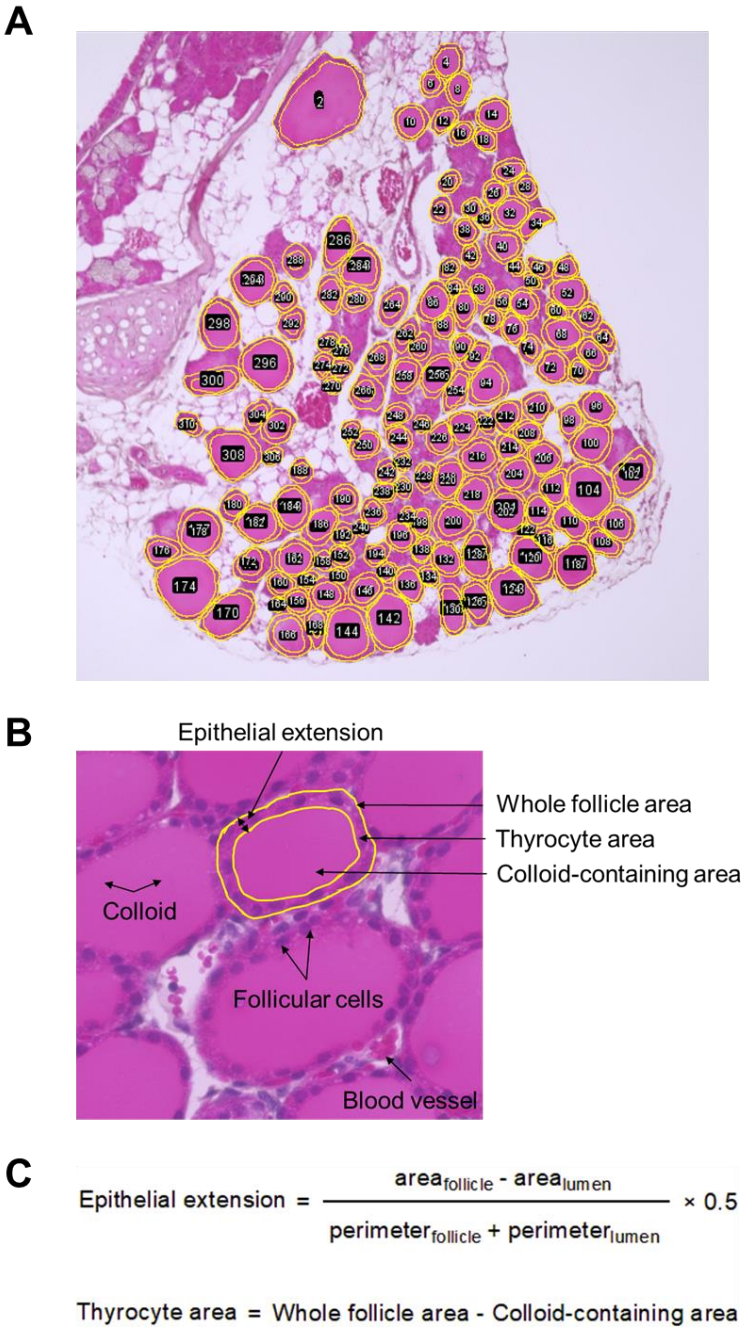

Figure 13: Schematic diagram of thyroid morphology analysis. A) The ImageJ software was used to process sections of the thyroid gland stained with hematoxylin and eosin, B) the inner and outer rings of each follicle were marked, and C) the epithelial extension and thyrocyte area were calculated using these formulas.

3.5.2 TH Measurement

Serum concentrations of total T4 and T3 were measured using radioimmunoassay kits (Total T3 RIA Kit RIA-4534 and Total T4 RIA Kit RIA-4533) from DRG Diagnostics GmbH (DE). The assays were performed following the manufacturer's instructions and previously described methods (131).

3.5.3 TSH Measurement

Serum TSH concentrations were determined using the Milliplex Map Mouse Pituitary Magnetic Bead Kit (MPTMAG-49K; EMD Millipore Corporation, MA, USA) on a Luminex 200 system (Luminex Corporation, ATX, USA) according to the manufacturer's instructions. The lowest detectable concentration was 1.9 pg/ml and the inter-assay variation was < 20% in this assay.

3.5.4 Dio1 Activity Measurement

Dio1 activity assays were performed as described in the literature (132). Liver samples were homogenized in 300 µl homogenization buffer followed by sonication for 10 sec using a sonicator. After centrifugation, the pellet was collected and the protein concentration was determined by BCA assay. 60 µg of liver samples were added to PCR tubes in quadruplicate with or without the addition of propylthiouracil (PTU). Reactions were started by adding 50 µl of MasterMix to obtain the desired final concentration of phosphate buffer (100 mM, 1 mM EDTA, pH 6.8), along with dithiothreitol (DTT, 40 mM) as cofactor and rT3 (10 µM) as substrate. After incubation for 2 h at 37°C with constant shaking, the reaction was stopped by centrifugation at 4°C. The reaction mixture was centrifuged, 75 µl of the supernatant was applied to a Dowex W50-X2 packed microtiter column, and the released iodide was eluted by adding 100 µl of 10% acetic acid (132). 12.5 µl of the eluted sample was mixed with 37.5 µl of 10% acetic acid, it was added to a microtiter plate, and the reaction was initiated by the addition of cerium solution (25 mM $(NH_4)_4Ce(SO_4)_4$ and 0.5 M H_2SO_4) and arsenite solution (25 mM $NaAsO_2$, 0.8 M NaCl and 0.5 M H_2SO_4), which was measured in a Sandell-Kolthoff reaction after further dilution (132, 133). Changes in absorbance (OD, at 416 nm) were determined at the start of the reaction and after 20 min, and absolute activity was estimated by interpolation from individually measured iodide standard curves (132).

3.6 Lipid Metabolism Detection

3.6.1 Quantitative Analysis of Non-Esterified Fatty Acids

Quantitative determination of NEFA levels in mouse serum was carried out with the enzymatic colorimetric technique using the NEFA (HR2) kit. NEFA was converted to acetyl-CoA by acyl-CoA synthase and then oxidized to 2,3-*trans*-enoyl-CoA and hydrogen peroxide by acyl-CoA oxidase. The enzymatic action of the peroxidase produced a blue/violet product which could be measured using a photometer. In a flat-bottomed 96-well plate, 5 µl of each standard and sample were added in duplicate and mix with 150 µl of Reagent R1. The plate was incubated at 37°C for 10 min. Then, 75 µl of Reagent R2 was added to each well and incubated for an additional 10 min at 37°C. After incubation, the samples and standard curves were measured using a photometer at a wavelength of 546 nm and calculate the sample concentrations accordingly.

3.6.2 Quantitative Analysis of Triglycerides

Quantitative determination of triglycerides in mouse serum and liver was carried out with a colorimetric enzymatic method using the DiaSys Triglyceride FS kit. 600 µl KOH was added to a weighed 50 mg of liver and incubated at 60°C for 5-6 h or until the tissue was completely digested. 500 µl of digested sample was added to 540 µl of 1 M $MgCl_2$ and mixed well. After incubation on ice for 10 min, the mixture was centrifuged at maximum speed for 30 min, and the supernatant was used as a sample for detection.

The activity of glycerol-3-phosphate oxidase produces a product that can be quantified photometrically. Therefore, 200 µl of the supplied reagents were added to 5 µl of standards and samples in a flat-bottomed 96-well plate and incubated at 37°C for 10 min before measuring the absorbance at a wavelength of 500 nm using a photometer. According to the standard curve obtained, the absorbance was correlated with the triglyceride concentration and used to calculate the concentration of the samples.

3.7 Statistical Analysis

The statistical tests used in this study are described in the figure legends. Data from animal experiments were presented as means and the standard error of the mean (SEM) was calculated. The animal experiments were neither randomized nor blinded to the

experimental conditions. For the analysis of single measurements from two independent groups, either Student’s t-test or the Mann-Whitney test was employed. In the case of repeated measurements from two groups, a two-way analysis of variance (ANOVA) with Šídák multiple comparison test was utilized. In situations involving single measurements from three groups, a one-way ANOVA with Dunnett’s multiple comparisons test was used. The Chi-squared test was used to evaluate differences in birth rates between mice of different genotypes. The Bonferroni correction was applied to the proteomics and RNA sequencing analyses to minimize the false discovery rate. The Grubb’s test was used to identify outliers in the data. All statistical analyses were performed using GraphPad Prism software.

4 Results

4.1 RetSat Shows High Expression in the Thyroid and is Regulated by Hypothyroidism and Iodide Overload in Mice

Tissue expression analysis revealed distinct patterns for RetSat and TPO in C57BL/6J mice. *Tpo* mRNA showed robust expression specifically in the thyroid, while being barely detectable in the liver and spleen (Ct > 35 cycles) (Figure 14A). Conversely, the liver demonstrated the highest levels of *RetSat* expression, whereas the spleen exhibited minimal expression. Notably, *RetSat* mRNA expression in the thyroid was 20% of its expression in the liver (Figure 14A). Furthermore, protein expression levels of RetSat in both the liver and thyroid paralleled their respective mRNA levels (Figure 14B). As is the case in humans (Figure 6B), immunostaining confirmed that RetSat protein was localized to thyrocytes in mice (Figure 14C). Notably, there was a gender-based disparity in thyroid *RetSat* mRNA expression, with male mice exhibiting higher levels compared to female mice of the same age (Figure 14D). To investigate the regulation of thyroid *RetSat* mRNA, male mice were subjected to various interventions to induce hyperthyroidism or hypothyroidism. Specifically, they were either repeatedly injected with T4 or treated with 0.1% MMI and 1% perchlorate in their drinking water. Upon comparison with untreated euthyroid mice of similar age, the expected TSH-dependent regulation pattern in the expression of *Tpo* and *Nis* was observed (Figure 14E). Conversely, thyroid expression of *RetSat* remained unchanged in hyperthyroid mice but showed a significant increase in hypothyroid mice (Figure 14E). Administration of iodide in drinking water leads to an increase in TSH levels and a decrease in serum T4 in mice (134), while a 7-day supplementation experiment with 0.05% NaI showed reduced *RetSat* expression levels in the thyroid (Figure 14F). NFE2-related transcription factor 2 (*Nrf2*) knockout did not affect *RetSat* expression or the iodide-induced downregulation of *RetSat* in another cohort of wt mice (Figure 14G). It is important to note that this model of iodide overload inhibits TG iodination, known as the Wolff-Chaikoff effect (135).

Taken together, these findings underscore the strong expression of *RetSat* in the mouse thyroid, with sex differences in expression levels. *RetSat* expression is induced by hypothyroidism and reduced by iodide overload, suggesting a functional role for RetSat in thyroid physiology.

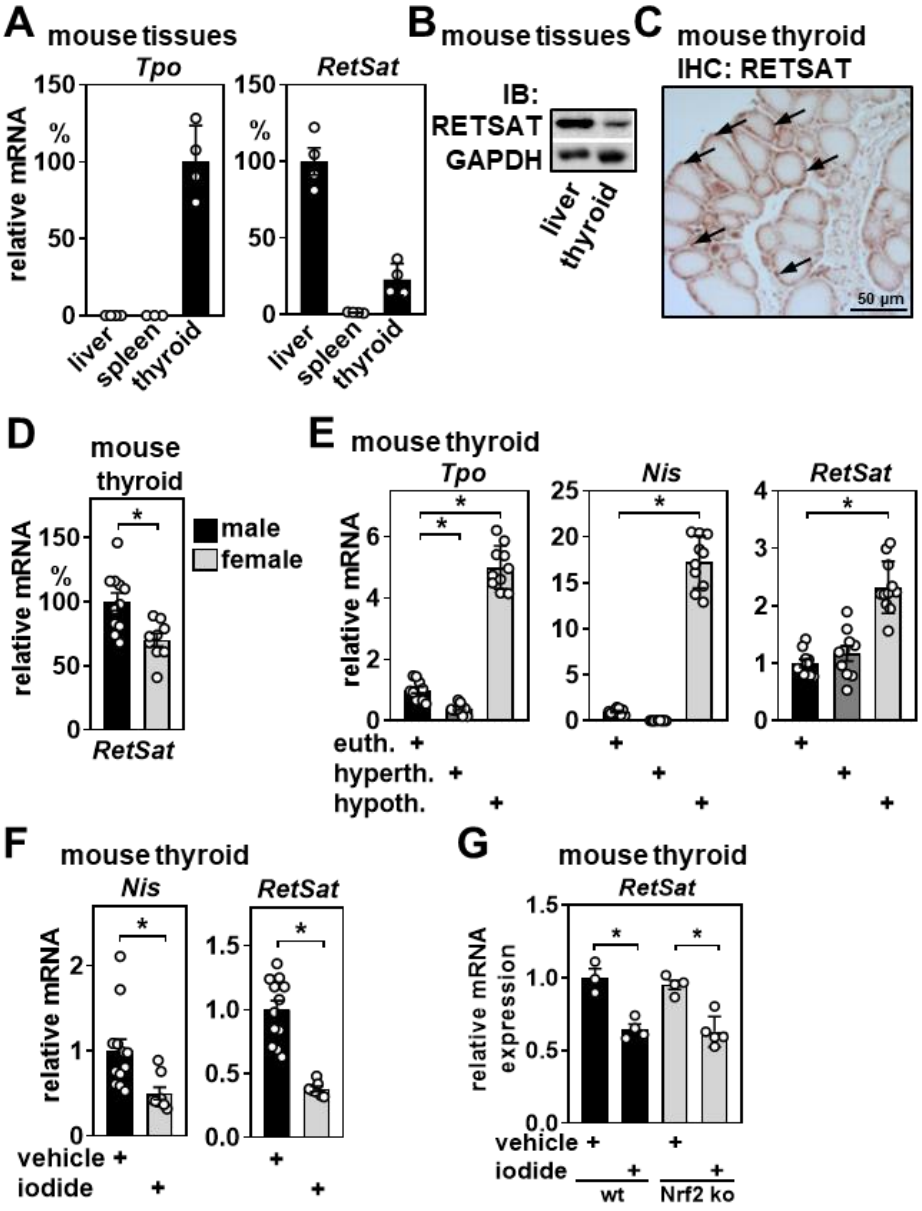

Figure 14: RetSat is highly expressed in the thyroid and regulated by hypothyroidism and iodide overload in mice. A) mRNA expression of thyrocyte-specific *Tpo* and of *RetSat* in liver, spleen, and thyroid was analyzed in male mice (n=4) by qPCR. B) Protein expression of RetSat was determined in male mice by immunoblotting. GAPDH served as loading control. C) RetSat protein was stained by immunohistochemistry in sections of murine thyroid gland, showing predominantly thyrocyte localization. D) Thyroid *RetSat* mRNA expression in 3-month-old male and female mice (n=11,9). E) Thyroid expression of indicated genes in eu-, hyper- and hypothyroid male mice (n=11,10,11) was analyzed by qPCR. F) Male mice (n=12,8) were supplemented with or without 0.05% sodium iodide in drinking water for 1 week and *Nis* and *RetSat* mRNA expression in the thyroid was determined by qPCR. G) Male wild-type (wt) or *Nrf2* knockout (ko) mice (n=3,4,4,5) were supplemented with vehicle or iodide for 1 week and *RetSat* mRNA expression in the thyroid was determined by RNA sequencing. Data are presented as individual data points and mean±SEM, analyzed using a Student's t-test (D, F(*RetSat*)), one-way ANOVA (E) and Mann-Whitney test (F(*Nis*)), **P*<0.05.

4.2 Establishment of Mouse Model with Thyrocyte-specific Deletion of *RetSat*

To investigate the role of RetSat in the thyroid, experiments were conducted in mice with targeted deletion of the *RetSat* gene specifically in thyrocytes. A previously generated mouse model with a floxed *RetSat* allele, encompassing exons 2 and 3 from a KOMP CSD (Retsattm1a (KOMP) Wtsi, ID: 27845), was utilized in conjunction with flippase-expressing mice for recombination to the floxed allele. The resulting mice were then backcrossed to C57BL/6J mice over six generations (127). Previous studies have demonstrated that deletion of specific amino acids within this motif leads to a lack of enzyme activity (89).

The mice carrying the floxed *RetSat* allele were bred with mice expressing Cre recombinase under the control of the human *TPO* promoter (128). Deletion of exons 2 and 3 is predicted to cause a frameshift and premature stop codon, resulting in a truncated protein (Figure 15A). Genotyping confirmed the presence of the wt and floxed *RetSat* alleles, establishing flox/flox homozygous mice for subsequent experiments (Figure 15B). *Cre* expression was specifically detected in the thyroid of Cre(+) mice expressing Cre recombinase (Figure 15C). The recombinant alleles lacked the dinucleotide binding motifs encoded by exons 2 and 3, which are crucial for the NADH/NADPH or FADH cofactors. Using qPCR primers to amplify the excised transcribed region, an approximately 70% reduction in *RetSat* mRNA expression was observed in female mice, regardless of whether the amplified exon regions were deleted by recombination or not (Figure 15D and Figure 14G), suggesting that the truncated transcript is unstable. Knockout efficiency was comparable in female (Figure 15D) and male (Figure 15E) mice. The analysis of RetSat protein expression was conducted through Western blotting (Figure 15F), densitometry (Figure 15G), and employing antibodies targeting the C-terminal epitope of the protein (89). The expression levels of RetSat protein in the thyroid glands of Cre(+) mice showed an approximately 80% reduction compared to Cre(-) mice (Figure 15F/G). This observation was further validated through immunohistochemistry results, as depicted in Figure 15H. These findings confirm the specific deletion of *RetSat* in thyrocytes in the established genetic mouse model.

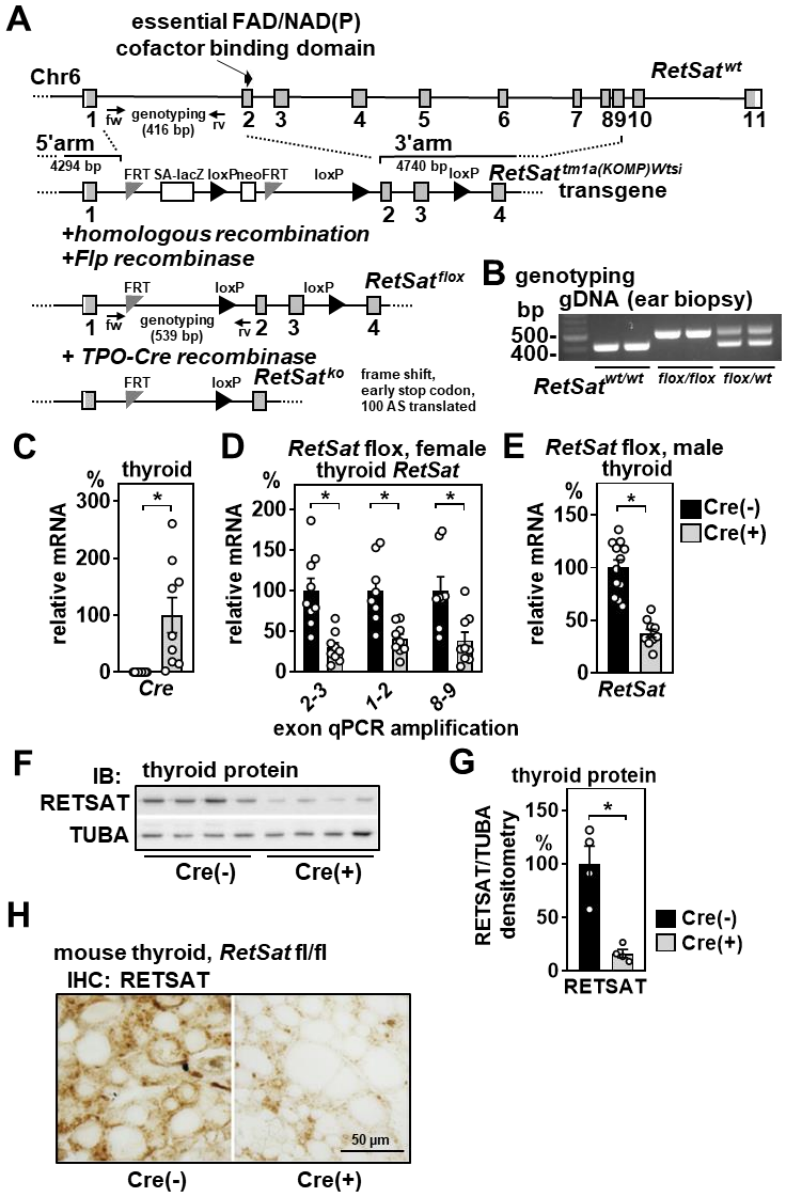

Figure 15: Generation and validation of thyrocyte-specific *RetSat* deletion in mice. Schematic view of the knockout strategy with the *RetSat* gene locus on top and the *RetSat* $^{tm1a(KOMP)Wtsi}$ construct used for homologous recombination shown below. After recombination and flippase (Flp)-mediated excision of the neo cassette, mice with floxed *RetSat* alleles were crossed with *TPO*-Cre expressing mice to induce thyrocyte-specific deletion of *RetSat*, lacking exons that encode a cofactor binding domain essential for its activity. B) Genotyping of wt- and floxed *RetSat* alleles yielding the expected amplification products depicted in A). Expression of C) Cre, D) *RetSat* mRNA amplifying parts of deleted (exons 2 and 3) and (exons 1 and 2) or undeleted (exons 8 and 9) regions of the transcript in female mouse thyroid (n=9,9). E) Expression of *RetSat* mRNA in male mouse thyroid (n=12,10). F) Protein in total thyroid of three-month-old Cre(-) and (+) female mice was determined by immunoblotting. TUBA served as loading control for the densitometric analysis of RetSat protein shown in G). H) RetSat immunohistochemistry of thyroid sections from Cre(-) and (+) mice. Data are presented as individual data points and mean±SEM, analyzed using a Student's t-test, **P*<0.05.

In the present investigation, a breeding experiment was conducted using two different genotypes of mice, denoted as *RetSat*$^{flox/flox}$/*TPO*-Cre(-) and *RetSat*$^{flox/wt}$/*TPO*-Cre(+). These genotypes were crossed to produce offspring with four different genotypes: *RetSat*$^{flox/flox}$/*TPO*-Cre(-), *RetSat*$^{flox/flox}$/*TPO*-Cre(+), *RetSat*$^{flox/wt}$/*TPO*-Cre(-), and *RetSat*$^{flox/wt}$/*TPO*-Cre(+).

Subsequent to genetic identification, a quantitative assessment of the population size for each genotype was performed. The birth rates for each genotype, along with the corresponding sample sizes, are presented in Table 18. The obtained data were subjected to analysis utilizing the Chi-squared test statistics. The results showed a decreasing trend in the birth rate of mice within the *RetSat*$^{flox/flox}$/*TPO*-Cre(+) group compared to the *RetSat*$^{flox/flox}$/*TPO*-Cre(-) group. Conversely, no striking difference was observed between the *RetSat*$^{flox/wt}$/*TPO*-Cre(-) and *RetSat*$^{flox/wt}$/*TPO*-Cre(+) groups. However, subsequent statistical analysis did not reveal a statistically significant difference. These results indicate that the effect of the thyrocyte-specific *RetSat* knockout on the birth rate of mice in this particular study did not reach a level of statistical significance.

Table 18: Chi-squared test analysis for genotype-phenotype correlations

genotyping (1034 animals)	Observed no. (%)	Expected no. (%)
RetSat$^{flox/flox}$/*TPO*-Cre(-)	283 (27%)	258.5 (25%)
RetSat$^{flox/flox}$/*TPO*-Cre(+)	239 (23%)	258.5 (25%)
RetSat$^{flox/wt}$/*TPO*-Cre(-)	257 (25%)	258.5 (25%)
RetSat$^{flox/wt}$/*TPO*-Cre(+)	255 (25%)	258.5 (25%)
Chi-squared test	χ^2=3.849	P=0.2782

4.3 Thyrocyte-specific Deletion of *RetSat* Increases TSH and Reduces Weight Gain in Female Mice

To investigate the role of *RetSat* in the thyroid, male and female mice were separated and divided into three age groups (3 months, 6 months and 15 months) and fed the normal diet. Female mice with thyrocyte-specific deletion of RetSat showed normal thyroid morphology in H&E staining, as shown in Figure 16A. Serum T3 and T4 levels were not different between the two groups, but interestingly, serum TSH levels were higher in

female Cre(+) mice than in Cre(-) mice, as shown in Figure 16B.

As shown in Figure 16C, all mice gained weight with age, but it is worth noting that 15-month-old female Cre(+) mice were lighter and gained weight more slowly than the control group. Body composition analysis revealed that Cre(+) mice had less fat mass than Cre(-) mice, but there was no significant difference in lean mass and free fluid, as shown in Figure 16D.

In the fed state, the blood glucose levels of the two groups of mice showed no significant difference, but Cre(+) mice had lower blood glucose levels than the control group, as shown in Figure 16E.

Heart weight was measured and divided by body weight, as heart weight is sensitive to TH levels (3), and no difference was observed between the two groups, as shown in Figure 16F. Interestingly, female Cre(+) mice were more active and consumed more food during the dark period than Cre(-) mice, as shown in Figure 16G/H. Energy expenditure in the Cre(+) group showed a slight increase during the day and at night, although the change was not statistically significant (Figure 16I). Surprisingly, the majority of observed metabolic changes indicated an increase in TH action in Cre(+) females, in contrast to unchanged circulating levels of T3 and T4. These results suggest that *RetSat* plays a role in regulating the HPT axis, mouse body composition, activity and food intake levels in female mice, with potential implications for metabolic disorders and thyroid function.

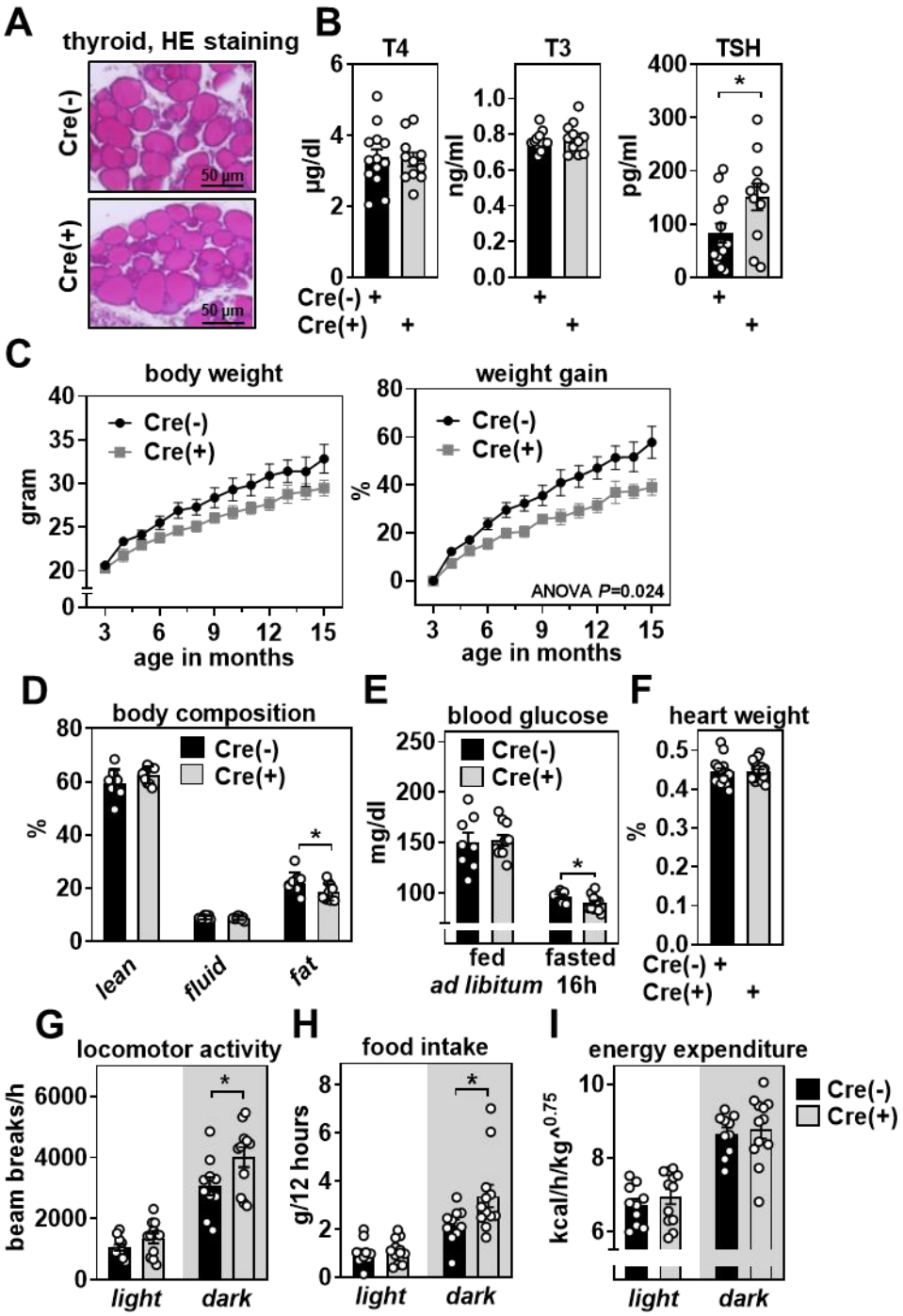

Figure 16: Deletion of *RetSat* in the thyroid of female mice increases TSH and reduces weight gain. A) Thyroids of 3-month-old mice of the indicated genotypes were stained by hematoxylin and eosin (H&E). B) Circulating thyroid hormone and thyroid-stimulating hormone (TSH) concentrations of mice (n=13,11) described in A). C) Body weight and body weight gain of mice (n=9,10) with the indicated genotypes. D) Body composition of 15-month-old Cre(+) and Cre(-) mice (n=9,10). E) Blood glucose levels of 6-month-old Cre(+) and Cre(-) mice (n=8,10). F) Relative heart weight of 6-month-old mice (n=14,19). G) Locomotor activity, H) food intake and I) energy expenditure during the light and dark phase of 6-month-old mice (n=10,12). Data are presented as single data points and mean±SEM, analyzed using a Student's t-test (B, D, E, F, G, H, I) or two-way ANOVA (C), **P*<0.05.

4.4 Thyrocyte-specific Deletion of *RetSat* does not Affect HPT Axis or Weight Gain in Male Mice

Given the established sex-specific responses of mice to alterations in the HPT axis (136), separate analyses were performed for female and male mice in the Cre(-) and Cre(+) groups. Male mice were divided into three groups according to age (3 months, 6 months and 15 months) and fed a normal diet like the female mice. Serum hormone and TSH levels showed no significant differences between Cre(+) and Cre(-) mice, as shown in Figure 17A. Although male mice gained weight with age, *RetSat* had no effect on body weight or body composition, as shown in Figure 17B/C, respectively. In addition, there were no significant differences in fed and fasting blood glucose levels between the two groups (Figure 17D). The male mice, similarly to the female mice, did not show any changes in heart weight (Figure 17E). However, it is worth noting that the male Cre(+) mice showed less activity than the Cre(-) mice, especially during the dark period (Figure 17F). The food intake results showed no difference between light and dark (Figure 17G). Consequently, following thyrocyte-specific depletion of *RetSat*, sex-specific differences in thyroid homeostasis and metabolic phenotypes were observed, rendering female mice more susceptible to functional impairment.

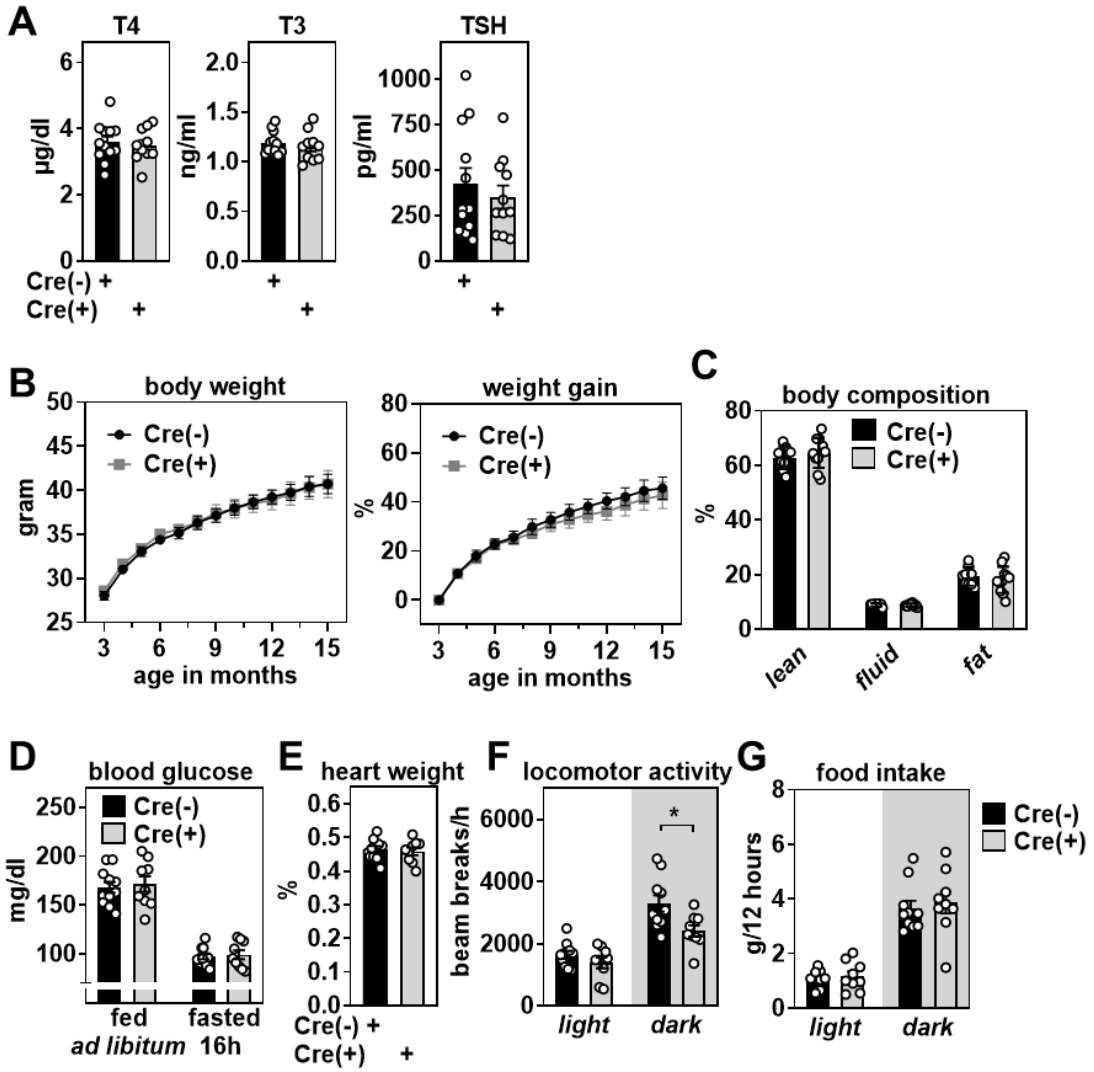

Figure 17: Deletion of *RetSat* in thyroids of male mice does not affect TSH or weight gain. A) Circulating thyroid hormone and thyroid-stimulated hormone (TSH) concentrations of 3-month-old male mice (n=12,10). B) Body weights and body weight gain in mice (n=9,11). with the indicated genotypes. C) Body composition of 15-month-old Cre(+) and Cre(-) mice (n=9,11). D) Blood glucose levels of 6-month-old Cre(+) and Cre(-) mice (n=11,9). E) Relative heart weight of 6-month-old mice (n=11,9). F) Locomotor activity and G) food intake during the light and dark phase of 6-month-old mice (n=10,9). Data are presented as individual data points and mean±SEM, analyzed using a Student's t-test (A, C, D, E, F, G) or two-way ANOVA (B), **P*<0.05.

4.5 Thyrocyte-specific Deletion of *RetSat* Leads to Increased TSH, Weight Gain and Altered Thyroid Morphology on HFD Challenge

Diet-induced obesity is on the rise around the world. Imbalances between energy intake, storage and expenditure play a critical role in diet-induced obesity. TH is a key regulator of energy metabolism, which regulates glucose and lipid metabolism. In contrast to female C57BL/6J mice, their male counterparts show a rapid increase in body weight and fat

mass when subjected to an HFD (137). To investigate the influence of metabolic challenge on *RetSat* thyrocyte-specific knockout mice, male mice were fed an HFD for 12 weeks. In spite of the weekly weight gain observed during the experimental period, the deletion of *RetSat* had no discernible impact on overall body weight, as depicted in Figure 18A. Following the dietary challenge, it was observed that male mice in the Cre(+) group exhibited a tendency towards higher serum T3 levels in comparison to their Cre(-) counterparts. However, no significant disparity in T4 levels was observed between the two groups. Figure 18B clearly shows that the Cre(+) mice had significantly higher TSH levels than the Cre(-) mice. As shown in Figure 18C, body composition analysis revealed that Cre(-) and Cre(+) mice exhibited similar proportions of lean body mass, body fluid mass, and fat mass. In addition, Figure 18D shows that Cre(+) mice had heavier hearts than Cre(-) mice. Additionally, it was observed that Cre(+) mice displayed greater activity during the dark period, as presented in Figure 18E. However, both groups of mice consumed similar amounts of food during both the light and dark periods, as evidenced by the data shown in Figure 18F. Taken together, male mice exhibited elevated TSH concentrations, increased body weight gain, and increased heart weight specifically in response to the additional stressor of the HFD on the HPT axis.

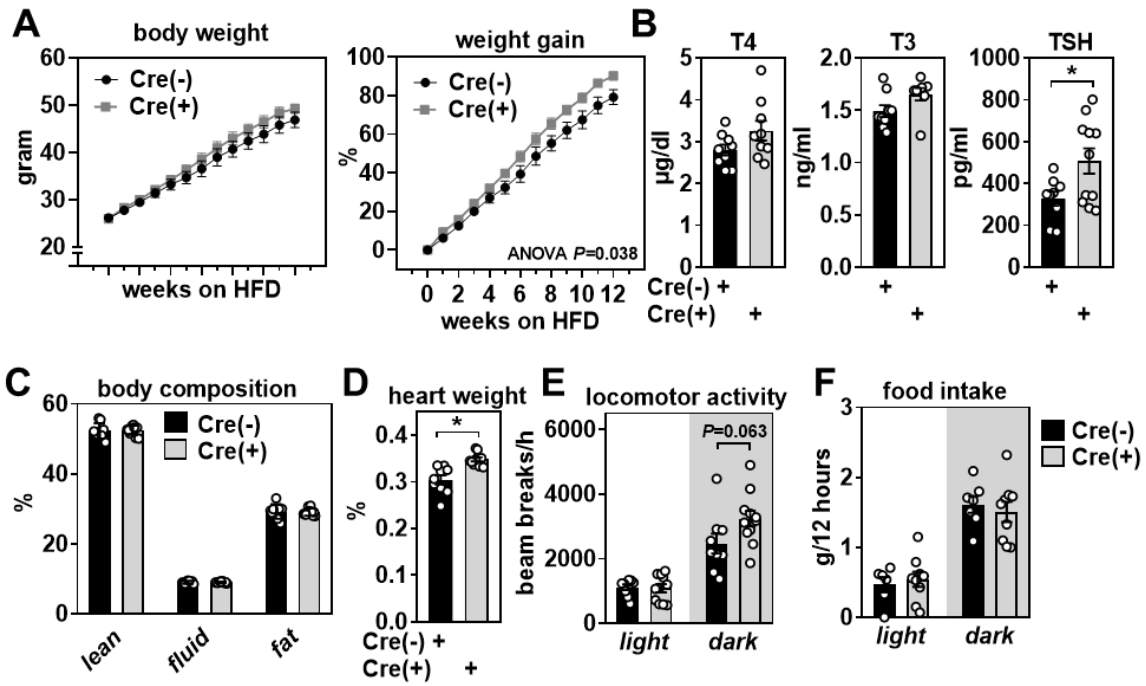

Figure 18: Deletion of *RetSat* in the thyroid of male mice increases TSH and weight gain upon high-fat diet feeding. A) Male mice of the indicated genotypes were fed a high-fat diet for 12 weeks, starting at 8 weeks of age, and body weight and weight gain were determined (n=9,11). B) Circulating thyroid hormone and thyroid-stimulated hormone (TSH) concentrations of mice (n

=9,11) after HFD feeding. C) Body composition of mice fed HFD. D) Relative heart weight of HFD-fed mice (n=9,11). E) Locomotor activity (n=9,11) and F) food intake (n=7,9) during the light and dark phase of HFD-fed mice. Data are presented as individual data points and mean±SEM, analyzed using a two-way ANOVA (A), Student's t-test (B (T4 and TSH), C, D,E, F) or Mann-Whitney test (B (T3)), *P<0.05.

Morphological changes in the thyroid gland are a reliable indicator of HPT axis dysfunction (138). Previous literature has shown that elevated TSH levels increase both the size and number of follicular cells (139). To investigate morphological changes in the thyroid gland, the glands were removed and subjected to H&E staining. The changes were observed under a light microscope and analyzed using ImageJ software (Figure 19A). Fat dispersion within the thyroid gland was observed in both genotypes, which may be due to the consumption of the HFD. TSH is the main trophic factor of the thyroid gland through its TSHR (25, 26). Compared to the thyroid gland of Cre(-) mice, the follicular epithelial cells of Cre(+) mice showed significant hypertrophy, with an increase in follicular lumen size, area and the thickness of follicular epithelial cells (Figure 19B/C/E); the distribution of areas containing colloids (Figure 19D) was not affected. These morphological changes suggest a higher level of thyrocyte activity in Cre(+) mice than in Cre(-) mice, which is consistent with the increased TSH levels in Cre(+) mice.

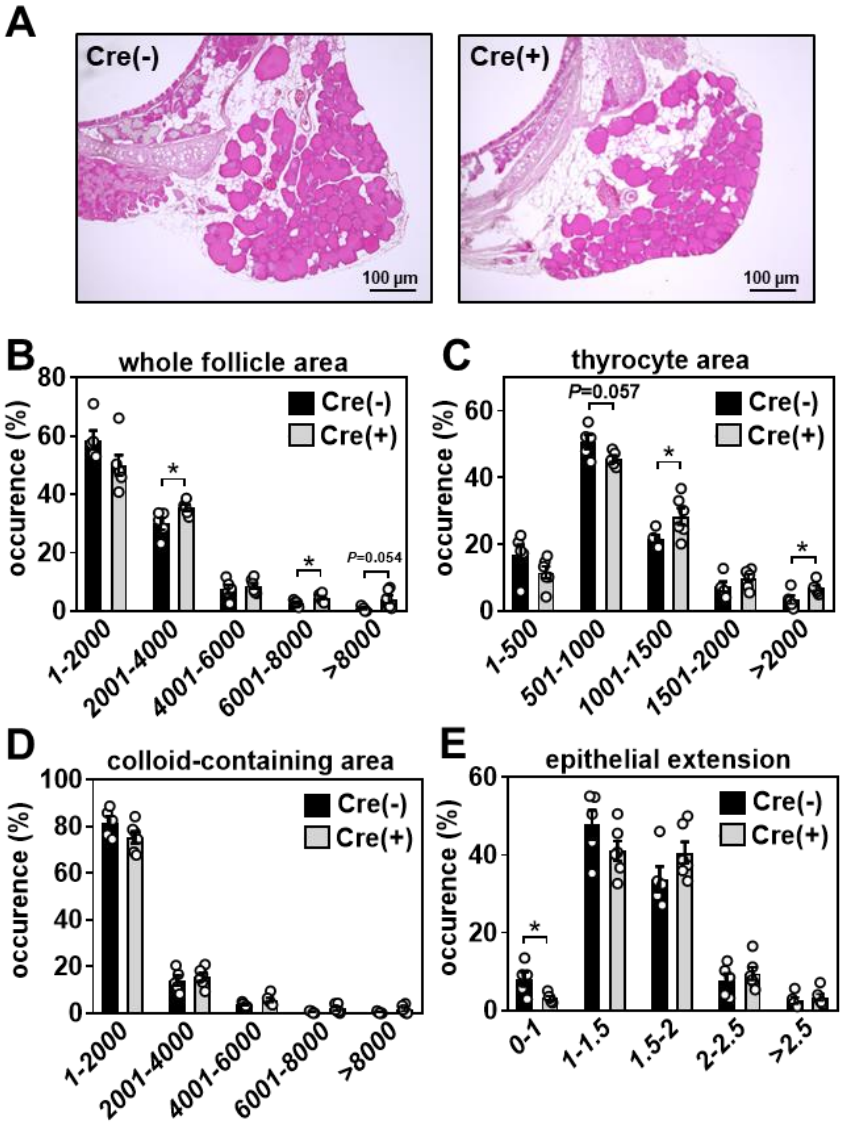

Figure 19: Deletion of *RetSat* in the thyroid of male mice alters thyroid morphology. A) Male mice (n=5,6) of the indicated genotypes were fed a high-fat diet for 12 weeks, starting at 8 weeks of age, and the thyroid gland morphology was analyzed. B) Whole follicle, C) Thyrocyte area, D) Colloid-containing area distribution, and E) epithelial extension in Cre(-) and Cre(+) mice. Data are presented as individual data points and mean±SEM, analyzed using a Student's t-test, **P*<0.05.

To investigate the transcriptional consequences of *RetSat* deletion in HFD-fed mice, thyroid gene expression was profiled by RNA sequencing (RNAseq). The analysis revealed that apart from reduced *RetSat* mRNA levels, only a few transcripts showed significant changes (false discovery rate (FDR) 5%). Among these transcripts, *Pcdhgc4* (a protocadherin), *Gtf2a1* (a transcription factor subunit), and *Spdef* (a transcription factor) showed more than 1.5-fold regulation (Figure 20A). These genes are not pseudogenes, but their specific functions in the thyroid have not been reported. To further explore

potential subtle regulations, the expression of canonical RAR target genes was visualized using a heat map (Figure 20B), which included *Cyp26a1*, *Cyp26b1*, *Lrat*, *Rarb*, *Rbp1*, *Smad3*, and *Stra6* (140-144). These target genes are known to be induced by all-*trans* retinoic acid (atRA), but there was no evidence of altered atRA responses in the thyroids of Cre(+) mice. Since RetSat is known to be an ER-associated protein (86, 89), the researchers investigated whether its deletion could induce ER stress in the thyroids of HFD-fed mice. However, analysis showed that there was no increase in the ratio of spliced (s) to unspliced (u) X-box binding protein 1 (*Xbp1*) transcripts (Figure 20C). This ratio serves as a highly sensitive marker of the unfolded protein response (UPR) in the ER, but no signs of dysregulated atRA signaling or ER stress were observed in HFD-fed mice due to *RetSat* deletion in the thyroid. In conclusion, deletion of *RetSat* in the thyroid of HFD-fed mice had limited transcriptional effects and did not appear to cause major dysregulation of atRA signaling or induce ER stress.

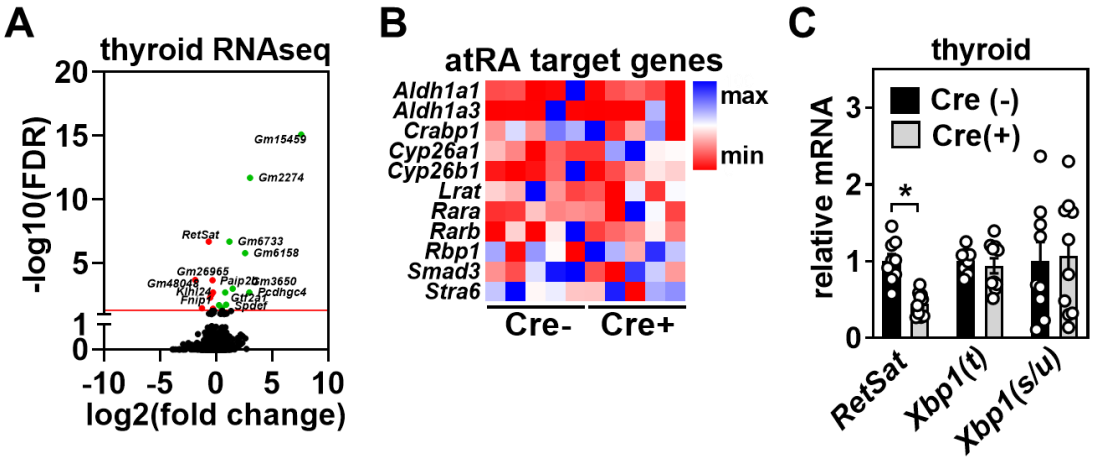

Figure 20: Deletion of *RetSat* in the thyroid of high-fat diet fed male mice has no major transcriptional effects. A) Significantly (FDR 5%) upregulated (green dots) and downregulated (red dots) genes in thyroids of Cre(+) mice (n=5,5). B) Expression heatmap of known RAR target genes in thyroids of Cre(-) and Cre(+) mice (n=5,5). C) Expression of *RetSat* and total/spliced/unspliced (t/s/u) *Xbp1* in thyroids of indicated mice (n=9,10). Data are presented as individual data points and mean±SEM, analyzed using a Student's t-test, **P*<0.05.

To investigate whether RetSat deficiency has an effect on blood glucose levels under an HFD, this study measured blood glucose levels in mice before feeding and after 16 h of fasting. The results showed no significant difference in blood glucose levels between male Cre(+) and Cre(-) mice before feeding and in the fasting state, as shown in Figure 21A. To investigate the effect of RetSat deficiency in the thyroid on glucose and insulin

tolerance, the ipGTT and ipITT were performed. After glucose injection, there was no significant change in blood glucose levels and no difference in the area under the curve between the two groups of mice, as shown in Figure 21B/C. *RetSat* deletion in the thyroid also caused no change in blood glucose levels compared to the insulin injected control group, as shown in Figure 21D/E. The findings indicate that deficiency of RetSat in the thyroid does not lead to a noteworthy impact on glucose and insulin tolerance in these mice.

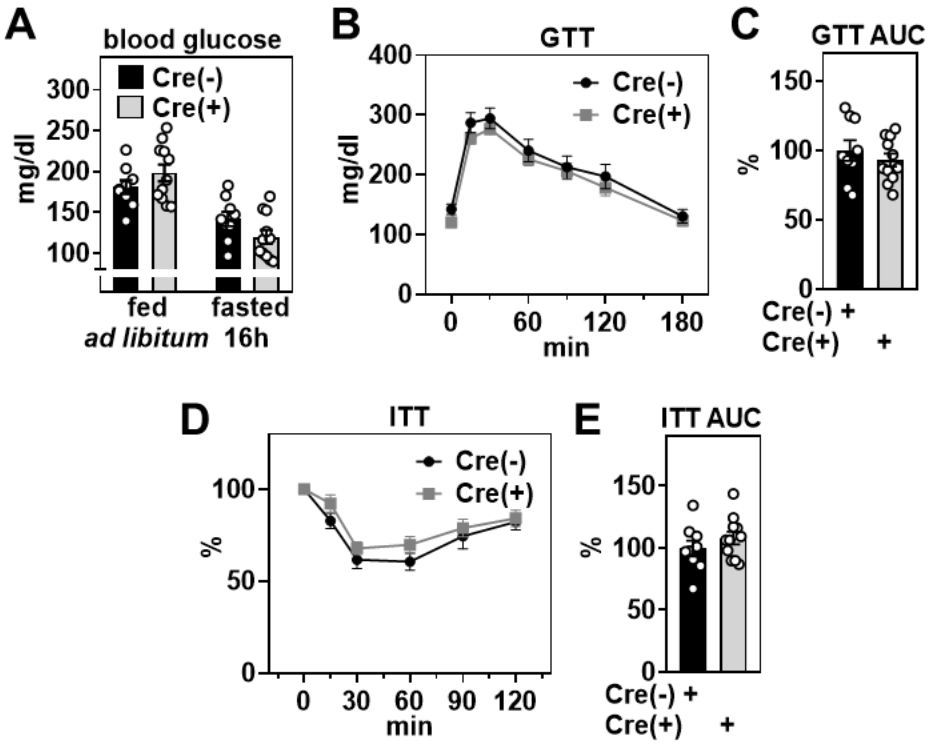

Figure 21: Deletion of *RetSat* in thyroids of male mice has no effect on blood glucose, glucose tolerance and insulin response in mice fed a high-fat diet. A) Male mice (n=9,11) of the indicated genotypes were fed a high-fat diet (HFD, 60% kcal fat) for 12 weeks, starting at 8 weeks of age, and *ad libitum* and fasted blood glucose were determined. B) Glucose tolerance, C) insulin responses, and D) and E) the corresponding area under the curve (AUC) calculations of HFD-fed mice (n=9,11). Data are presented as individual data points and mean±SEM, analyzed using a Student's t-test (A, C, E) or two-way ANOVA (B, D).

To further investigate the effects of *RetSat*-specific deletion in the thyroid under HFD conditions, this study examined lipid metabolism in mice. First, the expression of relevant genes in the liver was examined. Dio1 catalyzes the deiodination of T4, T3, and rT3 and can activate and inactivate TH; its expression and activity are important for studying the effects of TH on the liver (145). As shown in Figure 22A/B, the specific absence of RetSat

in the thyroid gland had no significant effect on the expression and activity of Dio1 in the liver. In addition, the *de novo* lipogenesis and TH target genes acetyl-CoA carboxylase 1 (*Acc1*), fatty acid synthase (*Fasn*), TH binding proteins *Ttr* and *Tbg,* and TH target gene TH-responsive spot 14 (*Spot14*) were downregulated in male Cre(+) mice. This suggests that *RetSat* in the thyroid plays an important role in hepatic gene regulation.

Triglycerides are the major storage form of lipids and are broken down into NEFA and glycerol during energy demands and transported to muscle and other tissue cells for energy production. Triglycerides play an important role in lipid metabolism. Liver and serum triglyceride levels were examined (Figure 22C and D), and there were no significant differences between Cre(-)/+ mice. Serum levels of NEFA were reduced in Cre(+) mice compared to Cre(-) mice, as depicted in Figure 22E.

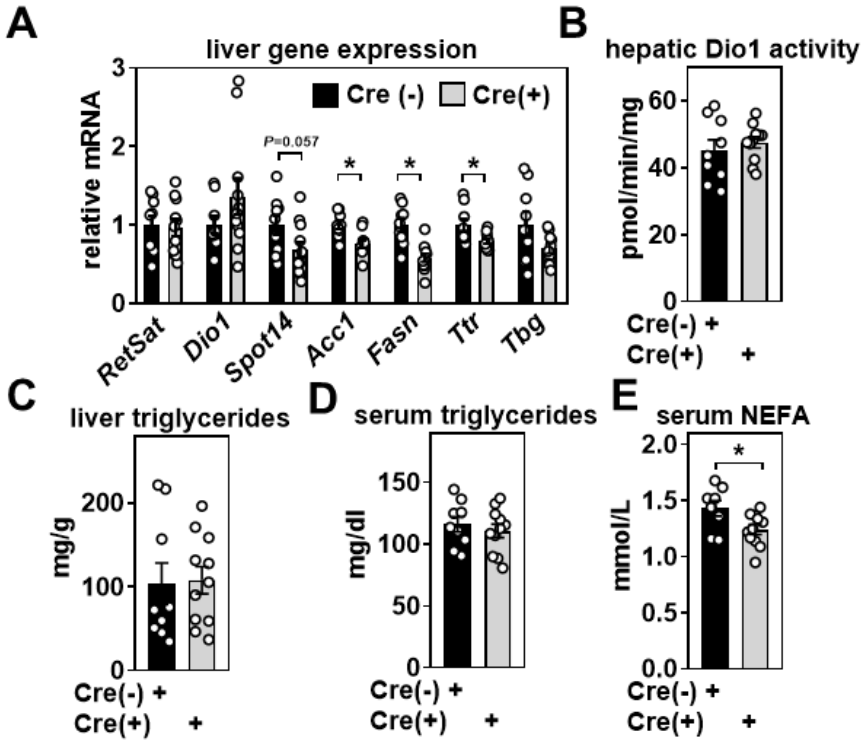

Figure 22: Deletion of *RetSat* in thyroids of male mice fed a high-fat diet affects lipid metabolism. Male mice (n=9,11) of the indicated genotypes were fed a high-fat diet (HFD, 60% kcal/fat) for 12 weeks, starting at 8 weeks of age, and A) hepatic gene expression was analyzed by qPCR. B) Dio1 activity in livers of Cre(-) and Cre(+) mice. C) Liver triglycerides in mice of the indicated genotypes. D) Serum triglycerides and E) NEFA in Cre(-) and Cre(+) mice. Data are presented as individual data points and mean±SEM, analyzed using a Student's t-test, **P*<0.05.

In conclusion, the results of the study showed that under HFD conditions, Cre(+) mice had increased thyrocyte activity compared to Cre(-) mice, as evidenced by elevated TSH

levels and hypertrophy of follicular epithelial cells. However, despite the thyroid RetSat deficiency, there was no significant effect on body weight, glucose metabolism and insulin tolerance in the mice. Thus, the results suggest that thyroid RetSat deficiency primarily affects thyroid morphology and local tissues when mice are challenged with HFD.

4.6 Thyrocyte-specific Deletion of *RetSat* Shows Higher TG Levels, Reduced Iodination of Low TG, and Signs of UPR Due to Iodide Overload

The literature suggests that RetSat is associated with ER stress (87) and that iodide overload can induce increased ROS levels in mice (134). Our collaborators Dr. Panos G. Ziros and Dr. Gerasimos P. Sykiotis found that iodide overload led to a decrease in the expression of *RetSat* and that this was independent of *Nrf2* (Figure 14G). To investigate whether Retsat deficiency affects the consequences of iodide overload in the thyroid, the same iodide overload mouse model was applied to 15-week-old Cre(-)/(+) mice by giving them water containing 0.05% NaI for one week.

There was no significant difference in serum T3, T4, TSH levels between the Cre(-) and Cre(+) groups (Figure 23A). Both the iodination and folding processes of TG are mediated by oxidative reactions (134). The results showed that TG protein levels were significantly higher in the thyroid of the Cre(+) group compared to the Cre(-) group, but iodinated TG was significantly reduced (Figure 23B/C). Interestingly, iodide overload leads to a decrease in both TG levels and TG iodination (134) as a phenomenon of the Wolff-Chaikoff effect (135). This suggests that RetSat is not essential for the decreased TG iodination observed during iodide overload. Studies in the literature have shown that iodide excess activates the XBP1-mediated unfolded protein response primarily in the mouse thyroid and thyroid-like organs, and that activation of UPR by thyrocytes is an adaptive mechanism of resistance to ER stress (146). In the iodide overload state, the antioxidant genes NAD(P)H quinone dehydrogenase 1 (*Nqo1*) and glutathione peroxidase 2 (*Gpx2*) are highly expressed and help thyrocytes maintain internal homeostasis by ameliorating oxidative damage (134). Dual oxidases (DUOX1 and DUOX2) are the specific member of the NADPH oxidase family responsible for the production of H_2O_2 necessary for TH synthesis (147, 148). As shown in Figure 23D, *RetSat*-specific deletion in the thyroid resulted in a decrease in *RetSat* mRNA expression,

no significant change in *Tg* and *Gpx2* expression, a downward trend in *Nqo1* and *Duox1* expression, and no change in total *Xbp1* expression in the iodide overload state, but an increase in *Xbp1* splicing was observed in the thyroid. Under ER stress, unspliced *Xbp1* mRNA is converted to the mature form encoding spliced *Xbp1*(149). The results reveal that RetSat deficiency in thyrocytes protects the thyroid from oxidation caused by iodide overload.

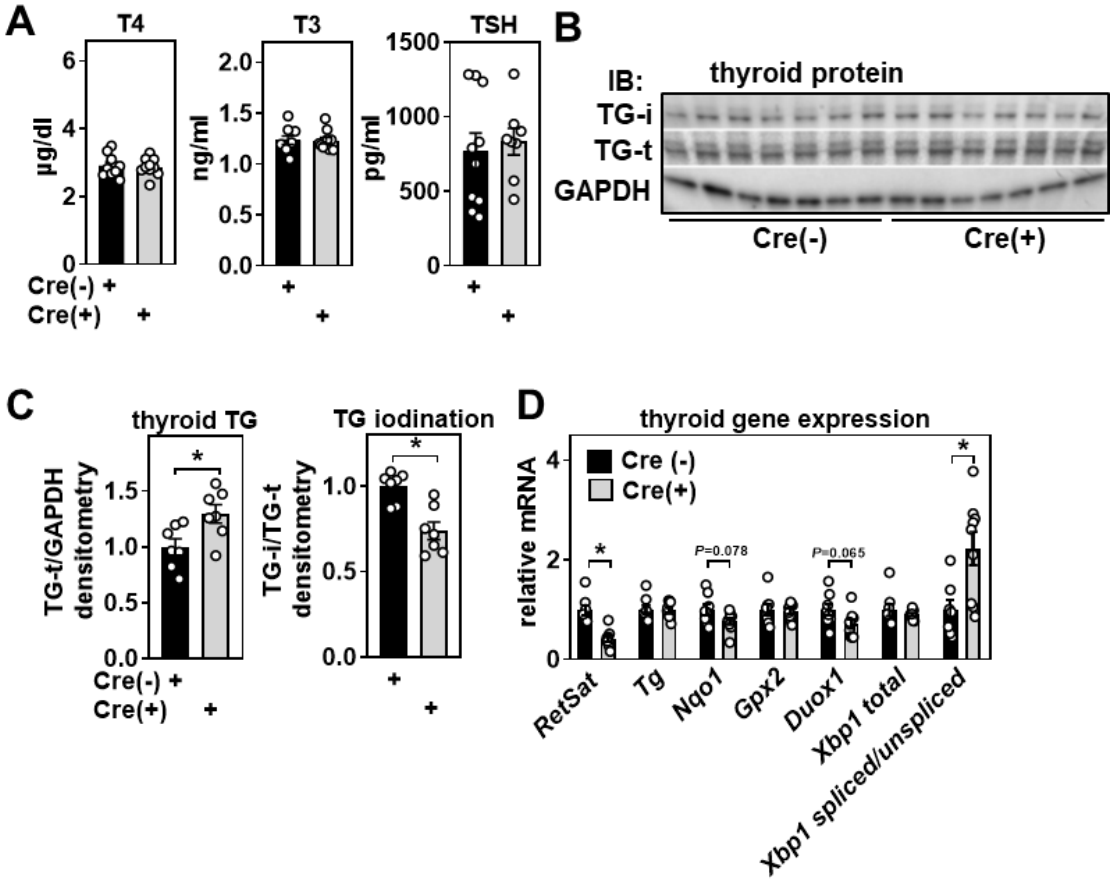

Figure 23: Deletion of *RetSat* in the thyroid of male mice reduces low TG iodination by iodide overload but shows signs of the unfolded protein stress response. Mice were supplemented with 0.05% sodium iodide in drinking water for 1 week and A) thyroid hormones and thyroid-stimulated hormone (TSH) concentrations were analyzed (n=9,10). B) Total and iodinated thyroglobulin (TG) protein were analyzed by immunoblotting. GAPDH served as loading control. C) Densitometric analysis of total and iodinated TG protein levels (n=7,7). D) Thyroid gene expression in mice (n=8,9) of the indicated genotype. Data are presented as individual data points and mean±SEM, analyzed using a Student's t-test, **P*<0.05.

5 Discussion

5.1 Expression and Location of RetSat in the Thyroid

Since the expression of RetSat in the mouse thyroid has not been reported, this study investigated the function of RetSat in the thyroid using C57BL/6J mice. The results showed that in wt mice, RetSat expression in the thyroid reached approximately 20% of the expression level in the liver (Figure 14A/B), and the liver was the organ with the highest expression of *RetSat* in mice. To further investigate the expression of RetSat in the mouse thyroid and the effects of hyperthyroidism and hypothyroidism on its expression, relevant experiments were performed in this study. The results showed that the expression level of *RetSat* in the thyroid gland did not change significantly in the hyperthyroidism model, but was significantly upregulated in the hypothyroidism model (Figure 14E). In addition, iodide is very important for the synthesis of TH. The research partner from the University Hospital of Lausanne (134) supplemented the drinking water with 0.05% NaI, carried out a 7-day experiment in wt mice, and found that the expression level of *RetSat* in the thyroid gland was downregulated (Figure 14G), which was consistent with the findings of this study (Figure 14F). Iodide overload in this model suppresses iodination of TG, and increases thyroidal oxidative stress (134).

Known *RetSat* transcriptional regulators such as FOXO1 and certain PPAR isoforms are expressed in thyrocytes (150-152); however, to fully understand their role in the observed dynamics, further experimental investigation is warranted. Notably, the influence of sex hormones on RetSat regulation remains unexplored, and its impact on gene expression requires detailed examination. In hypothyroid mice, it is plausible that the upregulation of thyroid *RetSat* is controlled by TSH regulation. However, in hyperthyroid mice, the expected decrease in expression of TSH responsive genes (e.g., *Tpo* and *Nis*) is observed, but this pattern is not reflected in the case of *RetSat*. Therefore, alternative regulatory mechanisms may be at play in hyperthyroid conditions, and further research is needed to fully understand them.

5.2 Evaluation of the Mouse Model

Similar to the liver-specific depletion of RetSat described above (94), the thyrocyte-specific knockout mouse model used in this study provides a more precise assessment

of RetSat functions in the thyroid, avoiding potential confounding influences from other organs seen in a global *RetSat* knockout model . The Cre-loxP system is a technology based on the interaction of the DNA recombinase Cre and the loxP sequence, which allows the selective knockout of target genes in specific tissues or cell types while preserving gene function in other areas (153). Models such as *TPO*-Cre, *Pax8*-Cre (154) and *Nkx2.1*-Cre (155) are widely used to achieve gene-specific deletion in the thyroid. However, *Pax8* and *Nkx2.1* are expressed in multiple organs, and the *Pax8*-Cre transgenic mouse model exhibits severe hypothyroidism (156). The thyroid gland is primarily composed of thyrocytes that express TPO, which is thyrocyte specific and present in approximately 92% of normal adult thyrocytes (128). The *Tpo* gene promoter was an ideal candidate for driving Cre expression in this study because it ensures that the recombinase enzyme is active only in thyrocytes, and RetSat is primarily localized to thyrocytes in the thyroid.

As expected, Cre expression was only detected in the thyroid in Cre(+) mice and resulted in an approximate 70% reduction in *RetSat* mRNA and protein expression (Figure 15C-G). This reduction was observed regardless of whether qPCR primer pairs were used to amplify the excised transcribed region (Figure 15D) or the remaining exons, indicating an impact on mRNA processing and/or stability. Notably, *RetSat* expression remained unaffected in other tissues, such as the liver (e.g. liver) (Figure 22A). Taken together, these findings confirm the successful thyrocyte-specific deletion of *RetSat* in this genetic mouse model. This is the first establishment of this mouse model, and its development holds significant importance in gaining profound insights into the functionality of RetSat within the thyroid.

5.3 Effect of Thyrocyte-specific Deletion of *RetSat* on Mouse Embryo Development

The birth rate of mice reflects various factors such as gene expression, physiological status, and environmental conditions. By studying changes in mouse birth rates, we can gain knowledge about the function of specific genes and their role in embryonic development.

In *RetSat*$^{flox/wt}$ heterozygous mice, both Cre(+) and Cre(-) mice followed the Mendelian inheritance laws. However, in *RetSat*$^{flox/flox}$ pure homozygotes, slightly higher than

expected birth rates in Cre(-) mice and slightly lower than expected birth rates in Cre(+) mice were observed. Although these observations are not statistically significant, due to the large sample size of 1034 individuals, they suggest that RetSat in the thyroid gland may play a role in embryonic development. RetSat deficiency may lead to abnormalities in the embryo at critical developmental stages, ultimately affecting birth rates (Table 18). This is the first report on the birth rate of mice deficient in RetSat.

Further studies are required to fully understand the precise the role of thyroid RetSat during embryogenesis. Nevertheless, these observations provide valuable clues for investigating the function of RetSat in embryonic development. These findings will guide future research and enhance our understanding of the significance of RetSat in the thyroid gland and embryonic development.

5.4 Sex-specific Effects of RetSat on the Thyroid Gland in Mice

Sex differences in thyroid disease prevalence have been reported in both mice and humans (136, 157, 158), with females having a higher susceptibility to thyroid disease than males. In hyper- or hypothyroidism, TH has significant effects on body weight, food and water intake, body temperature and heart rate in both male and female mice (136). Specifically, female mice showed a significant increase in activity in the open field test in the hyperthyroid state, while male mice showed no significant change (136). Furthermore, *Dio2* transcript levels in brown fat BAT were upregulated in male mice and downregulated in female mice in the hyperthyroid state, and this sex-specific change was evident with altered thyroid status (136).

With respect to the observed sex differences, it was hypothesized that since RetSat expression is higher in the thyroid of male mice (Figure 14D), its thyrocyte-specific loss would be more consequential in males than in females. To investigate the differential effects of thyrocyte-specific deletion of *RetSat* in male and female mice, I conducted a study to examine the performance of male and female mice following the absence of the *RetSat* gene under normal dietary conditions (Figure 16 and Figure 17). The results revealed that *RetSat* knockout decreases locomotor activity in male mice under normal dietary conditions. In contrast, in female mice, *RetSat* knockout resulted in altered TSH levels, fasting serum levels, body fat content and diet, suggesting that specific deletion of *RetSat* in the thyroid has a more significant effect in female mice.

The literature suggests that the HPT axis responds differently in male and female rats under fasting conditions, and that adult males have a stronger HPT axis response to starvation (159). Female rats exhibit greater resistance to reduced HPT axis activity after two weeks of food restriction compared to males, while even with a food intake reduction of less than 20% in males, there is a reduction in TRH and serum concentrations of TSH and leptin (160). However, in females with a 30% reduction in food intake, no significant changes in TRH expression and TSH levels are observed, even with a similar leptin concentration as in males (160). The HPT axis is activated in male rats and mice in the presence of energy excess due to HFD, but few studies have examined both male and female rodents (160-162). In HFD experiments with saturated and monounsaturated fatty acids for 40 consecutive days after weaning, male rats showed a twofold increase in serum leptin concentrations and a decrease in the T4/T3 ratio, whereas female rats showed a threefold increase in leptin concentrations, but no change in the T4/T3 ratio (160, 163). Although female mice and humans are more susceptible to thyroid disease, in this study, female mice did not exhibit significant weight gain under the HFD conditions, as indicated by the data. Therefore, male mice were employed as the subjects for this research.

The mechanisms by which deletion of the *RetSat* gene in the thyroid gland leads to phenotypic sex differences in mice are currently unclear. Metabolism is sexually dimorphic and therefore the phenotypic changes caused by gene deletion may be influenced by a number of complex causes (158). In the thyroid, sex differences due to gene deletion may be related to estrogen, which increases serum TBG and total T4 concentrations (136, 164, 165).

5.5 Effects of Thyrocyte-specific Deletion of *RetSat* might be Compensated

TH is essential for maintaining normal metabolism and physiological functions. When thyroid function is disrupted, the body initiates compensatory mechanisms to maintain normal physiological functions as well as possible.

In 2022, Liu *et al.* made an interesting discovery regarding Xb130 (also known as actin filament-associated protein 1-like 2 (AFAP1L2)) in mice. They found that *Xb130* knockout resulted in growth retardation at 2 weeks, but normal growth was fully restored by 14

weeks (166). Interestingly, no discernible phenotypic differences were observed in adult mice (167). Serum TH levels increase rapidly after birth in normal mice, but are initially low in Xb130-deficient mice (166). Xb130-deficient mice also have higher serum TSH levels compared to controls (166). However, by week 12, TH and TSH levels are nearly normalized in Xb130-deficient mice (166). This activation of compensatory mechanisms in thyroid tissue underscores the critical role of these pathways.

In this study, only adult mice were chosen as research subjects. Cre-mediated recombination was initiated at approximately embryonic day 14.5, coinciding with the onset of TPO expression during thyroid organogenesis (128). The study did not investigate the deletion of RetSat in juvenile mice. However, this does not eliminate the possibility of compensatory mechanisms restoring normal TH levels after inducing metabolic disturbances.

Specific knockout of *RetSat* in the thyroid resulted in elevated serum TSH in females on a normal diet (Figure 16B) and in males on an HFD (Figure 18B), while serum T3 and T4 levels did not change significantly. This suggests that RetSat is required to maintain adequate TSH sensitivity and to synthesize and secrete TH. The observed TSH and TH configuration is commonly called subclinical hypothyroidism, whereby increased TSH levels are required to maintain normal circulating TH concentrations, often preceding the appearance of reduced blood TH in patients (168). Thus, it is very likely that TSH is increased to maintain TH concentrations within the physiological range as a compensatory response to the loss of thyroid RetSat. This would also be consistent with the notion that since RetSat is not a thyrocyte-specific protein with specialized functions like TPO or TG, its expression in the thyrocytes, which are present in many cell types and tissues, is not essential for its response to TSH and for the synthesis and secretion of TH. It is possible that RetSat plays a role in the fine-tuning of the TSH response and the synthesis and secretion of TH by thyrocytes. TSH increases the size of the follicular cells (hypertrophy), and it increases the number of follicular cells (hyperplasia) (169, 170). Thyroid morphology also confirmed that thyrocytes enlarged in response to stimulation by higher levels of TSH after *RetSat* knockout (Figure 19).

In conclusion, RetSat knockout is likely to induce compensatory responses to maintain physiological TH levels.

5.6 Thyrocyte-specific Deletion of *RetSat* Shows Minimal Transcriptional Effects in the Thyroid

Deletion of *RetSat* resulted in minimal transcriptional consequences in the thyroid gland (Figure 20A), which is in contrast to the significant transcriptional changes that were observed in other cell types and tissues upon RetSat depletion (89, 94). Both the substrate (all-*trans*-retinol) and the product (all-*trans*-13,14-dihydroretinol) of RetSat can be stored as esters or further oxidized to the corresponding aldehydes or acids (171). atRA mediates its effects via the ligand-activated transcription factor RAR, which heterodimerizes with retinoid X receptors (RXR) (171). According to the latest research findings by Bi *et al*., the RNA-seq data demonstrates that deficiency of RetSat significantly activates the RAR signaling pathway in A549, HT1080, and H1299 cells (114). However, thyrocyte-specific deletion of *RetSat* did not result in increased expression of canonical RAR target genes in male HFD mice, as shown in Figure 20B. The possibility of reduced dihydroretinol generation, which could potentially lead to enhanced thyroid atRA synthesis and RAR activation, is unlikely to be involved. It has not been fully understood the exact mechanism by which thyroid RetSat deficiency affects TH homeostasis.

5.7 Thyrocyte-specific Deletion of *RetSat* Affects Metabolism in Normal Chow Female Mice

5.7.1 Thyrocyte-specific Deletion of *RetSat* Affects Lipid Metabolism in Normal Chow Female Mice

The hormones of the thyroid gland exert a significant influence on various metabolic processes in the body (68). Their most prominent and widely recognized roles are the enhancement of basal energy expenditure and their effects on protein, carbohydrate and lipid metabolism (68). The regulation of lipid homeostasis is a complex process requiring coordinated modulation between multiple target tissues (172). TH maintains lipid balance by influencing gene expression in target organs such as the liver and adipose tissue (172). TH affects the synthesis, mobilization and degradation of lipids, with degradation being more effected than synthesis (68). In the female normal chow mouse cohort, Cre(+) mice gained weight more slowly than Cre(-) mice, and had a lower fat content, lower fasting blood glucose levels and a higher food intake during the dark phase (Figure 16). These observations suggest that *RetSat* deletion in the thyroid affects lipid metabolism in mice.

Paradoxically, these results suggest an augmented TH bioactivity, which is challenging to reconcile with the concurrent rise in TSH levels and the presence of subclinical hypothyroidism.

Research suggests an association between TSH and abnormalities in lipid metabolism (158, 173). TSH is capable of promoting lipolysis (174-176) through activation of TSHR (176). The observed reduction in TSH-induced fat breakdown upon *TSHR* knockout in mice further substantiates this mechanism (177). In mice with thyrocyte-specific knockout of *RetSat*, there was a relative decrease in body weight and fat content among the Cre(+) group of female mice on a normal diet (Figure 16), which may be attributed to elevated serum TSH levels. However, the actions of TSH independent of the thyroid gland are still incompletely understood and remain a mystery.

The production of TH is subject to a complex regulation involving both positive and negative feedback mechanisms. Within this feedback loop, the synthesis and release of TRH plays a critical role. The elevated serum TSH levels observed in Cre(+) female mice suggest a potential increase in TRH levels. In a previous study, overexpression of diencephalic TRH (d*Trh*) in mice resulted in increased food and water intake, but significantly decreased body weight compared to the control group, as well as increased blood pressure, heart rate, and locomotor activity, independent of TH levels (178). In this same study, acute and subacute TRH overexpression was found to increase sympathetic tone, leading to cardiovascular and weight regulation abnormalities (178). Notably, the phenotypes observed in the TRH-overexpressing mice mirrored those found in female Cre(+) mice, suggesting a potential link between TRH levels and these findings, which requires further experimental validation.

5.7.2 Thyrocyte-specific Deletion of *RetSat* Reduces Fasting Blood Glucose in Female Mice on Normal Chow

It is well known that there is a strong association between obesity and an increased risk of diabetes (179); however, the correlation between weight and blood glucose in the normal weight range is not clear (180).

Ruhla *et al.* found that TSH has no association with fasting blood glucose based on a study of 1333 euthyroid volunteers (173). However, several studies showed that serum

TSH was positively associated with hyperglycemia in euthyroid individuals (181). TSH stimulates hepatic glucose production *in vivo* and *in vitro* (181). Another study found that in mice, TSHR knockout mice had reduced fasting glucose levels (182). Based on the above studies, the reduction in fasting blood glucose caused by deletion of *RetSat* in the thyroid gland of female mice was unlikely due to elevated TSH (Figure 16E).

The study found that TSH can stimulate the secretion of leptin (183), which has profound glucose-lowering and anti-lipogenic effects (184). Although leptin levels in mice were not measured in this study, the reduction in fasting blood glucose in female mice in the Cre(+) group may be due in part to an increase in leptin secretion induced by TSH (Figure 16E).

5.7.3 Thyrocyte-specific Deletion of *RetSat* Increases Locomotor Activity in Female Mice on Normal Chow

It is common knowledge that there is a significant correlation between locomotor activity level and body weight. Compared to Cre(-) female mice, Cre(+) female mice showed an increase in locomotor activity in the dark phase and a tendency towards reduced body weight, as shown in Figure 16 C/G. However, in 129sv/C57BL6 mice with RetSat deficiency under either a low-fat diet or HFD conditions, the weight gain in females and males is similar to that of the wt littermates (103). After backcrossing to a C57BL/6N strain, male *RetSat* deletion mice gain body weight on normal chow and HFD (109). This discrepancy could potentially be due to several factors, including thyrocyte-specific knockout effects, differences in mouse strains, and sex-specific responses.

The relationship between TSH and daily activity levels has been explored to a limited extent in the literature. Recent studies have found a negative association between TSH levels and lying down time in elderly individuals with normal thyroid function, particularly in women (185). Another study conducted in young men reported that short-term high-intensity exercise resulted in increased TSH and T4 levels, along with decreased T3 levels (186). However, these results were not fully confirmed in another study, where TSH and free triiodothyronine (fT3) levels were lower than pre-exercise levels after 24 h of rest following exercise in young male athletes (187). In addition, there was no significant correlation between TSH and changes in free thyroxine (fT4)/T4 levels (187). Although exercise can impact TSH levels, it remains unclear whether TSH levels have an effect on exercise activity in the presence of normal thyroid function.

A number of studies have shown that an increase in TRH levels leads to an increase in locomotor activity (178, 188, 189), with a dose-dependent relationship being observed (190, 191). In addition, the literature suggests that the effects of TRH on locomotor activity are mediated through the mesencephalic dopaminergic system (192-194). In the context of this study, the increased locomotor activity observed in Cre(+) mice may be related to the elevated TRH levels, which requires further experimental validation.

5.7.4 Thyrocyte-specific Deletion of *RetSat* Increases Food Intake in Female Mice on Normal Chow

Energy homeostasis, which involves the regulation of energy intake and expenditure, is critical for maintaining a stable weight and body composition. Normally, the body compensates for increased energy requirements due to exercise by increasing energy intake (195). However, an energy imbalance occurs when the body is unable to maintain a balance between energy intake and energy expenditure. The mechanisms underlying this compensation process are complex (196).

In this study, female Cre(+) mice showed increased nocturnal locomotor activity compared to controls (Figure 16G). Cre(+) mice had a higher food intake, which was likely due to the maintenance of stable body weight and body composition (Figure 16H). Although there was no significant difference in energy metabolism, Cre(+) mice had a slightly higher level of energy expenditure (Figure 16I), which may have contributed to their slower body weight gain compared to Cre(-) mice (Figure 16C).

A literature review found that food intake was greatly reduced after intracerebroventricular injection of TSH in rats (197). TSH can stimulate the secretion of leptin (183), thereby suppressing food intake (198). Therefore, the increased food intake of Cre(+) mice could not be explained by elevated TSH levels.

5.8 Thyrocyte-specific Deletion of *RetSat* Affects Metabolism in HFD Male Mice

5.8.1 Thyrocyte-specific Deletion of *RetSat* Affects Lipid Metabolism in HFD Male Mice

Obesity is mainly due to an imbalance between energy intake and energy expenditure.

TH plays an important role in regulating lipid, cholesterol and glucose metabolism in the liver (199). Therefore, analyzing the concentrations of circulating TH is often required in the search for the cause of obesity (200, 201). TH and TSH independently regulate the quality and function of adipose tissue, and in obese states, serum TSH levels are usually slightly elevated or above the reference range (200).

In animal models, a diet high in fat and simple carbohydrates significantly increased T3 and TSH levels (200, 202). Additionally, leptin receptors were significantly downregulated, leading to the development of leptin resistance (200). Although centrally acting leptin stimulates the HPT axis, elevated levels of leptin do not decrease appetite or increase energy expenditure (200).

In HFD male Cre(+) mice, as shown in Figure 18, food intake was not lower than in Cre(-) mice, and this did not lead to weight loss, despite an increase in locomotor activity, and energy expenditure was not increased. Deletion of *RetSat* in the thyroid did not result in significant changes in glucose metabolism and insulin sensitivity, as shown in Figure 21. The data are consistent with previous reports, in that RetSat-deficient mice have no alterations in glucose homeostasis under normal chow conditions，as well as insulin sensitivity under normal chow and HFD conditions (103, 109). HFD male Cre(+) mice exhibited a faster rate of weight gain than the Cre(-) group (Figure 18A), which is inconsistent with data from the normal chow female group (Figure 16C). Previous studies have shown that mice with whole body deletion of *RetSat* in the 129sv/C57BL6 genetic background showed no significant change in body weight on HFD compared to control mice; however, they showed an increase in fat mass (103). Male mice with RetSat depletion gain body weight when backcrossed to a C57BL/6N strain (109), which may be related to gender as well as diet.

Previous studies showed that TH induces expression of lipogenesis genes such as *Spot14, Fasn, Acc1*, and regulates hepatic NEFA uptake and TAG assembly (69, 199, 203, 204). However, as shown in Figure 22A, these genes were downregulated in the male HFD mice with *RetSat* deletion, indicating that they were not induced by T3. The liver obtains fatty acids from 3 major sources, i.e., uptake of NEFA from the blood, uptake of celiac residue, and *de novo* lipogenesis. Studies have shown that exogenous NEFA uptake is the largest single source of fatty acids in stored hepatic triacylglycerol (205). Serum NEFA levels were reduced (Figure 22E), while triglycerides remained unchanged

(Figure 22C), suggesting hepatic uptake of NEFA was increased. Lipolysis is the metabolic pathway by which triglycerides are hydrolyzed to glycerol and free fatty acids (206). The decrease in free fatty acid levels indicates that lipolysis is reduced. Paradoxically, TSH stimulates lipolysis in cultured adipocytes *in vitro* and increases serum free fatty acid levels *in vivo* (174), contradicting the above findings.

The hepatic secretion of three serum proteins, namely TTR, HSA, and TBG, orchestrates the systemic distribution of TH from its site of synthesis in the thyroid gland to various target tissues via the bloodstream (207, 208), thereby regulating the balance between free and total TH levels (209). TBG serves as the primary carrier for the majority of TH, followed by TTR due to its greater binding affinity for TH (54). TH has been observed to induce an upregulation of hepatic *Dio1* mRNA expression and a downregulation of *Tbg* mRNA expression in mouse models (210). No significant changes in *Ttr* mRNA levels were observed in the livers of hypothyroid or hyperthyroid rats (211), but they were reduced in the brains of T4-treated mice (76). According to the results in Figure 22A, there was a slight upward trend in *Dio1* gene expression in the liver and a significant decrease in *Ttr* gene expression in the thyrocyte-specific deletion of *RetSat*, as well as a slight decrease in *Tbg* gene expression. Although not all of these differences were statistically significant, it is hypothesized, however, that this phenomenon is due to a slight increase in serum TH (Figure 18). The regulation of TH concentration in the liver is not only dependent on the uptake of circulating TH, but is also locally activated and inactivated by iodothyronine deiodinases (209). Dio1 is involved in the activation of T4 to T3 and inactivation of TH, and is regulated by T3 (132, 209). The slightly increased hepatic Dio1 activity increases the likelihood of the hypothesis being true (Figure 22B). But in this study, the decreased expression of the lipogenesis gene was not caused by T3, and thus does not support the above hypothesis.

The process of lipogenesis and lipid metabolism entails intricate and multifaceted mechanisms. The mechanism of the changes in lipid metabolism caused by the specific deletion of *RetSat* in the thyroid gland under HFD needs further study.

5.8.2 Thyrocyte-specific Deletion of *RetSat* Affects Heart Weight in HFD Male Mice

There is a close relationship between the thyroid and the heart, with physicians noticing the effects of increased TH secretion on cardiovascular function more than 200 years ago

(3). Hyperthyroidism can cause tachycardia, while hypothyroidism can cause bradycardia. Hyperthyroidism increases total protein synthesis in cardiomyocytes, leading to increased heart weight and mild cardiac hypertrophy, which in turn increases the contractile state of the heart. Although the male HFD Cre(+) mice in this study were subclinically hypothyroid when considering their TSH and TH concentrations in the circulation, they had increased heart weights compared to Cre(-) mice. The current data cannot explain this finding and further research is needed to resolve this issue.

5.9 Retsat May be Involved in the Homeostasis of Oxidative Stress in Thyroid

The thyroid gland typically generates significant amounts of H_2O_2， which plays a critical role in oxidizing iodine to iodide, facilitating the iodination process of TG, and contributing to the synthesis of TH (212). These hormones are essentially iodinated derivatives of specific tyrosines found in TG (212). Negative feedback regulation of the HPT axis is the primary mechanism for maintaining stable serum TH levels. Iodide is actively transported into thyrocytes via the NIS on the basolateral membrane, then iodide is transported into the lumen by pendrin and is rapidly oxidized by TPO and H_2O_2, resulting in the covalent binding of iodide to tyrosyl residues of TG and the formation of monoiodotyrosine (MIT) and diiodotyrosine (DIT) in the TG molecule (213).

RetSat is a potent regulator of the cellular response to oxidative stress and ROS generation, and RetSat deficiency reduces ROS and lipid peroxide formation (109). PTU and MMI inhibit the TPO-H_2O_2 reaction and inhibit the action of NADPH oxidase, but not TPO itself (214-216). MMI degrades H_2O_2 in the cell-free system and interferes with thyroid H_2O_2 production (216). Perchlorate inhibits thyroid iodide uptake and subsequently reduces TH production. Perchlorate is a potent competitive inhibitor of the NIS (217) and has been found to inhibit iodide overload induced strong mitochondrial superoxide production (218). In the model of hypothyroidism caused by MMI and perchlorate, the increased expression of *RetSat* may be due to compensatory upregulation (Figure 14E). Therefore, in the hypothyroid models, the thyroid gland may maintain the levels of H_2O_2 and promote TH synthesis by regulating the expression of RetSat.

Decades ago, it was reported that high doses of iodide have an inhibitory effect on thyroid

function (219), a phenomenon known as the Wolff-Chaikoff effect (220, 221). After a period of time, NIS expression decreases, resulting in a decrease in intracellular iodide levels and a return to near normal levels of TH production (222, 223). Iodide exposure increases oxidative stress in the thyroid and also increases ROS levels in cell culture (134, 221, 224).

RetSat imparts sensitivity to peroxide stress (87), and iodide overload in mice triggers oxidative stress in thyrocytes, which subsequently results in the downregulation of *RetSat* expression (Figure 14F). Previous studies have found that reduced *RetSat* expression increases cellular resistance to hydrogen peroxide, and *RetSat* mediates H_2O_2-induced cell death (108, 112). Similarly, the levels of lipid peroxidation products were reduced in the livers of *RetSat* knockout mice fed normal or HFD (109). Therefore, this downregulation is believed to serve a protective role, protecting the cells from the detrimental effects of oxidative stress. Interestingly, an excess of iodide leads to a decrease in total TG levels, particularly in terms of TG iodination, so as to prevent excessive TH synthesis (134, 225). In contrast to *Nrf2* knockout, a key transcription factor to drive gene expression of the antioxidative defense in the thyroid, which resulted in decreased total TG protein levels and increased iodination levels (134), RetSat deficiency resulted in increased total TG levels and decreased iodination levels (Figure 23). This observation suggests that *RetSat* deletion in the thyroid may ameliorate oxidative stress in the thyroid under conditions of iodide excess. In the thyroid gland, NRF2 stimulates the transcription and protein synthesis of molecules with antioxidant and cytoprotective properties, including NQO1, GPX2 (226). GPX typically catalyzes the reduction of H_2O_2 or organic hydrogen peroxide to water or corresponding alcohols using glutathione as the reducing agent (227). When exposed to excessive levels of iodide, these antioxidant enzyme systems are further induced in response to the elevated levels of reactive oxygen species (212). RetSat deficiency had minimal impact on the expression of iodide-inducible genes (*Duox1*, *Nqo1*, and *Gpx2*), as depicted in Figure 22D. Under ER stress, unspliced *Xbp1* mRNA is converted to the mature form encoding spliced *Xbp1* to reduce ER stress (149). Additionally, iodide excess in Cre(+) mice resulted in increased *Xbp1* transcript splicing (Figure 22D), indicating heightened ER stress (228). This suggests that RetSat may be involved in antioxidant responses during iodide overload.

In summary, the expression of *RetSat* was decreased in the hypothyroid model in which

H_2O_2 was suppressed by perchlorate and MMI, and the expression was increased in the oxidative stress model caused by iodide excess, indicating that RetSat was involved in the homeostasis of thyroid oxidative stress.

6 Conclusions

RetSat is an oxidoreductase that has been implicated in the generation of dihydroretinol and which mediates cellular sensitivity to peroxide stress (87). This enzyme is expressed at higher levels in metabolically active tissues such as adipose tissue and liver (87). In adipocytes, RetSat promotes cell differentiation, but is downregulated under conditions of obesity (87). In the liver, the absence of RetSat alters hepatic lipid content and composition (87). However, the function of RetSat in other tissues has not been investigated yet.

RetSat's high expression in the human thyroid was reported (Figure 6). Consequently, the function of RetSat in the thyroid, an unexplored area, was investigated. The expression of RetSat in mouse thyroid tissue was initially examined. Notably, RetSat exhibited strong expression in the thyroid (Figure 14A), with gender differences observed between male and female mice (Figure 14D). Its levels were increased by inducing hypothyroidism (Figure 14E) and decreased by iodide overload in the mouse thyroid (Figure 14F). These findings offer novel insights into the regulation of RetSat expression in the thyroid.

To further investigate the function of RetSat in the thyroid, a mouse model with thyrocyte-specific deletion of *RetSat* was established (Figure 15). Utilizing this model, the phenotypic changes in male and female mice with thyrocyte-specific RetSat deficiency under normal diet conditions were observed. It was observed that the deficiency of RetSat in thyrocytes increased circulating TSH levels specifically in female mice (Figure 16), while this effect was not observed in male mice (Figure 17). The disruption of metabolic homeostasis due to thyrocyte-specific RetSat deficiency displayed a gender-dependent pattern. Although no significant impact was observed on circulating TH levels, various metabolic abnormalities were associated with this condition. Female Cre(+) mice exhibited reduced weight gain during the active dark phase, decreased fasting blood glucose levels, increased physical activity, and elevated food intake (Figure 16), which poses a challenge to reconcile with elevated TSH levels and subclinical hypothyroidism.

TH exert a significant influence on energy metabolism and their close association with obesity has been extensively studied. RetSat expression is known to be inhibited in the context of obesity. Therefore, the present study was designed to investigate the effects

of thyrocyte-specific RetSat deficiency in mice challenged with HFD. Male mice with thyrocyte-specific RetSat deficiency have exhibited elevated TSH levels when subjected to HFD (Figure 18B), and have larger follicle and thyrocyte areas (Figure 19). However, despite elevated TSH levels and subclinical hypothyroidism, the HFD-fed male Cre(+) mice experienced an increase in body weight (Figure 18A) and relative heart weight (Figure 18D), which is a sensitive indicator of TH action. Notably, the expression of specific TH genes encoding lipogenesis and TH-binding proteins was reduced in the liver (Figure 22A), indicating tissue-specific alterations in TH homeostasis. Interestingly, the activity of hepatic Dio1 (Figure 22B), which is responsible for local TH activation and/or inactivation, remained unaltered, adding complexity to the observed changes. While there were no changes in liver and serum triglyceride levels, circulating NEFA derived from adipose tissue were decreased (Figure 22). As a result, only male mice exposed to the HFD as an additional stressor exhibited elevated TSH concentrations, weight gain, and increased heart weight - phenomena that were absent in male mice on a normal diet.

Previous studies have shown that RetSat plays a role in mediating the sensitivity of various cell types to oxidative stress (87, 93, 108, 109, 114). In thyroid gland, TPO uses H_2O_2 to catalyze the organic iodination of inorganic iodide, a critical step in the synthesis of TH (229). Given that high iodide intake increases oxidative stress in the thyroid, this study aimed to investigate the effects of RetSat deficiency in mice using a high iodide challenge. It was observed that iodide overload resulted in the downregulation of *RetSat* mRNA expression in the thyroid (Figure 14F), and this downregulation may synergistically interact with another phenomenon, the Wolff-Chaikoff effect, which acts to protect the thyroid. Interestingly, no significant differences in TH and TSH levels were observed between Cre(-) and Cre(+) mice. Notably, studies have shown that thyroid lipid peroxidation induced by potassium iodate (KIO_3) is significantly lower compared to other tissues (230), indicating the adaptive capacity of the thyroid to maintain high iodide concentrations (229). However, in Cre(+) mice, there was a further decrease in thyroid iodinated glycerolipid content, and iodide overload led to increased *Xbp1* transcript splicing, indicating increased ER stress. These results suggest the involvement of RetSat in organelle antioxidant responses during iodide overload.

There are still many limitations in this study. The exact mechanism by which the loss of thyroid RetSat affects TH homeostasis remains to be elucidated. Known transcriptional

regulators of *RetSat*, such as FOXO1 and certain PPAR subtypes, require further experiments to determine whether they are involved in the regulation of RetSat in the thyroid. Thyrocyte-specific deletion of *RetSat* does not lead to increased expression of typical RAR target genes, suggesting that they are unlikely to be involved in reducing dihydroretinoid production. Further studies on the enzymatic activity of RetSat and alternative substrates are needed to investigate the mechanisms behind the observed phenotypes. Given the role of RetSat in oxidative physiology, and the differences in its expression in mouse models of iodide overload and hypothyroidism (both associated with oxidative stress), analysis of oxidized proteins (via Oxyblot) and oxidized lipids (via IHC for 4-HNE) will help to explain the role of RetSat in important antioxidant defense mechanisms in thyrocytes.

Regulation of RetSat by sex hormone factors has not been described. Due to the differences in RetSat expression between male and female mice and the different phenotypes after specific deletion in the thyroid, the investigation of the regulation of RetSat by sex hormones could provide valuable insights.

It is worth noting that in this model, *RetSat* is knocked out at about two weeks of embryonic age in mice, and the knockout mice have a lower birth rate compared to wt mice, although without statistical significance, and thus the study of RetSat-deficient mice at a young age or even during the embryonic period is warranted.

In spite of these limitations, this study provides the first comprehensive *in vivo* analysis of the regulation and function of RetSat in the thyroid gland. The establishment of a novel mouse model with thyrocyte-specific RetSat deficiency and the findings of this study will contribute to a deeper understanding of the tissue-specific functions of RetSat and its potential relevance in thyroid diseases.

7 Reference List

1. Mullur R, Liu YY, Brent GA. Thyroid hormone regulation of metabolism. Physiological Reviews. 2014;94(2):355-82.
2. Wikström L, Johansson C, Saltó C, Barlow C, Barros AC, Baas F, Forrest D, Thorén P, Vennström B. Abnormal heart rate and body temperature in mice lacking thyroid hormone receptor α1. The EMBO journal. 1998;17(2):455-61.
3. Kahaly GJ, Dillmann WH. Thyroid hormone action in the heart. Endocrine Reviews. 2005;26(5):704-28.
4. Klein I, Danzi S. Thyroid disease and the heart. Circulation. 2007;116(15):1725-35.
5. Althausen T, Stockholm M. Influence of the thyroid gland on absorption in the digestive tract. American Journal of Physiology-Legacy Content. 1938;123(3):577-88.
6. Bradley DJ, Towle HC, Young WS. Spatial and temporal expression of alpha- and beta-thyroid hormone receptor mRNAs, including the beta 2-subtype, in the developing mammalian nervous system. Journal of Neuroscience. 1992;12(6):2288-302.
7. Dussault JH, Ruel J. Thyroid hormones and brain development. Annual Review of Physiology. 1987;49(1):321-32.
8. Mundy GR, Shapiro JL, Bandelin JG, Canalis EM, Raisz LG. Direct stimulation of bone resorption by thyroid hormones. Journal of Clinical Investigation. 1976;58(3):529-34.
9. Burkhart JM, Jowsey J. Parathyroid and thyroid hormones in the development of immobilization osteoporosis. Endocrinology. 1967;81(5):1053-62.
10. Dempsey E, Astwood E. A determination of the rate of thyroid hormone secretion at various environmental temperatures. Endocrinology. 1943;32(6):509-18.
11. Jannini EA, Ulisse S, D'Armiento M. Thyroid hormone and male gonadal function. Endocrine Reviews. 1995;16(4):443-59.
12. Doufas AG, Mastorakos G. The hypothalamic‐pituitary‐thyroid axis and the female reproductive system. Annals of the New York Academy of Sciences. 2000;900(1):65-76.
13. MacCrimmon DJ, Wallace JE, Goldberg WM, Streiner DL. Emotional disturbance and cognitive deficits in hyperthyroidism. Psychosomatic Medicine. 1979;41(4):331-40.
14. Devereaux D, Tewelde SZ. Hyperthyroidism and thyrotoxicosis. Emergency Medicine Clinics. 2014;32(2):277-92.
15. Almandoz JP, Gharib H. Hypothyroidism: etiology, diagnosis, and management. Medical Clinics. 2012;96(2):203-21.
16. Stathatos N. Anatomy and physiology of the thyroid gland. The Thyroid and Its Diseases: A Comprehensive Guide for the Clinician. 2019:3-12.
17. Carvalho DP, Dupuy C. Thyroid hormone biosynthesis and release. Molecular and Cellular Endocrinology. 2017;458:6-15.
18. Szanto I, Pusztaszeri M, Mavromati M. H2O2 metabolism in normal thyroid cells and in thyroid tumorigenesis: focus on NADPH oxidases. Antioxidants. 2019;8(5):126.
19. Köhrle J. Selenium, Iodine and Iron–Essential Trace Elements for Thyroid Hormone Synthesis and Metabolism. International Journal of Molecular Sciences. 2023;24(4):3393.
20. Dai G, Levy O, Carrasco N. Cloning and characterization of the thyroid iodide transporter. Nature. 1996;379(6564):458-60.
21. Dohan O, De la Vieja A, Paroder V, Riedel C, Artani M, Reed M, Ginter CS, Carrasco N. The sodium/iodide Symporter (NIS): characterization, regulation, and medical significance. Endocrine Reviews. 2003;24(1):48-77.
22. Kaminsky SM, Levy O, Salvador C, Dai G, Carrasco N. Na(+)-I- symport activity is present in membrane vesicles from thyrotropin-deprived non-I(-)-transporting cultured thyroid cells. Proceedings of the National Academy of Sciences of the United States of America. 1994;91(9):3789-93.

23. Riedel C, Levy O, Carrasco N. Post-transcriptional regulation of the sodium/iodide symporter by thyrotropin. Journal of Biological Chemistry. 2001;276(24):21458-63.
24. Zaballos MA, Garcia B, Santisteban P. Gbetagamma dimers released in response to thyrotropin activate phosphoinositide 3-kinase and regulate gene expression in thyroid cells. Molecular Endocrinology. 2008;22(5):1183-99.
25. Postiglione MP, Parlato R, Rodriguez-Mallon A, Rosica A, Mithbaokar P, Maresca M, Marians RC, Davies TF, Zannini MS, De Felice M, Di Lauro R. Role of the thyroid-stimulating hormone receptor signaling in development and differentiation of the thyroid gland. Proceedings of the National Academy of Sciences of the United States of America. 2002;99(24):15462-7.
26. Szkudlinski MW, Fremont V, Ronin C, Weintraub BD. Thyroid-stimulating hormone and thyroid-stimulating hormone receptor structure-function relationships. Physiological Reviews. 2002;82(2):473-502.
27. Kleinau G, Worth CL, Kreuchwig A, Biebermann H, Marcinkowski P, Scheerer P, Krause G. Structural-Functional Features of the Thyrotropin Receptor: A Class A G-Protein-Coupled Receptor at Work. Frontiers in Endocrinology. 2017;8:86.
28. Laugwitz K-L, Allgeier A, Offermanns S, Spicher K, Van Sande J, Dumont JE, Schultz G. The human thyrotropin receptor: a heptahelical receptor capable of stimulating members of all four G protein families. Proceedings of the National Academy of Sciences. 1996;93(1):116-20.
29. Godbole A, Lyga S, Lohse MJ, Calebiro D. Internalized TSH receptors en route to the TGN induce local Gs-protein signaling and gene transcription. Nature Communications. 2017;8(1):443.
30. Dunn JT, Dunn AD. The importance of thyroglobulin structure for thyroid hormone biosynthesis. Biochimie. 1999;81(5):505-9.
31. Dunn JT, Dunn AD. Update on intrathyroidal iodine metabolism. Thyroid. 2001;11(5):407-14.
32. Avvedimento VE, Tramontano D, Ursini MV, Monticelli A, Di Lauro R. The level of thyroglobulin mRNA is regulated by TSH both in vitro and in vivo. Biochemical and Biophysical Research Communications. 1984;122(1):472-7.
33. Bjorkman U, Ekholm R, Ericson LE. Effects of thyrotropin on thyroglobulin exocytosis and iodination in the rat thyroid gland. Endocrinology. 1978;102(2):460-70.
34. Miccadei S, De Leo R, Zammarchi E, Natali PG, Civitareale D. The synergistic activity of thyroid transcription factor 1 and Pax 8 relies on the promoter/enhancer interplay. Molecular Endocrinology. 2002;16(4):837-46.
35. Grasberger H, Ringkananont U, Lefrancois P, Abramowicz M, Vassart G, Refetoff S. Thyroid transcription factor 1 rescues PAX8/p300 synergism impaired by a natural PAX8 paired domain mutation with dominant negative activity. Molecular Endocrinology. 2005;19(7):1779-91.
36. Gerard CM, Lefort A, Libert F, Christophe D, Dumont JE, Vassart G. Transcriptional regulation of the thyroperoxydase gene by thyrotropin and forskolin. Molecular and Cellular Endocrinology. 1988;60(2-3):239-42.
37. Uyttersprot N, Pelgrims N, Carrasco N, Gervy C, Maenhaut C, Dumont JE, Miot F. Moderate doses of iodide in vivo inhibit cell proliferation and the expression of thyroperoxidase and Na+/I- symporter mRNAs in dog thyroid. Molecular and Cellular Endocrinology. 1997;131(2):195-203.
38. Morand S, Chaaraoui M, Kaniewski J, Deme D, Ohayon R, Noel-Hudson MS, Virion A, Dupuy C. Effect of iodide on nicotinamide adenine dinucleotide phosphate oxidase activity and Duox2 protein expression in isolated porcine thyroid follicles. Endocrinology. 2003;144(4):1241-8.
39. Schweizer U, Chiu J, Köhrle J. Peroxides and peroxide-degrading enzymes in the thyroid. Antioxidants & Redox Signaling. 2008;10(9):1577-92.
40. Groeneweg S, van Geest FS, Peeters RP, Heuer H, Visser WE. Thyroid hormone transporters. Endocrine Reviews. 2020;41(2):146-201.
41. Friesema EC, Ganguly S, Abdalla A, Fox JEM, Halestrap AP, Visser TJ. Identification of monocarboxylate transporter 8 as a specific thyroid hormone transporter. Journal of Biological Chemistry. 2003;278(41):40128-35.

42. Di Cosmo C, Liao X-H, Dumitrescu AM, Philp NJ, Weiss RE, Refetoff S. Mice deficient in MCT8 reveal a mechanism regulating thyroid hormone secretion. The Journal of Clinical Investigation. 2010;120(9):3377-88.
43. Trajkovic-Arsic M, Müller J, Darras VM, Groba C, Lee S, Weih D, Bauer K, Visser TJ, Heuer H. Impact of monocarboxylate transporter-8 deficiency on the hypothalamus-pituitary-thyroid axis in mice. Endocrinology. 2010;151(10):5053-62.
44. Friesema EC, Grueters A, Biebermann H, Krude H, von Moers A, Reeser M, Barrett TG, Mancilla EE, Svensson J, Kester MH, Kuiper GG, Balkassmi S, Uitterlinden AG, Koehrle J, Rodien P, Halestrap AP, Visser TJ. Association between mutations in a thyroid hormone transporter and severe X-linked psychomotor retardation. Lancet. 2004;364(9443):1435-7.
45. Dumitrescu AM, Liao X-H, Best TB, Brockmann K, Refetoff S. A novel syndrome combining thyroid and neurological abnormalities is associated with mutations in a monocarboxylate transporter gene. The American Journal of Human Genetics. 2004;74(1):168-75.
46. Schwartz CE, May MM, Carpenter NJ, Rogers RC, Martin J, Bialer MG, Ward J, Sanabria J, Marsa S, Lewis JA. Allan-Herndon-Dudley syndrome and the monocarboxylate transporter 8 (MCT8) gene. The American Journal of Human Genetics. 2005;77(1):41-53.
47. Wirth EK, Roth S, Blechschmidt C, Hölter SM, Becker L, Racz I, Zimmer A, Klopstock T, Gailus-Durner V, Fuchs H. Neuronal 3′, 3, 5-triiodothyronine (T3) uptake and behavioral phenotype of mice deficient in Mct8, the neuronal T3 transporter mutated in Allan–Herndon–Dudley syndrome. Journal of Neuroscience. 2009;29(30):9439-49.
48. De Souza E, Dias G, Cardoso R, Lima L, Fortunato R, Visser T, Vaisman M, Ferreira A, Carvalho D. MCT8 is downregulated by short time iodine overload in the thyroid gland of rats. Hormone and Metabolic Research. 2015;47(12):910-5.
49. Refetoff S. Thyroid hormone serum transport proteins. Endotext [internet]. 2023.
50. Janssen ST, Janssen OE. Directional thyroid hormone distribution via the blood stream to target sites. Molecular and Cellular Endocrinology. 2017;458:16-21.
51. Pappa T, Ferrara AM, Refetoff S. Inherited defects of thyroxine-binding proteins. Best Practice & Research Clinical Endocrinology & Metabolism. 2015;29(5):735-47.
52. Holt EH, Lupsa B, Lee GS, Bassyouni H, Peery HE. Goodman's basic medical endocrinology: Academic Press; 2021.
53. Richardson SJ. Evolutionary changes to transthyretin: evolution of transthyretin biosynthesis. The FEBS journal. 2009;276(19):5342-56.
54. Vieira M, Saraiva MJ. Transthyretin: a multifaceted protein. Biomolecular Concepts. 2014;5(1):45-54.
55. Danforth E, Jr., Burger A. The role of thyroid hormones in the control of energy expenditure. Clinics in Endocrinology and Metabolism. 1984;13(3):581-95.
56. Kim B. Thyroid hormone as a determinant of energy expenditure and the basal metabolic rate. Thyroid. 2008;18(2):141-4.
57. Sokoloff L, Roberts PA, Januska MM, Kline JE. Mechanisms of stimulation of protein synthesis by thyroid hormones in vivo. Proceedings of the National Academy of Sciences of the United States of America. 1968;60(2):652-9.
58. Ojamaa K, Samarel AM, Kupfer JM, Hong C, Klein I. Thyroid hormone effects on cardiac gene expression independent of cardiac growth and protein synthesis. American Journal of Physiology. 1992;263(3 Pt 1):E534-40.
59. Tarım ÖF. Thyroid hormones and growth in health and disease. Journal of Clinical Research in Pediatric Endocrinology. 2011;3(2):51-5.
60. Williams GR. Actions of thyroid hormones in bone. Endokrynologia Polska. 2009;60(5):380-8.
61. Salvatore D, Simonides WS, Dentice M, Zavacki AM, Larsen PR. Thyroid hormones and skeletal muscle—new insights and potential implications. Nature Reviews Endocrinology. 2014;10(4):206-14.
62. Brent GA. Mechanisms of thyroid hormone action. The Journal of Clinical Investigation. 2012;122(9):3035-43.

63. Klein I, Ojamaa K. Thyroid hormone and the cardiovascular system. New England Journal of Medicine. 2001;344(7):501-9.
64. Middleton W. Thyroid hormones and the gut. Gut. 1971;12(2):172.
65. Silva JE. Thermogenic mechanisms and their hormonal regulation. Physiological Reviews. 2006;86(2):435-64.
66. Cannon B, Nedergaard J. Brown adipose tissue: function and physiological significance. Physiological Reviews. 2004;84(1):277-359.
67. Fedorenko A, Lishko PV, Kirichok Y. Mechanism of fatty-acid-dependent UCP1 uncoupling in brown fat mitochondria. Cell. 2012;151(2):400-13.
68. Pucci E, Chiovato L, Pinchera A. Thyroid and lipid metabolism. International Journal of Obesity and Related Metabolic Disorders. 2000;24 Suppl 2(2):S109-12.
69. Sinha RA, Singh BK, Yen PM. Direct effects of thyroid hormones on hepatic lipid metabolism. Nature Reviews Endocrinology. 2018;14(5):259-69.
70. Lee WY, Suh JY, Rhee EJ, Park JS, Sung KC, Kim SW. Plasma CRP, apolipoprotein A-1, apolipoprotein B and Lpa levels according to thyroid function status. Archives of Medical Research. 2004;35(6):540-5.
71. Hatziagelaki E, Paschou SA, Schön M, Psaltopoulou T, Roden M. NAFLD and thyroid function: pathophysiological and therapeutic considerations. Trends in Endocrinology and Metabolism. 2022.
72. Müller M, Acheson K, Jequier E, Burger A. Thyroid hormone action on lipid metabolism in humans: a role for endogenous insulin. Metabolism. 1990;39(5):480-5.
73. Ness GC, Pendleton LC, Li YC, Chiang JY. Effect of thyroid hormone on hepatic cholesterol 7 alpha hydroxylase, LDL receptor, HMG-CoA reductase, farnesyl pyrophosphate synthetase and apolipoprotein A-I mRNA levels in hypophysectomized rats. Biochemical and Biophysical Research Communications. 1990;172(3):1150-6.
74. Duntas LH, Brenta G. The effect of thyroid disorders on lipid levels and metabolism. Medical Clinics. 2012;96(2):269-81.
75. Jackson-Hayes L, Song S, Lavrentyev EN, Jansen MS, Hillgartner FB, Tian L, Wood PA, Cook GA, Park EA. A thyroid hormone response unit formed between the promoter and first intron of the carnitine palmitoyltransferase-Ialpha gene mediates the liver-specific induction by thyroid hormone. Journal of Biological Chemistry. 2003;278(10):7964-72.
76. Niedowicz DM, Wang W-X, Price DA, Nelson PT. Modulating Thyroid Hormone Levels in Adult Mice: Impact on Behavior and Compensatory Brain Changes. Journal of Thyroid Research. 2021;2021.
77. Chattergoon NN. Thyroid hormone signalling and consequences for cardiac development. The Journal of endocrinology. 2019;242(1):T145.
78. Mariotti S, Beck-Peccoz P. Physiology of the hypothalamic-pituitary-thyroid axis. Endotext. 2021.
79. Mondal S, Raja K, Schweizer U, Mugesh G. Chemistry and biology in the biosynthesis and action of thyroid hormones. Angewandte Chemie International Edition. 2016;55(27):7606-30.
80. Ortiga‐Carvalho TM, Chiamolera MI, Pazos‐Moura CC, Wondisford FE. Hypothalamus‐pituitary‐thyroid axis. Comprehensive Physiology. 2011;6(3):1387-428.
81. Duntas L. New insights into the hypothalamic-pituitary-thyroid axis. Acta Endocrinologica (Bucharest). 2016;12(2):125.
82. Sabatino L, Vassalle C, Del Seppia C, Iervasi G. Deiodinases and the three types of thyroid hormone deiodination reactions. Endocrinology and Metabolism. 2021;36(5):952-64.
83. Bianco AC, Dumitrescu A, Gereben B, Ribeiro MO, Fonseca TL, Fernandes GW, Bocco BM. Paradigms of dynamic control of thyroid hormone signaling. Endocrine Reviews. 2019;40(4):1000-47.
84. Park H, Kreunen SS, Cuttriss AJ, DellaPenna D, Pogson BJ. Identification of the carotenoid isomerase provides insight into carotenoid biosynthesis, prolamellar body formation, and photomorphogenesis. Plant Cell. 2002;14(2):321-32.
85. Breitenbach J, Vioque A, Sandmann G. Gene sll0033 from Synechocystis 6803 encodes a carotene isomerase involved in the biosynthesis of all-E lycopene. Zeitschrift Fur Naturforschung Section C-a Journal Of Biosciences. 2001;56(9-10):915-7.

86. Moise AR, Kuksa V, Imanishi Y, Palczewski K. Identification of all-trans-retinol:all-trans-13,14-dihydroretinol saturase. Journal of Biological Chemistry. 2004;279(48):50230-42.
87. Weber P, Flores RE, Kiefer MF, Schupp M. Retinol Saturase: more than the name suggests. Trends in Pharmacological Sciences. 2020;41(6):418-27.
88. Dailey TA, Dailey HA. Identification of an FAD superfamily containing protoporphyrinogen oxidases, monoamine oxidases, and phytoene desaturase. Expression and characterization of phytoene desaturase of Myxococcus xanthus. Journal of Biological Chemistry. 1998;273(22):13658-62.
89. Schupp M, Lefterova MI, Janke J, Leitner K, Cristancho AG, Mullican SE, Qatanani M, Szwergold N, Steger DJ, Curtin JC, Kim RJ, Suh MJ, Albert MR, Engeli S, Gudas LJ, Lazar MA. Retinol saturase promotes adipogenesis and is downregulated in obesity. Proceedings of the National Academy of Sciences of the United States of America. 2009;106(4):1105-10.
90. Moise AR, von Lintig J, Palczewski K. Related enzymes solve evolutionarily recurrent problems in the metabolism of carotenoids. Trends in Plant Science. 2005;10(4):178-86.
91. Moise AR, Isken A, Dominguez M, de Lera AR, von Lintig J, Palczewski K. Specificity of zebrafish retinol saturase: formation of all-trans-13,14-dihydroretinol and all-trans-7,8- dihydroretinol. Biochemistry. 2007;46(7):1811-20.
92. Toomey MB, Lind O, Frederiksen R, Curley RW, Jr., Riedl KM, Wilby D, Schwartz SJ, Witt CC, Harrison EH, Roberts NW, Vorobyev M, McGraw KJ, Cornwall MC, Kelber A, Corbo JC. Complementary shifts in photoreceptor spectral tuning unlock the full adaptive potential of ultraviolet vision in birds. Elife. 2016;5:e15675.
93. Shin D-J, Joshi P, Hong S-H, Mosure K, Shin D-G, Osborne TF. Genome-wide analysis of FoxO1 binding in hepatic chromatin: potential involvement of FoxO1 in linking retinoid signaling to hepatic gluconeogenesis. Nucleic Acids Research. 2012;40(22):11499-509.
94. Heidenreich S, Witte N, Weber P, Goehring I, Tolkachov A, von Loeffelholz C, Döcke S, Bauer M, Stockmann M, Pfeiffer AF. Retinol saturase coordinates liver metabolism by regulating ChREBP activity. Nature Communications. 2017;8(1):384.
95. Sun Y, Ng L, Lam W, Lo CK-C, Chan P-T, Yuen Y-L, Wong P-F, Tsang DS-C, Cheung W-T, Lee SS-T. Identification and characterization of a novel mouse peroxisome proliferator-activated receptor a-regulated and starvation-induced gene, Ppsig. The International Journal of Biochemistry & Cell Biology. 2008;40(9):1775-91.
96. Wu C, Orozco C, Boyer J, Leglise M, Goodale J, Batalov S, Hodge CL, Haase J, Janes J, Huss JW, 3rd, Su AI. BioGPS: an extensible and customizable portal for querying and organizing gene annotation resources. Genome Biology. 2009;10(11):R130.
97. Su AI, Wiltshire T, Batalov S, Lapp H, Ching KA, Block D, Zhang J, Soden R, Hayakawa M, Kreiman G, Cooke MP, Walker JR, Hogenesch JB. A gene atlas of the mouse and human protein-encoding transcriptomes. Proceedings of the National Academy of Sciences of the United States of America. 2004;101(16):6062-7.
98. Uhlen M, Fagerberg L, Hallstrom BM, Lindskog C, Oksvold P, Mardinoglu A, Sivertsson A, Kampf C, Sjostedt E, Asplund A, Olsson I, Edlund K, Lundberg E, Navani S, Szigyarto CA, Odeberg J, Djureinovic D, Takanen JO, Hober S, Alm T, Edqvist PH, Berling H, Tegel H, Mulder J, Rockberg J, Nilsson P, Schwenk JM, Hamsten M, von Feilitzen K, Forsberg M, Persson L, Johansson F, Zwahlen M, von Heijne G, Nielsen J, Ponten F. Proteomics. Tissue-based map of the human proteome. Science. 2015;347(6220):1260419.
99. Gu J, Li Z, Sun Y, Wei LL. Identification of functional peroxisome proliferator-activated receptor alpha response element in the human Ppsig gene. Biochemistry (Mosc). 2011;76(2):253-9.
100. Hall RK, Yamasaki T, Kucera T, Waltner-Law M, O'Brien R, Granner DK. Regulation of phosphoenolpyruvate carboxykinase and insulin-like growth factor-binding protein-1 gene expression by insulin. The role of winged helix/forkhead proteins. Journal of Biological Chemistry. 2000;275(39):30169-75.
101. Green H, Meuth M. An established pre-adipose cell line and its differentiation in culture. Cell. 1974;3(2):127-33.

102. Guilherme A, Virbasius JV, Puri V, Czech MP. Adipocyte dysfunctions linking obesity to insulin resistance and type 2 diabetes. Nature Reviews: Molecular Cell Biology. 2008;9(5):367-77.
103. Moise AR, Lobo GP, Erokwu B, Wilson DL, Peck D, Alvarez S, Dominguez M, Alvarez R, Flask CA, de Lera AR, von Lintig J, Palczewski K. Increased adiposity in the retinol saturase-knockout mouse. FASEB Journal. 2010;24(4):1261-70.
104. Spiegelman BM, Flier JS. Obesity and the regulation of energy balance. Cell. 2001;104(4):531-43.
105. Sustarsic EG, Ma T, Lynes MD, Larsen M, Karavaeva I, Havelund JF, Nielsen CH, Jedrychowski MP, Moreno-Torres M, Lundh M, Plucinska K, Jespersen NZ, Grevengoed TJ, Kramar B, Peics J, Hansen JB, Shamsi F, Forss I, Neess D, Keipert S, Wang J, Stohlmann K, Brandslund I, Christensen C, Jorgensen ME, Linneberg A, Pedersen O, Kiebish MA, Qvortrup K, Han X, Pedersen BK, Jastroch M, Mandrup S, Kjaer A, Gygi SP, Hansen T, Gillum MP, Grarup N, Emanuelli B, Nielsen S, Scheele C, Tseng YH, Faergeman NJ, Gerhart-Hines Z. Cardiolipin Synthesis in Brown and Beige Fat Mitochondria Is Essential for Systemic Energy Homeostasis. Cell Metabolism. 2018;28(1):159-74 e11.
106. Sarang Z, Joós G, Garabuczi É, Rühl R, Gregory CD, Szondy Z. Macrophages engulfing apoptotic cells produce nonclassical retinoids to enhance their phagocytic capacity. The Journal of Immunology. 2014;192(12):5730-8.
107. Sarang Z, Saghy T, Budai Z, Ujlaky-Nagy L, Bedekovics J, Beke L, Mehes G, Nagy G, Ruhl R, Moise AR, Palczewski K, Szondy Z. Retinol Saturase Knock-Out Mice are Characterized by Impaired Clearance of Apoptotic Cells and Develop Mild Autoimmunity. Biomolecules. 2019;9(11):737.
108. Nagaoka-Yasuda R, Matsuo N, Perkins B, Limbaeck-Stokin K, Mayford M. An RNAi-based genetic screen for oxidative stress resistance reveals retinol saturase as a mediator of stress resistance. Free Radical Biology and Medicine. 2007;43(5):781-8.
109. Pang X-Y, Wang S, Jurczak MJ, Shulman GI, Moise AR. Retinol saturase modulates lipid metabolism and the production of reactive oxygen species. Archives of Biochemistry and Biophysics. 2017;633:93-102.
110. Xu D, Yang C, Shen Q, Pan S, Liu Z, Zhang T, Zhou X, Lei M, Chen P, Yang H, Zhang T, Guo Y, Zhan X, Chen Y, Shi P. A single mutation underlying phenotypic convergence for hypoxia adaptation on the Qinghai-Tibetan Plateau. Cell Research. 2021;31(9):1032-5.
111. Li J, Cao F, Yin H-l, Huang Z-j, Lin Z-t, Mao N, Sun B, Wang G. Ferroptosis: past, present and future. Cell Death & Disease. 2020;11(2):88.
112. Dubreuil MM, Morgens DW, Okumoto K, Honsho M, Contrepois K, Lee-McMullen B, Traber GM, Sood RS, Dixon SJ, Snyder MP. Systematic identification of regulators of oxidative stress reveals non-canonical roles for peroxisomal import and the pentose phosphate pathway. Cell Reports. 2020;30(5):1417-33. e7.
113. Chidawanyika T, Mark KM, Supattapone S. A genome-wide CRISPR/Cas9 screen reveals that riboflavin regulates hydrogen peroxide entry into HAP1 cells. Mbio. 2020;11(4):10.1128/mbio. 01704-20.
114. Bi G, Liang J, Shan G, Bian Y, Chen Z, Huang Y, Lu T, Li M, Besskaya V, Zhao M, Fan H, Wang Q, Gan B, Zhan C. Retinol saturase mediates retinoid metabolism to impair a ferroptosis defense system in cancer cells. Cancer Research. 2023:CAN-22-3977.
115. Galan-Caridad JM, Harel S, Arenzana TL, Hou ZE, Doetsch FK, Mirny LA, Reizis B. Zfx controls the self-renewal of embryonic and hematopoietic stem cells. Cell. 2007;129(2):345-57.
116. Chan JY, Poon PHY, Zhang Y, Ng CW, Piao WY, Ma M, Yip KY, Chan AB, Lui VWY. Case Report: exome sequencing reveals recurrent RETSAT mutations and a loss-of-function POLDIP2 mutation in a rare undifferentiated tongue sarcoma. F1000Research. 2018;7.
117. Sahin U, Derhovanessian E, Miller M, Kloke BP, Simon P, Lower M, Bukur V, Tadmor AD, Luxemburger U, Schrors B, Omokoko T, Vormehr M, Albrecht C, Paruzynski A, Kuhn AN, Buck J, Heesch S, Schreeb KH, Muller F, Ortseifer I, Vogler I, Godehardt E, Attig S, Rae R, Breitkreuz A, Tolliver C, Suchan M, Martic G, Hohberger A, Sorn P, Diekmann J, Ciesla J, Waksmann O, Bruck AK, Witt M, Zillgen M, Rothermel A, Kasemann B, Langer D, Bolte S, Diken M, Kreiter S, Nemecek R, Gebhardt C, Grabbe S, Holler C, Utikal J, Huber C, Loquai C, Tureci O. Personalized RNA mutanome vaccines mobilize poly-specific therapeutic immunity against cancer. Nature. 2017;547(7662):222-6.
118. Jiang X, He Y, Shen Q, Duan L, Yuan Y, Tang L, Shi Y, Liu B, Zhai H, Shi P, Yang C, Chen Y. RETSAT Mutation Selected for Hypoxia Adaptation Inhibits Tumor Growth. Front Cell Dev Biol. 2021;9:744992.

119. Tu Q, Liu X, Yao X, Li R, Liu G, Jiang H, Li K, Chen Q, Huang X, Chang Q, Xu G, Zhu H, Shi P, Zhao B. RETSAT associates with DDX39B to promote fork restarting and resistance to gemcitabine based chemotherapy in pancreatic ductal adenocarcinoma. Journal of Experimental and Clinical Cancer Research. 2022;41(1):274.
120. McAninch EA, Bianco AC. Thyroid hormone signaling in energy homeostasis and energy metabolism. Annals of the New York Academy of Sciences. 2014;1311(1):77-87.
121. Fontenelle L, Feitosa M, Severo J, Freitas T, Morais J, Torres-Leal F, Henriques G, do Nascimento Marreiro D. Thyroid function in human obesity: underlying mechanisms. Hormone and Metabolic Research. 2016;48(12):787-94.
122. Reinehr T. Obesity and thyroid function. Molecular and Cellular Endocrinology. 2010;316(2):165-71.
123. Kowalik MA, Columbano A, Perra A. Thyroid hormones, thyromimetics and their metabolites in the treatment of liver disease. Frontiers in Endocrinology. 2018;9:382.
124. Den Hartog MT, De Boer M, Veenboer GJ, De Vijlder JJ. Generation and characterization of monoclonal antibodies directed against noniodinated and iodinated thyroglobulin, among which are antibodies against hormonogenic sites. Endocrinology. 1990;127(6):3160-5.
125. Singh VK, Mangalam AK, Dwivedi S, Naik S. Primer premier: program for design of degenerate primers from a protein sequence. Biotechniques. 1998;24(2):318-9.
126. Ye J, Coulouris G, Zaretskaya I, Cutcutache I, Rozen S, Madden TL. Primer-BLAST: a tool to design target-specific primers for polymerase chain reaction. BMC Bioinformatics. 2012;13:1-11.
127. Heidenreich S. Neue Regulatoren des zellulären Glukosestoffwechsels: Freie Universitaet Berlin (Germany); 2019.
128. Kusakabe T, Kawaguchi A, Kawaguchi R, Feigenbaum L, Kimura S. Thyrocyte-specific expression of Cre recombinase in transgenic mice. Genesis. 2004;39(3):212-6.
129. Schneider CA, Rasband WS, Eliceiri KW. NIH Image to ImageJ: 25 years of image analysis. Nature Methods. 2012;9(7):671-5.
130. Friedrichs B, Tepel C, Reinheckel T, Deussing J, von Figura K, Herzog V, Peters C, Saftig P, Brix K. Thyroid functions of mouse cathepsins B, K, and L. Journal of Clinical Investigation. 2003;111(11):1733-45.
131. Wirth EK, Rijntjes E, Meyer F, Köhrle J, Schweizer U. High T3, low T4 serum levels in Mct8 deficiency are not caused by increased hepatic conversion through type i deiodinase. European Thyroid Journal. 2015;4(Suppl. 1):87-91.
132. Renko K, Kerp H, Pape J, Rijntjes E, Burgdorf T, Führer D, Köhrle J. Tentative Application of a Streamlined Protocol to Determine Organ-Specific Regulations of Deiodinase 1 and Dehalogenase Activities as Readouts of the Hypothalamus-Pituitary-Thyroid-Periphery-Axis. Frontiers in Toxicology. 2022;4.
133. Renko K, Hoefig CS, Dupuy C, Harder L, Schwiebert C, Köhrle J, Schomburg L. A nonradioactive DEHAL assay for testing substrates, inhibitors, and monitoring endogenous activity. Endocrinology. 2016;157(12):4516-25.
134. Ziros PG, Habeos IG, Chartoumpekis DV, Ntalampyra E, Somm E, Renaud CO, Bongiovanni M, Trougakos IP, Yamamoto M, Kensler TW, Santisteban P, Carrasco N, Ris-Stalpers C, Amendola E, Liao XH, Rossich L, Thomasz L, Juvenal GJ, Refetoff S, Sykiotis GP. NFE2-Related Transcription Factor 2 Coordinates Antioxidant Defense with Thyroglobulin Production and Iodination in the Thyroid Gland. Thyroid. 2018;28(6):780-98.
135. Wolff J, Chaikoff I. Plasma inorganic iodide as a homeostatic regulator of thyroid function. Journal of Biological Chemistry. 1948;174:555-64.
136. Rakov H, Engels K, Hönes GS, Strucksberg K-H, Moeller LC, Köhrle J, Zwanziger D, Führer D. Sex-specific phenotypes of hyperthyroidism and hypothyroidism in mice. Biology of Sex Differences. 2016;7(1):1-13.
137. Benz V, Bloch M, Wardat S, Böhm C, Maurer L, Mahmoodzadeh S, Wiedmer P, Spranger J, Foryst-Ludwig A, Kintscher U. Sexual dimorphic regulation of body weight dynamics and adipose tissue lipolysis. PloS One. 2012;7(5):e37794.

138. Dumont JE, Lamy F, Roger P, Maenhaut C. Physiological and pathological regulation of thyroid cell proliferation and differentiation by thyrotropin and other factors. Physiological Reviews. 1992;72(3):667-97.
139. Hood A, Liu YP, Gattone VH, 2nd, Klaassen CD. Sensitivity of thyroid gland growth to thyroid stimulating hormone (TSH) in rats treated with antithyroid drugs. Toxicological Sciences. 1999;49(2):263-71.
140. Kawaguchi R, Yu J, Honda J, Hu J, Whitelegge J, Ping P, Wiita P, Bok D, Sun H. A membrane receptor for retinol binding protein mediates cellular uptake of vitamin A. Science. 2007;315(5813):820-5.
141. Muenzner M, Tuvia N, Deutschmann C, Witte N, Tolkachov A, Valai A, Henze A, Sander LE, Raila J, Schupp M. Retinol-binding protein 4 and its membrane receptor STRA6 control adipogenesis by regulating cellular retinoid homeostasis and retinoic acid receptor α activity. Molecular and Cellular Biology. 2013;33(20):4068-82.
142. Fedders R, Muenzner M, Weber P, Sommerfeld M, Knauer M, Kedziora S, Kast N, Heidenreich S, Raila J, Weger S. Liver-secreted RBP4 does not impair glucose homeostasis in mice. Journal of Biological Chemistry. 2018;293(39):15269-76.
143. Steinhoff JS, Wagner C, Taschler U, Wulff S, Kiefer MF, Petricek KM, Wowro SJ, Oster M, Flores RE, Yang N, Li C, Meng Y, Sommerfeld M, Weger S, Henze A, Raila J, Lass A, Schupp M. Acute retinol mobilization by retinol-binding protein 4 in mouse liver induces fibroblast growth factor 21 expression. Journal of Lipid Research. 2022;63(10):100268.
144. Bouillet P, Sapin V, Chazaud C, Messaddeq N, Décimo D, Dollé P, Chambon P. Developmental expression pattern of Stra6, a retinoic acid-responsive gene encoding a new type of membrane protein. Mechanisms of Development. 1997;63(2):173-86.
145. Bruinstroop E, van der Spek AH, Boelen A. Role of hepatic deiodinases in thyroid hormone homeostasis and liver metabolism, inflammation, and fibrosis. European Thyroid Journal. 2023;12(3).
146. Yu J, Shen S, Yan Y, Liu L, Luo R, Liu S, Wu Y, Li Y, Jiang J, Ying H. Iodide Excess Inhibits Thyroid Hormone Synthesis Pathway Involving XBP1-Mediated Regulation. Nutrients. 2023;15(4):887.
147. Rigutto S, Hoste C, Dumont JE, Corvilain B, Miot F, De Deken X. Duox1 is the main source of hydrogen peroxide in the rat thyroid cell line PCCl3. Experimental Cell Research. 2007;313(18):3892-901.
148. Rigutto S, Hoste C, Grasberger H, Milenkovic M, Communi D, Dumont JE, Corvilain B, Miot F, De Deken X. Activation of dual oxidases Duox1 and Duox2. Journal of Biological Chemistry. 2009;284(11):6725-34.
149. Park S-M, Kang T-I, So J-S. Roles of XBP1s in transcriptional regulation of target genes. Biomedicines. 2021;9(7):791.
150. Franz F, Weidinger C, Krause K, Gimm O, Dralle H, Führer D. The transcriptional regulation of FOXO genes in thyrocytes. Hormone and Metabolic Research. 2016;48(09):601-6.
151. Yu J, Koenig RJ. Thyroid-Specific PPAR γ Deletion Is Benign in the Mouse. Endocrinology. 2018;159(3):1463-8.
152. Antonelli A, Ferrari SM, Frascerra S, Pupilli C, Mancusi C, Metelli MR, Orlando C, Ferrannini E, Fallahi P. CXCL9 and CXCL11 Chemokines Modulation by Peroxisome Proliferator-Activated Receptor-α Agonists Secretion in Graves' and Normal Thyrocytes. The Journal of Clinical Endocrinology & Metabolism. 2010;95(12):E413-E20.
153. Branda CS, Dymecki SM. Talking about a revolution: The impact of site-specific recombinases on genetic analyses in mice. Developmental Cell. 2004;6(1):7-28.
154. Bouchard M, Souabni A, Busslinger M. Tissue‐specific expression of cre recombinase from the Pax8 locus. Genesis. 2004;38(3):105-9.
155. Tiozzo C, Danopoulos S, Lavarreda-Pearce M, Baptista S, Varimezova R, Al Alam D, Warburton D, Virender R, De Langhe S, Di Cristofano A. Embryonic epithelial Pten deletion through Nkx2. 1-cre leads to thyroid tumorigenesis in a strain-dependent manner. Endocrine-Related Cancer. 2012;19(2):111.
156. Fuziwara CS, Kimura ET. MicroRNAs in thyroid development, function and tumorigenesis. Molecular and Cellular Endocrinology. 2017;456:44-50.

157. Rakov H, Engels K, Hönes GS, Brix K, Köhrle J, Moeller LC, Zwanziger D, Führer D. Sex-specific phenotypes of hyperthyroidism and hypothyroidism in aged mice. Biology of Sex Differences. 2017;8:1-11.
158. Meng Z, Liu M, Zhang Q, Liu L, Song K, Tan J, Jia Q, Zhang G, Wang R, He Y, Ren X, Zhu M, He Q, Wang S, Li X, Hu T, Liu N, Upadhyaya A, Zhou P, Zhang J. Gender and Age Impacts on the Association Between Thyroid Function and Metabolic Syndrome in Chinese. Medicine (Baltimore). 2015;94(50):e2193.
159. Joseph-Bravo P, Lazcano I, Jaimes-Hoy L, Gutierrez-Mariscal M, Sanchez-Jaramillo E, Uribe RM, Charli JL. Sexually dimorphic dynamics of thyroid axis activity during fasting in rats. Front Biosci (Landmark Ed). 2020;25(7):1305-23.
160. Parra-Montes de Oca MA, Sotelo-Rivera I, Gutiérrez-Mata A, Charli J-L, Joseph-Bravo P. Sex dimorphic responses of the hypothalamus-pituitary-thyroid axis to energy demands and stress. Frontiers in Endocrinology. 2021;12:746924.
161. Joseph-Bravo P, Gutiérrez-Mariscal M, Jaimes-Hoy L, Charli J. Thyroid axis and energy balance: focus on animals and implications for humankind. Handbook of Famine, Starvation, Nutrient Deprivation Springer Nature: Cham, Switzerland. 2017:1-28.
162. Xia SF, Duan XM, Hao LY, Li LT, Cheng XR, Xie ZX, Qiao Y, Li LR, Tang X, Shi YH, Le GW. Role of thyroid hormone homeostasis in obesity-prone and obesity-resistant mice fed a high-fat diet. Metabolism. 2015;64(5):566-79.
163. Toniazzo AP, Arcego DM, Lazzaretti C, Lampert C, Weis SN, Proto-Siqueira R, Krolow R, Dalmaz C. Sex-specific effects of prepubertal stress and high-fat diet on leptin signaling in rats. Nutrition. 2018;50:18-25.
164. Engbring NH, Engstrom WW. Effects of estrogen and testosterone on circulating thyroid hormone. Journal of Clinical Endocrinology and Metabolism. 1959;19(7):783-96.
165. Arafah BM. Increased need for thyroxine in women with hypothyroidism during estrogen therapy. New England Journal of Medicine. 2001;344(23):1743-9.
166. Sugihara J, Wong A, Shimizu H, Zhao J, Cho H-R, Wang Y, Refetoff S, Arvan P, Liu M. Thyroidal Transcriptomic Profiles of Pathoadaptive Responses to Congenital Hypothyroidism in XB130 Knockout Mice. Cells. 2022;11(6):975.
167. Zhao J, Wang Y, Wakeham A, Hao Z, Toba H, Bai X, Keshavjee S, Mak TW, Liu M. XB130 deficiency affects tracheal epithelial differentiation during airway repair. PloS One. 2014;9(10):e108952.
168. Biondi B, Duntas LH. Subclinical hypothyroidism. The Thyroid and Its Diseases: A Comprehensive Guide for the Clinician. 2019:255-63.
169. Stubner D, Gartner R, Greil W, Gropper K, Brabant G, Permanetter W, Horn K, Pickardt CR. Hypertrophy and hyperplasia during goitre growth and involution in rats--separate bioeffects of TSH and iodine. Acta Endocrinologica. 1987;116(4):537-48.
170. Paynter OE, Burin GJ, Jaeger RB, Gregorio CA. Goitrogens and thyroid follicular cell neoplasia: evidence for a threshold process. Regulatory Toxicology and Pharmacology. 1988;8(1):102-19.
171. Moise AR, Alvarez S, Dominguez M, Alvarez R, Golczak M, Lobo GP, von Lintig J, de Lera AR, Palczewski K. Activation of retinoic acid receptors by dihydroretinoids. Molecular Pharmacology. 2009;76(6):1228-37.
172. Zhu X, Cheng S-y. New insights into regulation of lipid metabolism by thyroid hormone. Current Opinion in Endocrinology, Diabetes, and Obesity. 2010;17(5):408.
173. Ruhla S, Weickert MO, Arafat AM, Osterhoff M, Isken F, Spranger J, Schofl C, Pfeiffer AF, Mohlig M. A high normal TSH is associated with the metabolic syndrome. Clinical Endocrinology. 2010;72(5):696-701.
174. Gagnon AM, Antunes TT, Ly T, Pongsuwan P, Gavin C, Lochnan HA, Sorisky A. Thyroid-stimulating hormone stimulates lipolysis in adipocytes in culture and raises serum free fatty acid levels in vivo. Metabolism. 2010;59(4):547-53.
175. Felske D, Gagnon A, Sorisky A. Interacting effects of TSH and insulin on human differentiated adipocytes. Hormone and Metabolic Research. 2014:681-5.
176. Janson A, Karlsson FA, Micha-Johansson G, Bolme P, Bronnegard M, Marcus C. Effects of stimulatory and inhibitory thyrotropin receptor antibodies on lipolysis in infant adipocytes. Journal of Clinical Endocrinology and Metabolism. 1995;80(5):1712-6.

177. Elgadi A, Zemack H, Marcus C, Norgren S. Tissue-specific knockout of TSHr in white adipose tissue increases adipocyte size and decreases TSH-induced lipolysis. Biochemical and Biophysical Research Communications. 2010;393(3):526-30.
178. Landa MS, García SI, Schuman ML, Peres Diaz LS, Aisicovich M, Pirola CJ. Cardiovascular and body weight regulation changes in transgenic mice overexpressing thyrotropin-releasing hormone (TRH). Journal of Physiology and Biochemistry. 2020;76:599-608.
179. Johnson RJ, Sánchez-Lozada LG, Andrews P, Lanaspa MA. Perspective: a historical and scientific perspective of sugar and its relation with obesity and diabetes. Advances in Nutrition. 2017;8(3):412-22.
180. Chiu CJ, Wray LA, Beverly EA. Relationship of glucose regulation to changes in weight: a systematic review and guide to future research. Diabetes/Metabolism Research and Reviews. 2010;26(5):323-35.
181. Biondi B, Kahaly GJ, Robertson RP. Thyroid dysfunction and diabetes mellitus: two closely associated disorders. Endocrine Reviews. 2019;40(3):789-824.
182. Wang T, Xu J, Bo T, Zhou X, Jiang X, Gao L, Zhao J. Decreased fasting blood glucose is associated with impaired hepatic glucose production in thyroid-stimulating hormone receptor knockout mice. Endocrine Journal. 2013;60(8):941-50.
183. Menendez C, Baldelli R, Camina JP, Escudero B, Peino R, Dieguez C, Casanueva FF. TSH stimulates leptin secretion by a direct effect on adipocytes. Journal of Endocrinology. 2003;176(1):7-12.
184. Pereira S, Cline DL, Glavas MM, Covey SD, Kieffer TJ. Tissue-specific effects of leptin on glucose and lipid metabolism. Endocrine Reviews. 2021;42(1):1-28.
185. Di Blasio A, Di Dalmazi G, Izzicupo P, Bucci I, Giuliani C, Di Baldassarre A, Cecchi F, Molino Lova R, Vannetti F, Napolitano G, Macchi C. Serum TSH and Daily Physical Activity in a Cohort of Nonagenarians: Results from the Mugello Study. Journal of Functional Morphology and Kinesiology. 2022;7(3):56.
186. Ciloglu F, Peker I, Pehlivan A, Karacabey K, İlhan N, Saygin O, Ozmerdivenli R. Exercise intensity and its effects on thyroid hormones. Neuroendocrinology letters. 2005;26(6):830-4.
187. Moore A, Timmerman S, Brownlee K, Rubin D, Hackney A. Strenuous, fatiguing exercise: relationship of cortisol to circulating thyroid hormones. International Journal of Endocrinology and Metabolism. 2005;3(1):18-24.
188. Masserano JM, King C. TRH increases locomotor activity in rats after injection into the hypothalamus. European Journal of Pharmacology. 1981;69(2):217-9.
189. Lechan RM, Fekete C. The TRH neuron: a hypothalamic integrator of energy metabolism. Progress in Brain Research. 2006;153:209-35.
190. Sharp T, Bennett G, Marsden C, Tulloch I. A comparison of the locomotor effects induced by centrally injected TRH and TRH analogues. Regulatory Peptides. 1984;9(4):305-15.
191. Ushijima I, Mizuki Y, Hara T, Watanabe K, Hirano H, Yamada M, Glavin GB. Effects of acute and long-term treatments with thyrotropin-releasing hormone on locomotor activity and jumping behavior in mice. Pharmacology Biochemistry and Behavior. 1986;24(5):1423-8.
192. Miyamoto M, Nagawa Y. Mesolimbic involvement in the locomotor stimulant action of thyrotropin-releasing hormone (TRH) in rats. European Journal of Pharmacology. 1977;44(2):143-52.
193. Andrews J, Sahgal A. The effects of thyrotropin-releasing hormone, metabolites and analogues on locomotor activity in rats. Regulatory Peptides. 1983;7(2):97-109.
194. Heal D, Green A. Administration of thyrotropin releasing hormone (TRH) to rats releases dopamine in n. accumbens but not n. caudatus. Neuropharmacology. 1979;18(1):23-31.
195. Westerterp KR. Physical activity, food intake, and body weight regulation: insights from doubly labeled water studies. Nutrition Reviews. 2010;68(3):148-54.
196. Bosy-Westphal A, Hägele FA, Müller MJ. What is the impact of energy expenditure on energy intake? Nutrients. 2021;13(10):3508.
197. Lin MT, Chu PC, Leu SY. Effects of TSH, TRH, LH and LHRH on thermoregulation and food and water intake in the rat. Neuroendocrinology. 1983;37(3):206-11.
198. Attele AS, Shi ZQ, Yuan CS. Leptin, gut, and food intake. Biochemical Pharmacology. 2002;63(9):1579-83.

199. Sinha RA, Singh BK, Yen PM. Thyroid hormone regulation of hepatic lipid and carbohydrate metabolism. Trends in Endocrinology and Metabolism. 2014;25(10):538-45.
200. Walczak K, Sieminska L. Obesity and thyroid Axis. International Journal of Environmental Research Public Health. 2021;18(18):9434.
201. Pasquali R, Casanueva F, Haluzik M, van Hulsteijn L, Ledoux S, Monteiro MP, Salvador J, Santini F, Toplak H, Dekkers OM. European Society of Endocrinology Clinical Practice Guideline: Endocrine work-up in obesity. European Journal of Endocrinology of the European Federation of Endocrine Societies. 2020;182(1):G1-G32.
202. Swarnalatha NB, Roy N, Gouda MM, Moger R, Abraham A. High-fat, simple-carbohydrate diet intake induces hypothalamic–pituitary–thyroid axis dysregulation in C57BL/6J male mice. Applied Physiology, Nutrition, Metabolism. 2018;43(4):371-80.
203. Zhang D, Wei Y, Huang Q, Chen Y, Zeng K, Yang W, Chen J, Chen J. Important Hormones Regulating Lipid Metabolism. Molecules. 2022;27(20):7052.
204.Sinha RA, Bruinstroop E, Singh BK, Yen PM. Nonalcoholic fatty liver disease and hypercholesterolemia: roles of thyroid hormones, metabolites, and agonists. Thyroid. 2019;29(9):1173-91.
205. Mashek DG. Hepatic fatty acid trafficking: multiple forks in the road. Advances in Nutrition. 2013;4(6):697-710.
206. Duncan RE, Ahmadian M, Jaworski K, Sarkadi-Nagy E, Sul HS. Regulation of lipolysis in adipocytes. Annual Review of Nutrition. 2007;27:79-101.
207. Richardson SJ. Cell and molecular biology of transthyretin and thyroid hormones. International Review of Cytology. 2007;258:137-93.
208. Palha JA. Transthyretin as a thyroid hormone carrier: function revisited. Clinical Chemistry and Laboratory Medicine. 2002;40(12):1292-300.
209. Seifert J, Chen Y, Schöning W, Mai K, Tacke F, Spranger J, Köhrle J, Wirth EK. Hepatic Energy Metabolism under the Local Control of the Thyroid Hormone System. International Journal of Molecular Sciences. 2023;24(5):4861.
210. Engels K, Rakov H, Zwanziger D, Moeller LC, Homuth G, Köhrle J, Brix K, Führer D. Differences in mouse hepatic thyroid hormone transporter expression with age and hyperthyroidism. European Thyroid Journal. 2015;4(Suppl. 1):81-6.
211. Blay P, Nilsson C, Owman C, Aldred A, Schreiber G. Transthyretin expression in the rat brain: effect of thyroid functional state and role in thyroxine transport. Brain Research. 1993;632(1-2):114-20.
212. Chartoumpekis DV, Ziros PG, Georgakopoulos-Soares I, Smith AAT, Marques AC, Ibberson M, P AK, Habeos I, Trougakos IP, Khoo NKH, Sykiotis GP. The Transcriptomic Response of the Murine Thyroid Gland to Iodide Overload and the Role of the Nrf2 Antioxidant System. Antioxidants (Basel). 2020;9(9):884.
213. Mansourian A. Metabolic pathways of tetraidothyronine and triidothyronine production by thyroid gland: a review of articles. Pakistan Journal of Biological Sciences. 2011;14(1):1.
214. Sugawara M, Sugawara Y, Wen K. Methimazole and propylthiouracil increase cellular thyroid peroxidase activity and thyroid peroxidase mRNA in cultured porcine thyroid follicles. Thyroid. 1999;9(5):513-8.
215. Sugawara M. Reactive oxygen species and thyroid diseases. Systems Biology of Free Radicals Antioxidants. 2014;1:3521-38.
216. Ferreira AC, de Carvalho Cardoso L, Rosenthal D, de Carvalho DP. Thyroid Ca2+/NADPH-dependent H2O2 generation is partially inhibited by propylthiouracil and methimazole. European Journal of Biochemistry. 2003;270(11):2363-8.
217. De Groef B, Decallonne BR, Van der Geyten S, Darras VM, Bouillon R. Perchlorate versus other environmental sodium/iodide symporter inhibitors: potential thyroid-related health effects. European Journal of Endocrinology of the European Federation of Endocrine Societies. 2006;155(1):17-25.
218. Yao X, Li M, He J, Zhang G, Wang M, Ma J, Sun Y, Zhang W, Li L. Effect of early acute high concentrations of iodide exposure on mitochondrial superoxide production in FRTL cells. Free Radical Biology and Medicine. 2012;52(8):1343-52.

219. Morton M, Chaikoff I, Rosenfeld S. Inhibiting effect of inorganic iodide on the formation in vitro of thyroxine and diiodotyrosine by surviving thyroid tissue. Journal of Biological Chemistry. 1944;154:381-7.
220. Wolff J, Chaikoff IL. Plasma inorganic iodide, a chemical regulator of normal thyroid function. Endocrinology. 1948;42(6):468-71.
221. Leoni SG, Kimura ET, Santisteban P, De la Vieja A. Regulation of thyroid oxidative state by thioredoxin reductase has a crucial role in thyroid responses to iodide excess. Molecular Endocrinology. 2011;25(11):1924-35.
222. Wolff J, Chaikoff IL, Goldberg R, Meier J. The temporary nature of the inhibitory action of excess iodine on organic iodine synthesis in the normal thyroid. Endocrinology. 1949;45(5):504-13, illust.
223. Leung AM, Braverman LE. Consequences of excess iodine. Nature Reviews Endocrinology. 2014;10(3):136-42.
224. Liu J, Mao C, Dong L, Kang P, Ding C, Zheng T, Wang X, Xiao Y. Excessive iodine promotes pyroptosis of thyroid follicular epithelial cells in Hashimoto's thyroiditis through the ROS-NF-κB-NLRP3 pathway. Frontiers in Endocrinology. 2019;10:778.
225. Thanas C, Ziros PG, Chartoumpekis DV, Renaud CO, Sykiotis GP. The Keap1/Nrf2 signaling pathway in the thyroid—2020 update. Antioxidants. 2020;9(11):1082.
226. Renaud CO, Ziros PG, Chartoumpekis DV, Bongiovanni M, Sykiotis GP. Keap1/Nrf2 signaling: a new player in thyroid pathophysiology and thyroid cancer. Frontiers in Endocrinology. 2019;10:510.
227. Pei J, Pan X, Wei G, Hua Y. Research progress of glutathione peroxidase family (GPX) in redoxidation. Frontiers in Pharmacology. 2023;14:1147414.
228. Wang F-M, Chen Y-J, Ouyang H-J. Regulation of unfolded protein response modulator XBP1s by acetylation and deacetylation. Biochemical Journal. 2011;433(1):245-52.
229. Karbownik-Lewińska M, Stępniak J, Iwan P, Lewiński A. Iodine as a potential endocrine disruptor—a role of oxidative stress. Endocrine. 2022;78(2):219-40.
230. Iwan P, Stepniak J, Karbownik-Lewinska M. Pro-Oxidative Effect of KIO3 and Protective Effect of Melatonin in the Thyroid—Comparison to Other Tissues. Life. 2021;11(6):592.

Statutory Declaration

“I, Na Yang, by personally signing this document in lieu of an oath, hereby affirm that I prepared the submitted dissertation on the topic **“Retinol Saturase as a Novel Regulator of Thyroid Function and Energy Homeostasis”, “Retinol Saturase als neuer Regulator der Schilddrüsenfunktion und Energiestoffwechsel”** independently and without the support of third parties, and that I used no other sources and aids than those stated.

All parts which are based on the publications or presentations of other authors, either in letter or in spirit, are specified as such in accordance with the citing guidelines. The sections on methodology (in particular regarding practical work, laboratory regulations, statistical processing) and results (in particular regarding figures, charts and tables) are exclusively my responsibility.

Furthermore, I declare that I have correctly marked all of the data, the analyses, and the conclusions generated from data obtained in collaboration with other persons, and that I have correctly marked my own contribution and the contributions of other persons (cf. declaration of contribution). I have correctly marked all texts or parts of texts that were generated in collaboration with other persons.

My contributions to any publications to this dissertation correspond to those stated in the below joint declaration made together with the supervisor. All publications created within the scope of the dissertation comply with the guidelines of the ICMJE (International Committee of Medical Journal Editors; http://www.icmje.org) on authorship. In addition, I declare that I shall comply with the regulations of Charité – Universitätsmedizin Berlin on ensuring good scientific practice.

I declare that I have not yet submitted this dissertation in identical or similar form to another Faculty.

The significance of this statutory declaration and the consequences of a false statutory declaration under criminal law (Sections 156, 161 of the German Criminal Code) are known to me.”

Date Signature

Curriculum Vitae

My curriculum vitae does not appear in the electronic version of my paper for reasons of data protection.

Publication List

Li C, Kiefer MF, Dittrich S, Flores RE, Meng Y, **Yang N**, Wulff S, Gohlke S, Sommerfeld M, Wowro SJ, Petricek KM, Durbeck D, Spranger L, Mai K, Scholz H, Schulz TJ, Schupp M. Adipose retinol saturase is regulated by beta-adrenergic signaling and its deletion impairs lipolysis in adipocytes and acute cold tolerance in mice. Molecular Metabolism. 2024;79:101855.

Steinhoff JS, Wagner C, Taschler U, Wulff S, Kiefer MF, Petricek KM, Wowro SJ, Oster M, Flores RE, **Yang N**, Li C, Meng Y, Sommerfeld M, Weger S, Henze A, Raila J, Lass A, Schupp M. Acute retinol mobilization by retinol-binding protein 4 in mouse liver induces fibroblast growth factor 21 expression. Journal of Lipid Research. 2022;63(10):100268.

Oster M, Galhuber M, Krstic J, Steinhoff JS, Lenihan-Geels G, Wulff S, Kiefer MF, Petricek KM, Wowro SJ, Flores RE, **Yang N**, Li C, Meng Y, Reinisch I, Sommerfeld M, Weger S, Habisch H, Madl T, Schulz TJ, Prokesch A, Schupp M. Hepatic p53 is regulated by transcription factor FOXO1 and acutely controls glycogen homeostasis. Journal of Biological Chemistry. 2022;298(9):102287.

Heidenreich S, Weber P, Stephanowitz H, Petricek KM, Schutte T, Oster M, Salo AM, Knauer M, Goehring I, **Yang N**, Witte N, Schumann A, Sommerfeld M, Muenzner M, Myllyharju J, Krause E, Schupp M. The glucose-sensing transcription factor ChREBP is targeted by proline hydroxylation. Journal of Biological Chemistry. 2020;295(50):17158-68.

Han J[1], **Yang N**[1], Zhang F, Zhang C, Liang F, Xie W, Chen W. Rhizoma Anemarrhenae extract ameliorates hyperglycemia and insulin resistance via activation of AMP-activated protein kinase in diabetic rodents. Journal of Ethnopharmacology. 2015;172:368-76. (Co-first author)

Han J, Yi J, Liang F, Jiang B, Xiao Y, Gao S, **Yang N**, Hu H, Xie WF, Chen W. X-3, a mangiferin derivative, stimulates AMP-activated protein kinase and reduces hyperglycemia and obesity in db/db mice. Molecular and Cellular Endocrinology. 2015;405:63-73.

Acknowledgments

First and foremost, I would like to express my sincere gratitude to my supervisor, Prof. Dr Michael Schupp. Throughout my research, Prof. Dr. Michael Schupp's expertise and guidance have helped to clarify the direction of my research, provided invaluable guidance and advice, and fostered my ability to think critically and conduct independent research.

I extend my heartfelt thanks to Dr. Eva Katrin Wirth, an expert in the field of thyroid, for her collaboration and dedication, providing an expert perspective and contribution to the study and helping me to deepen my understanding of the research questions.

My appreciation goes out to my colleagues and friends in the laboratory, Yueming Meng, Julia Steinhoff, Marie Kiefer, Sascha Wulff, Manuela Sommerfeld, Moritz Oster, Dr. Sylvia Wowro, Konstantin Petricek, Roberto Flores, Pamela Weber, Catrin Taupp, Till Schütte and Sarah Dittrich. In this learning environment I have grown and learned with them, shared the joys and challenges of the experiments, and exchanged many valuable experiences and knowledge. Their suggestions and discussions have been instrumental in helping me to complete this thesis. Their friendship and spirit of collaboration has made me feel warm and connected in this laboratory.

I express my gratitude to everyone who contributed to this work. Dr. Panos G. Ziros and Dr. Gerasimos P. Sykiotis provided important data support, Beata Hoeft, Dr. Anna Foryst Ludwig, Marie Christin Gaerz, Vartiter Seher provided technical support, Dr. Carrie Stalpers and Dr. Xavier De Deken provided the I-TG antibody. They made the study more informative and comprehensive.

I also want to thank all the other academics and experts who contributed to this study. They provided valuable advice and conversations. Their expertise and enthusiasm have inspired me to continue to improve and progress.

To my family, I am deeply indebted. Throughout my studies, they have been my strongest support and backing. They have given me unconditional love and understanding and have always encouraged me to persevere, no matter how difficult the times may be. Without your unwavering support, I would not have been able to achieve this academic milestone.

Lastly, I am grateful to the Deutsche Forschungsgemeinschaft for generously funding this research project. In addition, I would like to sincerely appreciate the China Scholarship Council and the Stiftung Charité for their invaluable support in providing me with the scholarship. Their contributions have been instrumental in making this research endeavor possible.

Certificate of the Accredited Statistician

CHARITÉ

CharitéCentrum für Human- und Gesundheitswissenschaften

Charité | Campus Charité Mitte | 10117 Berlin

Institut für Biometrie und klinische Epidemiologie (iBikE)

Direktor: Prof. Dr. Frank Konietschke

Postanschrift:
Charitéplatz 1 | 10117 Berlin
Besucheranschrift:
Reinhardtstr. 58 | 10117 Berlin

Tel. +49 (0)30 450 562171
frank.konietschke@charite.de
https://biometrie.charite.de/

Name, Vorname: Yang, Na
Emailadresse: na.yang@charite.de
Matrikelnummer: 226072
PromotionsbetreuerIn: Prof. Dr. rer. nat. Michael Schupp
Promotionsinstitution / Klinik: Institute of Parmacology

Bescheinigung

Hiermit bescheinige ich, dass Frau *Na Yang* innerhalb der Service Unit Biometrie des Instituts für Biometrie und klinische Epidemiologie (iBikE) bei mir eine statistische Beratung zu einem Promotionsvorhaben wahrgenommen hat. Folgende Beratungstermine wurden wahrgenommen:

- Termin 1: 14.11.2022

Folgende wesentliche Ratschläge hinsichtlich einer sinnvollen Auswertung und Interpretation der Daten wurden während der Beratung erteilt:

- Prüfung der Normalverteilung
- Der t-Test für unabhängige Stichproben
- One-way und Two-way ANOVA

Diese Bescheinigung garantiert nicht die richtige Umsetzung der in der Beratung gemachten Vorschläge, die korrekte Durchführung der empfohlenen statistischen Verfahren und die richtige Darstellung und Interpretation der Ergebnisse. Die Verantwortung hierfür obliegt allein dem Promovierenden. Das Institut für Biometrie und klinische Epidemiologie übernimmt hierfür keine Haftung.

Datum: 04.07.2023

Name der Beraterin: Pimrapat Gebert

Pimrapat Gebert
Digital unterschrieben von Pimrapat Gebert
Datum: 2023.07.04 08:45:35 +02'00'

Unterschrift BeraterIn, Institutsstempel

CHARITÉ
UNIVERSITÄTSMEDIZIN BERLIN
Institut für Biometrie und Klinische Epidemiologie
Campus Charité Mitte
Charitéplatz 1 | D-10117 Berlin
Sitz: Reinhardtstr. 58